Cell Biology & Development

| Cell Biol Dev | vol. 9 | no. 1 | June 2025 | E-ISSN 2580-4499|

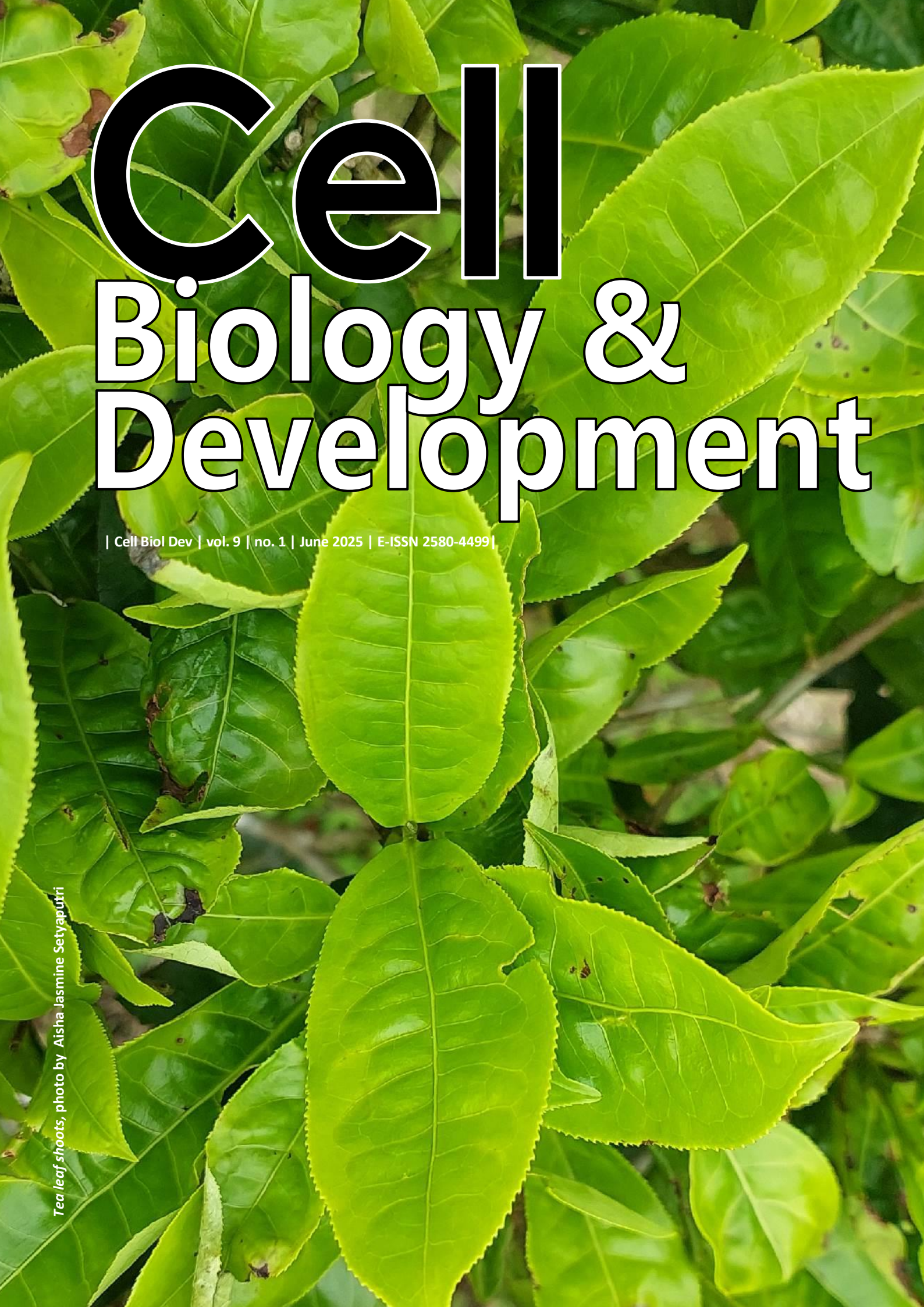

Tea leaf shoots, photo by Aisha Jasmine Setyaputri

Cell Biology & Development

| Cell Biol Dev | vol. 9 | no. 1 | June 2025 | E-ISSN 2580-4499|

Published semiannually **PRINTED IN INDONESIA**

9 772580 449173

Cell Biology & Development

| Cell Biol Dev | vol. 9 | no. 1 | June 2025 |

ONLINE
http://smujo.id/cbd

e-ISSN
2580-4499

PUBLISHER
Smujo International

ASSOCIATION
Society for Indonesian Biodiversity

INSTITUTION
Indonesian Legumes and Tuber Crops Research Institute, Malang, Indonesia

OFFICE ADDRESS
Indonesian Legumes and Tuber Crops Research Institute. Jl. Raya Kendalpayak Km 8, Po. Box 66, Malang 65101, East Java, Indonesia. Tel.: +62-341-801468, Fax.: +62-341-801496, email: editors@smujo.id

PERIOD OF ISSUANCE
June, December

Society for Indonesian Biodiversity

Indonesian Legumes and Tuber Crops Research Institute, Malang, Indonesia

Published by Smujo International for The Society for Indonesian Biodiversity and Indonesian Legumes and Tuber Crops Research Institute, Malang, Indonesia

GUIDANCE FOR AUTHORS

Aims and Scope ***Cell Biology and Development*** **(Cell Biol Dev)** encourages submission of manuscripts dealing with all aspects of the cells biology, plant molecular biology and biotechnology including organelles and cellular compartments, trafficking and turnover, signaling, motility, adhesion, cell division, differentiation and programmed cell death, regeneration, organogenesis and somatic embryogenesis, gene transfer, gene flow, secondary metabolites, metabolic engineering, impact of transgene(s), physiological, pharmacological, and toxic response of cellular systems; genomics and genetics, metabolism, abiotic and biotic stress, phytopathology, gene transfer and expression, molecular pharming, systems biology, nanobiotechnology, genome editing, phenomics and synthetic biology.

Article types The journal seeks for: (i) **Research papers**, (ii) **Reviews**, and (iii) **Short communications**. Original full-length research manuscripts are limited to 8,000 words (including tables and figures) or proportional to articles in this publication number (beyond that, it should be with notice). Review articles are also limited to 8,000 words, while Short communications should be less than 2,500 words, except for pre-study (can be more).

Submission The journal only accepts online submissions through the open journal system **(https://smujo.id/cbd/about/submissions)** or, for login problems, email the editors at unsjournals@gmail.com (or editors@smujo.id). Submitted manuscripts should be the original works of the author(s). Please ensure that the manuscript is submitted using the template, which can be found at (https://biodiversitas.mipa.uns.ac.id/D/template.doc). The manuscript must be accompanied by a cover letter containing the article title, the first name and last name of all the authors, and a paragraph describing the claimed novelty of the findings versus current knowledge. Please also provide a list of five potential reviewers in your cover letter. They should come from outside your institution and better from three different countries. Submission of a manuscript implies the submitted work has not been published (except as part of a thesis or report, or abstract) and is not being considered for publication elsewhere. When a group writes a manuscript, all authors should read and approve the final version of the submitted manuscript and its revision; and agree on the submission of manuscripts for this journal. All authors should have made substantial contributions to the concept and design of the research, acquisition of the data and its analysis, drafting the manuscript, and correcting the revision. All authors must be responsible for the work's quality, accuracy, and ethics.

Ethics Author(s) must be obedient to the law and/or ethics in treating the object of research and pay attention to the legality of material sources and intellectual property rights.

Copyright If the manuscript is accepted for publication, the author(s) still hold the copyright and retain publishing rights without restrictions. For the new invention, authors must manage its patent before publication.

Open Access The journal is committed to free-open access that does not charge readers or their institutions for access. Readers are entitled to read, download, copy, distribute, print, search, or link to the full texts of articles, as long as not for commercial purposes. The license type is CC-BY-NC-SA.

Acceptance Only articles written in US English are accepted for publication. Manuscripts will be reviewed by editors and invited reviewers (double-blind review) according to their disciplines. Authors will generally be notified of acceptance, rejection, or need for revision within 1 to 2 months of receipt. Manuscripts will be rejected if the content does not align with the journal scope, does not meet the standard quality, is in an inappropriate format, or contains complicated grammar, dishonesty (i.e., plagiarism, duplicate publications, fabrication of data, citations manipulation, etc.), or ignoring correspondence in three months. The primary criteria for publication are scientific quality and significance. **Uncorrected proofs** will be sent to the corresponding author by system or email as .doc or .docx files for checking and correcting typographical errors. The corrected proofs should be returned in 7 days to avoid publication delays. The accepted papers will be published online in chronological order at any time but printed at the end of each month.

Free of charge This publication is dedicated entirely to the advancement of science and technology, therefore author(s) or author institution(s) are not subject to publication fees. **Reprint** Authors or other parties may freely download and distribute. However, a printed request will be charged. It may be purchased when ordering by sending back the uncorrected proofs by email.

Manuscript preparation Manuscript is typed on A4 (210x297 mm^2) paper size, in a single column, single space, 10-point (10 pt) Times New Roman font. The margin text is 3 cm from the top, 2 cm from the bottom, and 1.8 cm from the left and right. Smaller lettering sizes can be applied in presenting tables and figures (9 pt). Word processing program or additional software can be used; however, it must be PC compatible, use the template, and be Microsoft Word based (.doc or .rtf; not .docx). **Scientific names** of species (incl. subspecies, variety, etc.) should be written in italics, except in italicized sentences. Scientific names (genus, species, author) and cultivar or strain should be mentioned completely for the first time mentioning it in the body text, especially for taxonomic manuscripts. The genus name can be shortened after the first mention, except in early sentences, or where this may generate confusion; name of the author can be eliminated after the first mention. For example, *Rhizopus oryzae* L. UICC 524 can be written hereinafter as *R. oryzae* UICC 524. Using trivial names should be avoided. **Biochemical and chemical nomenclature** should follow the order of the IUPAC-IUB. For DNA sequences, it is better to use Courier New font. Standard chemical abbreviations can be applied for common and clear used, for example, completely written butilic hydroxyl toluene (BHT) to be BHT hereinafter. **Metric measurements** should use IS denominations, and other systems should use equivalent values with the denomination of IS mentioned first. A dot should not follow abbreviations like g, mg, mL, etc. Minus index (m^{-2}, L^{-1}, h^{-1}) suggested being used, except in things like "per-plant" or "per-plot." **Mathematical equations** can be written down in one column with text; in that case, they can be written separately. **Numbers** one to ten are written in words, except if it relates to measurement, while values above them are written in number, except in early sentences. The fraction should be expressed in decimal. In the text, it should be used "%" rather than "percent." Avoid expressing ideas with complicated sentences and verbiage/phrasing, and use efficient and effective sentences.

The title of the article should be written in compact, clear, and informative sentence, preferably not more than 20 words. Name of author(s) should be completely written, especially for the first and the last name. **Name and institution** address should also be completely written with street name and number (location), postal code, telephone number, facsimile number, and email address. We choose local names in Bahasa Indonesia for universities in Indonesia. The mention of "strata" program, should be avoided. Manuscript written by a group, author for correspondence along with address is required (marked with "♥"). **The title page** (first page) should include title of the article, full name(s), institution(s) and address(es) of the author(s); the corresponding authors detailed postage and e-mail addresses (P), and phone (O) and fax numbers (O).

Abstract A concise abstract is required (about 200 words). The abstract should be informative and state briefly the aim of the research, the principal results and major conclusions. An abstract is often presented separately from the article, thus it must be able to stand alone (completely self-explanatory). References should not be cited, but if essential, then cite the author(s) and year(s). Abbreviations should be avoided, but if essential, they must be defined at their first mention. **Keywords** are about five words, covering scientific and local name (if any), research themes, and special methods used; and sorted from A to Z. **Abbreviations** (if any): All important abbreviations must be defined at their first mention there. **Running title** is about five words.

Introduction is about 600 words, covering the aims of the research and provide an adequate background, avoiding a detailed literature survey or a summary of the results. **Materials and Methods** should emphasize on the procedures and data analysis. **Results and Discussion** should be written as a series of connecting sentences, however, for a manuscript with long discussion should be divided into subtitles. Thorough discussion represents the causal effect mainly explains why and how the results of the research were taken place, and do not only re-express the mentioned results in the form of sentences. **Concluding** sentence should be given at the end of the discussion. **Acknowledgements** are expressed in a brief; all sources of institutional, private and corporate financial support for the work must be fully acknowledged, and any potential conflicts of interest are noted.

Figures and Tables of a maximum of three pages should be clearly presented. The title of a picture is written down below the picture, while the title of a table is written above the table. Colored figures can only be accepted if the information in the manuscript can lose without those images; the chart is preferred to use black and white images. The author could consign any picture or photo for the front cover, although it does not print in the manuscript. All images property of others should be mentioned the source. Author is suggested referring to Wikipedia for international boundaries and Google Earth for satellite imagery. If not specifically mentioned, it is assumed to refer to these sources. **There is no appendix**, all data or data analysis is incorporated into Results and Discussions. For broad data, it can be displayed on the website as a supplement.

References Preferably 80% of it comes from scientific journals published in the last 10 years. In the text, give the author names followed by the year of publication and arrange from oldest to newest and from A to Z; in citing an article written by two authors, both of them should be mentioned; however, for three and more authors only the first author is mentioned followed by et al. For example, Saharjo and Nurhayati (2006) or (Boonkerd 2003a, b, c; Sugiyarto 2004; El-Bana and Nijs 2005; Balagadde et al. 2008; Webb et al. 2008). Extent citation should be avoided, as shown with the word "cit." Reference to unpublished data and personal communication should not appear in the list but should be cited in the text only (e.g., Rifai MA 2007, pers. com. (personal communication); Setyawan AD 2007, unpublished data). In the reference list, the references should be listed in alphabetical order. Names of journals should be abbreviated. Always use the standard abbreviation of a journal's name according to the **ISSN List of Title Word Abbreviations** (www.issn.org/2-22661-LTWA-online.php). Please include DOI links for journal papers. The following examples are for guidance.

Journal:

Saharjo BH, Nurhayati AD. 2006. Domination and composition structure change at hemic peat natural regeneration following burning; a case study in Pelalawan, Riau Province. Biodiversitas 7: 154-158. DOI: 10.13057/biodiv/d070213.

The usage of "et al." in long author lists will also be accepted:

Smith J. Jones M Jr. Houghton L et al. 1999. Future of health insurance. N Engl J Med 965: 325-329. DOI: 10.10007/s002149800025.

Book:

Rai MK, Carpinella C. 2006. Naturally Occurring Bioactive Compounds. Elsevier, Amsterdam.

Chapter in the book:

Webb CO, Cannon CH, Davies SJ. 2008. Ecological organization, biogeography, and the phylogenetic structure of rainforest tree communities. In: Carson W, Schnitzer S (eds.). Tropical Forest Community Ecology. Wiley-Blackwell, New York.

Abstract:

Assaeed AM. 2007. Seed production and dispersal of *Rhazya stricta*. 50th annual symposium of the International Association for Vegetation Science, Swansea, UK, 23-27 July 2007.

Proceeding:

Alikodra HS. 2000. Biodiversity for development of local autonomous government. In: Setyawan AD, Sutarno (eds.). Toward Mount Lawu National Park; Proceeding of National Seminary and Workshop on Biodiversity Conservation to Protect and Save Germplasm in Java Island. Universitas Sebelas Maret, Surakarta, 17-20 July 2000. [Indonesian]

Thesis, Dissertation:

Sugiyarto. 2004. Soil Macro-invertebrates Diversity and Inter-Cropping Plants Productivity in Agroforestry System based on Sengon. [Dissertation]. Universitas Brawijaya, Malang. [Indonesian]

Information from the internet:

Balagadde FK, Song H, Ozaki J, Collins CH, Barnet M, Arnold FH, Quake SR, You L. 2008. A synthetic *Escherichia coli* predator-prey ecosystem. Mol Syst Biol 4: 187. DOI: 10.1038/msb.2008.24. www.molecularsystembiology.com.

THIS PAGE INTENTIONALLY LEFT BLANK

CELL BIOLOGY & DEVELOPMENT
Volume 9, Number 1, June 2025
Pages: 1-11

E-ISSN: 2580-4499
DOI: 10.13057/cellbioldev/v090101

Optimizing KCl seed priming to enhance salinity tolerance in *Capsicum frutescens*

LUTVIA FATIKAH SARI, SOLICHATUN♥, WIDYA MUDYANTINI
Department of Biology, Faculty of Mathematics and Natural Sciences, Universitas Sebelas Maret. Jl. Ir. Sutami 36A Surakarta 57126, Central Java, Indonesia. Tel./fax.: +62-271-663375, ♥email: solichatun@staff.uns.ac.id

Manuscript received: 26 July 2024. Revision accepted: 13 February 2025.

Abstract. *Sari LF, Solichatun, Mudyantini W. 2025. Optimizing KCl seed priming to enhance salinity tolerance in* Capsicum frutescens*. Cell Biol Dev 9: 1-11.* Salinity is a major abiotic stress that poses a challenge to crop productivity, particularly in coastal agricultural zones. However, there is hope on the horizon. The use of potassium chloride (KCl) for seed osmopriming has emerged as a potential strategy to enhance plant tolerance under saline conditions. This method improves seed vigor and early-stage resilience, offering a promising solution to the salinity problem. This study aimed to evaluate the effect of KCl-based osmopriming on the growth and physiological responses of cayenne pepper (*Capsicum frutescens*) under different levels of salinity stress. We applied a completely randomized design (CRD) with two factors four KCl concentrations (0, 50, 100, and 200 ppm) and three salinity levels (0, 1,000, and 2,000 ppm NaCl)—using a hydroponic system. The parameters measured included germination percentage, plant height, root length, leaf number, leaf area, shoot-to-root ratio, biomass (fresh and dry weight), total chlorophyll content, and leaf proline levels. The results showed that osmopriming with 50-100 ppm KCl significantly improved plant height, leaf area, and biomass under 1,000 ppm salinity stress, while 200 ppm KCl reduced growth under high salinity (2,000 ppm), suggesting ion toxicity. Physiological traits such as total chlorophyll and proline content exhibited non-significant changes, but trends indicated improved stress responses in primed plants. These findings demonstrate that low-dose KCl osmopriming is a promising pre-sowing treatment to enhance the early growth performance of cayenne pepper under moderate salinity. However, further field validation and biochemical profiling are recommended to optimize its application, highlighting the importance of your potential contribution to this research.

Keywords: Cayenne pepper, *Capsicum frutescens*, hydroponics, physiological response, potassium chloride

INTRODUCTION

Cayenne pepper (*Capsicum frutescens* L.) is an important horticultural crop with high economic and nutritional value, widely cultivated in tropical and subtropical regions, including Indonesia. The fruit is rich in vitamins, antioxidants, and capsaicinoids, which contribute to its use in food, medicine, and industry (Aisy and Rachmawati 2022). However, despite its adaptability to a wide range of agroecological zones, pepper production is highly sensitive to abiotic stresses, particularly salinity. Sea level rise due to climate change and unsustainable irrigation practices has accelerated soil salinization, which now threatens extensive lowland agricultural areas, including Indonesia's northern coastal plains (Bappenas 2010; Karolinoerita and Yusuf 2020).

Salinity affects plant development through complex physiological and biochemical disruptions. High salt concentrations reduce water potential in the rhizosphere, limit nutrient uptake, and induce osmotic and oxidative stress in plant tissues (Costa et al. 2018). In *Capsicum* species, exposure to saline conditions typically leads to reductions in seed germination, root and shoot growth, chlorophyll content, and fruit yield (Sobir et al. 2018; Barus et al. 2021). Salt stress also disrupts ion homeostasis, where toxic levels of Na^+ and Cl^- accumulate and interfere with the uptake of essential elements such as K^+, Ca^{2+}, and Mg^{2+} (Putri et al. 2017). Consequently, the development of low-cost, scalable strategies to improve crop tolerance to salinity is crucial for sustaining production in marginal lands.

Seed priming is one such strategy that has garnered significant attention due to its simplicity and effectiveness. It involves controlled hydration of seeds prior to sowing, allowing pre-germinative metabolic activities to occur without actual radicle emergence (Devika et al. 2021). Osmopriming, a specific priming technique using osmotic solutions such as polyethylene glycol (PEG) or inorganic salts, has shown promise in enhancing plant performance under abiotic stress (Ruan et al. 2002; Wahyuni and Kartika 2022). By inducing partial metabolic activation, osmoprimed seeds often exhibit faster and more synchronized germination, improved seedling vigor, and improved stress tolerance.

Among various osmotic agents, potassium chloride (KCl) offers dual advantages of being a priming solute and a source of K^+, an essential macronutrient involved in osmoregulation, enzyme activation, and stomatal function (Dong et al. 2020). Research by Aloui et al. (2014) on bell peppers demonstrated that KCl priming improved salinity tolerance through enhanced chlorophyll accumulation and proline synthesis. Likewise, Solichatun et al. (2022) reported that KCl priming significantly improved the growth and water-deficit resistance of *Capsicum annuum*. These effects

are generally attributed to priming-induced physiological memory, whereby the plant's stress response systems are preconditioned to react more effectively upon subsequent stress exposure (Aranega-Bou et al. 2014; Savvides et al. 2016).

Despite its potential, the effects of KCl osmopriming on *Capsicum frutescens*, particularly under different salinity levels, remain poorly understood. Most prior studies have focused on *C. annuum* or model crops such as rice and wheat, often neglecting locally important cultivars like cayenne pepper (Naz et al. 2014; Ibrahim 2016). Furthermore, while hydroponic systems offer a controlled platform for isolating the effects of salinity, they are rarely used in priming studies despite their ability to eliminate soil heterogeneity as a confounding factor. The integration of seed priming with hydroponic cultivation under salt stress conditions could offer new insights into plant adaptation mechanisms and early growth regulation.

The physiological indicators most commonly associated with salinity tolerance include growth metrics (e.g., height, biomass), photosynthetic pigments (e.g., chlorophyll a and b), and osmoprotectant accumulation (e.g., proline) (Bates et al. 1973; Chun et al. 2018). Proline accumulation is a particularly important marker, as it contributes to osmotic balance, membrane stability, and free radical scavenging under stress (Liang et al. 2013). When measured alongside chlorophyll content and morphometric data, these parameters can provide a comprehensive picture of plant responses to osmotic and ionic stress. Nonetheless, few studies have examined these indicators collectively in *C. frutescens* under salinity gradients.

Therefore, this study aimed to investigate the effect of KCl-based seed osmopriming on the growth and physiological responses of cayenne pepper grown under varying salinity stress levels in a hydroponic system. Specifically, we evaluated plant height, root length, leaf area, shoot-to-root ratio, biomass accumulation, chlorophyll content, and proline levels across a range of KCl priming concentrations (0-200 ppm) and salinity treatments (0-2,000 ppm NaCl). It is hypothesized that low-to-moderate doses of KCl will improve seedling vigor and physiological resilience, especially under moderate salinity. At the same time, excessive KCl concentrations may induce antagonistic effects due to ionic imbalance.

The findings of this study are expected to contribute to the development of cost-effective, pre-sowing seed enhancement technologies for smallholder farmers dealing with salinized environments. Moreover, the integration of morphological and physiological assessments under controlled conditions can provide a scientific basis for field validation, and breeding programs focused on abiotic stress resilience in chili peppers and other solanaceous crops.

MATERIALS AND METHODS

Study period and location

The experiment was conducted over five months, from January to May 2023. All experimental procedures were carried out under controlled conditions at two facilities within Universitas Sebelas Maret, Surakarta, Indonesia. The initial stages including seed sorting, osmopriming, germination testing, and physiological assays were performed in the Laboratory of the Undergraduate Biology Program, Faculty of Mathematics and Natural Sciences. Subsequent seedling growth, salinity treatment, and plant maintenance were conducted in semi-controlled environment in the Greenhouse of the Integrated Laboratory Unit, Universitas Sebelas Maret. The location was selected for its controlled microclimate, which ensured consistent temperature and humidity levels during the experimental period, thereby minimizing external variability and supporting accurate interpretation of treatment effects.

Plant materials and experimental design

The plant material used in this study consisted of cayenne pepper (*Capsicum frutescens*) seeds collected from fully ripe fruits (≥ 3 months old, weighing 3-4 g) obtained from local farmers in Gatak Hamlet, Pucanganom Village, Srumbung Sub-district, Magelang District, Central Java, Indonesia. Seeds were extracted manually, shade-dried, and sorted for uniformity in size, color, and shape using the Munsell Color Chart for Plant Tissue as a reference standard.

The experiment followed a factorial completely randomized design (CRD) with two independent variables: (i) KCl osmopriming concentrations at 0 ppm, 50 ppm, 100 ppm, and 200 ppm, and (ii) Salinity levels imposed through NaCl at 0 ppm, 1,000 ppm, and 2,000 ppm. These treatments resulted in 12 unique combinations, each replicated three times, for a total of 36 experimental units. The treatment matrix is presented in Table 1. Each treatment group consisted of 10 germinated seedlings grown in individual polybag units placed on a floating hydroponic setup. Seedlings were maintained for 28 days after transplanting (DAT) in a hydroponic nutrient solution supplemented with NaCl based on treatment designation.

Environmental variables such as temperature (average 27±2°C), relative humidity (60-80%), and photoperiod (12 h light:12 h dark) were kept constant throughout the growth period in the greenhouse. The nutrient solution was refreshed every two to three days to maintain ionic balance and prevent nutrient depletion. Electrical conductivity (EC) and pH were monitored routinely using a digital EC-pH meter to ensure treatment consistency.

Table 1. Treatment combinations based on KCl priming concentration and NaCl-induced salinity stress

Salinity (NaCl)	0 ppm KCl	50 ppm KCl	100 ppm KCl	200 ppm KCl
0 ppm	N0K0	N0K1	N0K2	N0K3
1,000 ppm	N1K0	N1K1	N1K2	N1K3
2,000 ppm	N2K0	N2K1	N2K2	N2K3

Osmopriming procedure

Osmopriming was performed by soaking dry cayenne pepper seeds in aqueous potassium chloride (KCl) solutions with four concentration levels: 0 ppm (control), 50 ppm, 100 ppm, and 200 ppm. For each treatment, 30 seeds were immersed in 100 mL of KCl solution and incubated at room temperature (25-28°C) for 24 hours under continuous aeration. Following priming, the seeds were air-dried at ambient temperature for 24 hours to restore their original moisture content, allowing for safe storage and handling before sowing.

To assess water uptake during the priming phase, the initial and final weights of seed batches were recorded using an analytical balance (±0.001 g accuracy). The relative increase in seed mass served as an indicator of imbibition efficiency. Seeds were subsequently subjected to a viability test using the tetrazolium (TZ) method (see Section 2.4), and only those with viability ≥ 90% were used for germination and planting.

All KCl solutions were prepared using analytical-grade KCl (Merck) dissolved in distilled water, and concentrations were verified using a conductivity meter to ensure consistency across treatments. The entire priming protocol was adapted from established methods for solanaceous crops (Elouaer and Hannachi 2012; Solichatun et al. 2022), with minor modifications to suit the seed morphology of *C. frutescens*.

Seed viability and germination test

The viability of the primed and unprimed seeds was determined using the 1% tetrazolium (TZ) test, following the method of Copeland and McDonald (2001) with minor adaptations. A total of 30 seeds per treatment were first soaked in distilled water for 24 hours to initiate imbibition. Seeds were then longitudinally bisected and submerged in a 1% solution of 2,3,5-triphenyl tetrazolium chloride at room temperature (28-30°C) for 24 hours in darkness. Viable tissues exhibited uniform red staining due to the enzymatic reduction of tetrazolium into insoluble red formazan.

The viability percentage was calculated as follows:

$$\text{Viability (\%)} = (\text{Number of viable seeds} / \text{Total number of seeds}) \times 100$$

Only seeds that showed clear red coloration in the embryo and cotyledons were considered viable. Seeds that failed to stain or exhibited patchy discoloration were excluded from further experimental use. The results of the viability test are visually illustrated in Figure 1.

Germination tests were conducted using the between-paper method on moistened filter paper placed in sterile Petri dishes. Each dish contained 10 seeds, with three replications per treatment (n=30 seeds per treatment). Seeds were kept at ambient temperature (~26°C) for 14 days, and the filter paper was regularly moistened with distilled water. Seeds were considered germinated when the radicle length reached ≥2 mm (Rhomadhon and Khotimah 2015).

Germination percentage was calculated using the formula:

$$\text{Germination (\%)} = (\text{Number of germinated seeds} / \text{Total seeds sown}) \times 100$$

Sprout length (from base to tip) was measured at the end of the germination period using a millimeter-scale ruler.

Salinity treatment and plant cultivation

After 14 days of germination, uniform seedlings from each priming treatment group were transplanted into a hydroponic culture system using rock wool cubes as the growing medium. The hydroponic system consisted of floating trays positioned on containers filled with nutrient solution. The nutrient solution was based on the commercial AB mix formula for vegetative growth, supplemented with NaCl to simulate salinity stress.

Three salinity levels were applied by adjusting NaCl concentrations in the nutrient solution to 0 ppm (control), 1,000 ppm (moderate), and 2,000 ppm (high). Salinity levels were monitored using a digital EC meter, and nutrient solutions were replaced every 2-3 days to maintain ion stability and avoid nutrient imbalances. The electrical conductivity (EC) values were kept within target ranges corresponding to the respective NaCl treatments (approximately 0.8-1.0 dS/m for control; 2.0-2.5 dS/m for 1,000 ppm NaCl; and 4.0-4.5 dS/m for 2,000 ppm NaCl), in line with previous studies on solanaceous crops under saline conditions (Ghafoor et al. 2004; Sobir et al. 2018).

Each treatment unit consisted of a single plant grown in an individual polybag filled with Rockwool and placed into the floating hydroponic tray. All trays were arranged randomly within the greenhouse to minimize spatial variation. Environmental conditions were semi-controlled, with natural lighting, daily temperatures ranging from 26-30°C, and relative humidity between 60-80%. Plants were maintained for 28 days after transplanting (DAT), during which growth and physiological parameters were recorded at weekly or endpoint intervals.

The hydroponic system was selected to ensure uniform salinity exposure, eliminate soil heterogeneity, and provide a precise evaluation of osmopriming effectiveness under controlled ionic conditions. This approach also enabled the isolation of salt stress effects from other edaphic variables, as recommended by previous controlled-environment salinity trials (Elouaer and Hannachi 2012; Dong et al. 2020).

Observational parameters

The effect of KCl osmopriming and salinity stress was evaluated using a comprehensive set of morphological and physiological parameters. Measurements were conducted either periodically (weekly) or at harvest (28 days after transplanting). Each parameter was assessed on three replicate plants per treatment, and values were expressed as means ± standard deviation (Table 2).

Data analysis

All experimental data were statistically analyzed using IBM SPSS Statistics version 26.0. Prior to analysis, data were checked for normality (Shapiro-Wilk test) and homogeneity of variance (Levene's test). Parameters that met the assumptions of parametric analysis were subjected to a two-way analysis of variance (ANOVA) to determine the main and interaction effects of KCl priming and salinity stress. Where significant differences were found ($P<0.05$),

Duncan's Multiple Range Test (DMRT) at the 5% significance level was used for post hoc comparisons among treatment means. All results are presented as mean ± standard deviation (SD) based on three biological replicates per treatment. For visualization purposes, selected data were plotted using GraphPad Prism 9.0 and Matplotlib in Python, with error bars representing standard deviations. Treatment-specific comparison tables and bar plots support interpretations of interaction effects between priming and salinity levels.

To facilitate comparative visualization across parameters with different units (e.g., cm, g, mg/g FW), standardized scores were calculated for Figure 2. Each variable was normalized using min-max scaling across all treatments using the formula:

$$\text{Standardized score} = (X - X_{min}) / (X_{max} - X_{min})$$

This transformation produced unitless values ranging from 0 to 1, allowing for the joint plotting of growth and physiological traits on a comparable scale. For proline content, the standardized values were inversely scaled to reflect the inverse relationship between proline accumulation and plant tolerance.

RESULTS AND DISCUSSION

Seed viability and germination performance

The viability of cayenne pepper seeds after osmopriming treatment was assessed using the 1% tetrazolium test. As shown in Figure 1, viable seeds exhibited clear red staining in both the embryo and cotyledon regions, indicating active dehydrogenase enzyme activity and intact respiratory function. All treatments including control and KCl-primed groups achieved high viability percentages, ranging from 96.67% to 100%. Notably, seeds primed with 50 ppm KCl showed 100% viability across all replicates. However, no statistically significant differences ($P>0.05$) were observed among treatments, indicating that KCl osmopriming neither impaired nor enhanced seed viability under non-stress conditions.

Table 2. Summary of observational parameters and measurement methods

Parameter	Description	Measurement method/reference
Plant height (cm)	Distance from the stem base to apex	Measured weekly using a ruler
Root length (cm)	Length from root collar to tip	Measured post-harvest after washing
Number of leaves	Count of fully expanded leaves	Weekly count: apical initials excluded
Leaf area (cm²)	Estimated individual leaf surface area	Gravimetric replica method (Sitompul and Guritno 1995)
Shoot-to-root ratio	Biomass allocation between shoots and roots	Fresh weight ratio at harvest
Fresh weight (g)	Total plant biomass, including water content	Weighed immediately post-harvest
Dry weight (g)	Biomass after removal of water content	Oven-dried at 60°C for 72 hours
Chlorophyll (mg/g FW)	Total chlorophyll content in fresh leaves	Acetone extract, UV-Vis at 645/663 nm (Hendry and Grime 1993)
Proline (M)	Leaf proline concentration as a stress marker	Acid-ninhydrin method (Bates et al. 1973)

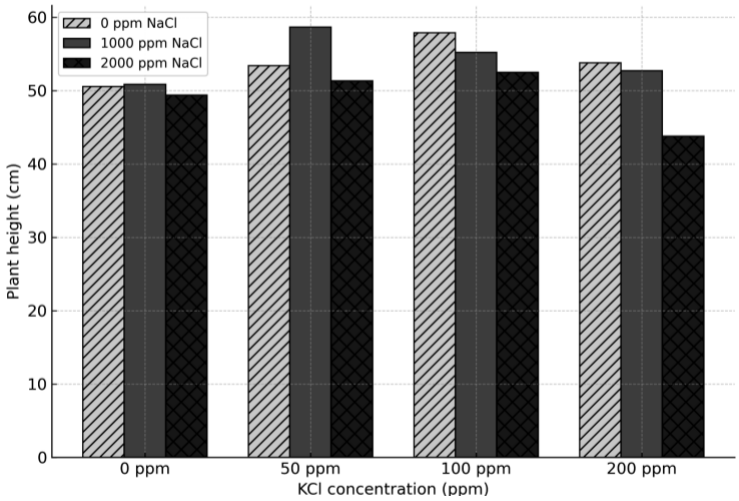

Figure 1. Average plant height of *Capsicum frutescens* under different KCl priming concentrations and salinity levels (NaCl). Bars represent mean ± SD (n=3).

In terms of germination performance, the seeds germinated successfully in all treatment groups within 14 days, with radicle emergence ≥2 mm. The germination percentage ranged from 96.67% to 100%, and the sprout length ranged from 2.37 mm to 3.30 mm (Table 3). Although the 50 ppm KCl treatment resulted in the highest germination rate (100%), it did not significantly differ from the other treatments ($P > 0.05$). Similarly, sprout length varied slightly across treatments, with the longest sprouts recorded in the control group (3.30 mm). None of the osmoprimed treatments produced significantly longer or shorter sprouts than the control, suggesting that osmopriming had limited effect on early seedling vigor in the absence of salinity stress.

These findings are consistent with previous studies showing that moderate KCl priming does not negatively affect seed viability or germination in *Capsicum* spp. (Aloui et al. 2014; Solichatun et al. 2022). The uniformity of results indicates that the seeds used in this study had inherently high physiological quality, and that the benefits of osmopriming are more likely to manifest at post-germination stages, particularly under abiotic stress conditions such as salinity.

Vegetative growth under salinity stress

Plant height was significantly affected by both KCl osmopriming and salinity stress ($P<0.05$), with a notable interaction between the two factors. As presented in Table 4, the tallest plants were observed under 1,000 ppm NaCl salinity combined with 50 ppm KCl priming, reaching an average height of 58.67 cm, which was significantly higher than most other treatment combinations. In contrast, the shortest plants (43.80 cm) were recorded in the group treated with 200 ppm KCl under 2,000 ppm NaCl salinity, suggesting that excessive K^+ input may have had an antagonistic effect under high ionic stress. Relative to the non-primed treatment at 1,000 ppm NaCl (N1K0), the 50 ppm KCl treatment (N1K1) improved plant height by approximately 21.2%, while the 100 ppm KCl treatment (N1K2) yielded a 27.8% increase in height. This indicates a dose-responsive benefit of moderate KCl priming on shoot elongation under moderate salinity.

These findings highlight the dual role of KCl priming: moderate concentrations (50-100 ppm) can enhance plant height under mild-to-moderate salinity, whereas higher concentrations (200 ppm) may lead to ion toxicity or K^+-Na^+ imbalance under high salinity. This is consistent with previous reports that potassium-mediated osmotic regulation supports turgor maintenance and elongation growth under salinity stress (Dong et al. 2020; Solichatun et al. 2022). However, excessive K^+ uptake may disrupt the selective absorption of other essential cations, particularly calcium and magnesium, leading to growth inhibition (Putri et al. 2017).

Root length, in contrast, was not significantly influenced by KCl priming or salinity treatments individually or in combination ($P>0.05$), as shown in Table 5. While some variations were observed, such as the longest average root length (26.93 cm) in plants treated with 200 ppm KCl under 1,000 ppm NaCl, these differences were not statistically meaningful. The shortest roots (20.20 cm) were found in the 50 ppm KCl + 2,000 ppm NaCl group.

Table 3. Germination percentage and sprout length of cayenne pepper (*Capsicum frutescens*) seeds after KCl osmopriming treatment

KCl concentration	Germination (%)	Sprout length (mm)
0 ppm (control)	96.67 ± 2.89^{a}	3.30 ± 0.41^{a}
50 ppm	100.00 ± 0.00^{a}	2.37 ± 0.38^{a}
100 ppm	96.67 ± 2.89^{a}	3.20 ± 0.33^{a}
200 ppm	96.67 ± 2.89^{a}	2.47 ± 0.36^{a}

Note: Values are means ± SD (n=3). Identical germination percentages across K0, K2, and K3 treatments reflect consistently high seed viability. Means followed by the same letter in a column are not significantly different at P>0.05 (DMRT)

Table 4. Average height (cm) of cayenne pepper plants after KCl priming and NaCl salinity treatment

Salinity (NaCl)	0 ppm KCl	50 ppm KCl	100 ppm KCl	200 ppm KCl
0 ppm	50.57 ± 1.2^{abc}	53.40 ± 1.5^{bcd}	57.87 ± 1.1^{cd}	53.80 ± 1.3^{bcd}
1,000 ppm	50.87 ± 1.4^{bc}	58.67 ± 1.6^{d}	55.23 ± 1.5^{bcd}	52.70 ± 1.2^{bcd}
2,000 ppm	49.37 ± 1.0^{ab}	51.33 ± 1.3^{bcd}	52.50 ± 1.2^{bcd}	43.80 ± 1.4^{a}

Note: Values are means ± SD (n=3). Different letters indicate significant differences at P<0.05 (DMRT)

Table 5. Average root length (cm) of cayenne pepper plants after KCl priming and NaCl salinity treatment

Salinity (NaCl)	0 ppm KCl	50 ppm KCl	100 ppm KCl	200 ppm KCl
0 ppm	20.47 ± 1.2^{a}	21.80 ± 1.3^{a}	22.33 ± 1.4^{a}	24.33 ± 1.2^{a}
1,000 ppm	25.80 ± 1.0^{a}	20.83 ± 1.5^{a}	26.60 ± 1.1^{a}	**26.93 ± 1.4^{a}**
2,000 ppm	23.30 ± 1.1^{a}	**20.20 ± 1.3^{a}**	21.97 ± 1.2^{a}	23.03 ± 1.4^{a}

Note: Values are means ± SD (n=3). No significant differences at P>0.05 (DMRT)

The lack of significant change in root length suggests that osmopriming may preferentially enhance shoot elongation rather than root expansion under hydroponic salinity stress. While KCl priming may help maintain cellular turgor in shoots, root systems are more directly exposed to salt ions and may suffer from osmotic inhibition or nutrient competition, as previously observed in *Pisum sativum* and *C. annuum* (Aloui et al. 2014; Naz et al. 2014). This decoupling between shoot and root responses implies that osmopriming benefits are organ-specific, favoring aboveground biomass development under salinity without necessarily promoting deeper rooting.

Compared to the non-primed control under 1,000 ppm NaCl, seeds primed with 100 ppm KCl exhibited a 27.8% increase in shoot height and a 23.4% increase in shoot dry weight, suggesting enhanced cell elongation and water uptake capacity. These improvements indicate that moderate KCl priming helps maintain shoot turgor and promotes biomass production under moderate salinity stress.

Leaf number and leaf area

The number of leaves per plant was significantly influenced by both salinity stress and KCl osmopriming, with a clear interaction effect ($P<0.05$). As shown in Table 6, the highest leaf count was recorded in plants treated with 100 ppm KCl under 1,000 ppm NaCl, averaging 11.67 leaves per plant. This was significantly higher than the control group (8.33 leaves) and the high-stress group treated with 200 ppm KCl under 2,000 ppm NaCl (6.67 leaves), which exhibited the lowest leaf number. Compared to the non-primed control under 1,000 ppm NaCl (N1K0), the 100 ppm KCl treatment (N1K2) resulted in a 40.0% increase in leaf number. Even the 50 ppm KCl treatment (N1K1) increased leaf number by 24.0%, indicating that moderate priming supports active leaf initiation under saline conditions.

These findings suggest that moderate KCl priming (50-100 ppm) can partially counteract the adverse effects of salinity on leaf development, likely by sustaining metabolic activity and delaying salt-induced senescence (Costa et al. 2018). Conversely, excessive priming (200 ppm) under severe salinity may result in additive ion toxicity, suppressing leaf initiation.

The leaf area showed a similar pattern of response (Table 7), with the largest leaf area (195.92 cm²) observed in plants treated with 50 ppm KCl under non-saline conditions. In contrast, the smallest leaf area (137.75 cm²) occurred in the 200 ppm KCl + 2,000 ppm NaCl group. The interaction between priming and salinity was significant ($P<0.05$), indicating that both factors influenced leaf expansion capacity. Under 1,000 ppm NaCl, plants primed with 100 ppm KCl produced leaves with an average area of 177.24 cm², which represents a 14.8% increase compared to the non-primed control (154.34 cm²). This suggests that KCl priming not only enhances leaf initiation but also promotes expansion under salinity stress.

Increased leaf area under moderate KCl priming is likely associated with enhanced cell turgor and membrane integrity, facilitating cell expansion even under osmotic stress. This is in agreement with studies showing that potassium availability regulates stomatal conductance, water uptake, and cell wall extensibility under saline conditions (Dong et al. 2020; Chun et al. 2018). Conversely, plants exposed to high salt levels and high priming doses showed restricted leaf growth, possibly due to metabolic disruption and ion imbalance. These physiological constraints may include disrupted protein synthesis, oxidative stress, and limited osmotic adjustment, which jointly suppress leaf development under high combined ionic load.

These results support the hypothesis that moderate KCl priming (50-100 ppm) enhances both leaf number and expansion, particularly under mild to moderate salinity stress. However, high priming doses combined with high salinity tend to reduce leaf development, indicating that the priming effect is dose-dependent and context-sensitive.

Table 6. The average number of leaves per plant under different KCl priming and salinity treatments

Salinity (NaCl)	0 ppm KCl	50 ppm KCl	100 ppm KCl	200 ppm KCl
0 ppm	8.33 ± 0.6^{b}	10.00 ± 0.5^{bc}	11.00 ± 0.5^{c}	9.33 ± 0.6^{bc}
1,000 ppm	9.00 ± 0.6^{bc}	11.00 ± 0.6^{c}	**11.67 ± 0.6^{c}**	10.00 ± 0.5^{bc}
2,000 ppm	8.00 ± 0.5^{b}	9.00 ± 0.6^{bc}	10.00 ± 0.6^{bc}	**6.67 ± 0.6^{a}**

Note: Values are means ± SD (n=3). Means followed by different letters in a column indicate significant differences at $P<0.05$ (DMRT)

Table 7. Average leaf area (cm²) of cayenne pepper under KCl priming and salinity stress

Salinity (NaCl)	0 ppm KCl	50 ppm KCl	100 ppm KCl	200 ppm KCl
0 ppm	157.33 ± 2.4^{bc}	195.92 ± 2.8^{c}	179.81 ± 2.6^{c}	170.97 ± 2.3^{bc}
1,000 ppm	153.64 ± 2.7^{b}	177.37 ± 2.4^{c}	164.22 ± 2.5^{bc}	153.48 ± 2.4^{b}
2,000 ppm	147.83 ± 2.5^{b}	148.90 ± 2.3^{b}	153.67 ± 2.6^{b}	137.75 ± 2.3^{a}

Note: Values are means ± SD (n=3). Means followed by different letters in a column are significantly different at $P < 0.05$ (DMRT)

Shoot-to-root ratio and biomass accumulation

The shoot-to-root ratio reflects the plant's resource allocation strategy under stress and was found to be significantly influenced by the interaction between KCl osmopriming and salinity levels ($P<0.05$). As presented in Table 8, the highest shoot-to-root ratio (3.35) was recorded in the group receiving 100 ppm KCl under 1,000 ppm NaCl, suggesting that this combination promoted greater shoot biomass accumulation relative to root development. Conversely, the lowest ratio (1.89) was found in the control group without priming under non-saline conditions. Relative to the unprimed control at 1,000 ppm NaCl, the 100 ppm KCl treatment increased the shoot-to-root ratio by 28.4%, indicating a shift in biomass partitioning favoring shoot growth. This reallocation may support enhanced photosynthetic area and transpiration surface under moderate stress conditions.

The increase in shoot-to-root ratio under optimal priming and moderate salinity suggests a favorable shift toward above-ground biomass allocation, possibly due to improved osmotic adjustment and photosynthetic activity. These findings align with reports that potassium priming enhances shoot vigor and water use efficiency under salt stress (Elouaer and Hannachi 2012; Solichatun et al. 2022). Nonetheless, a disproportionately high shoot-to-root ratio might also indicate a trade-off, where investment in root development is reduced, potentially compromising water uptake capacity and stress buffering over prolonged exposure.

In terms of total fresh and dry biomass, significant differences were observed among treatments ($P<0.05$). As shown in Table 9, the highest fresh weight (35.87 g) was recorded in the 100 ppm KCl + 1,000 ppm NaCl treatment, followed closely by the 50 ppm KCl + 0 ppm NaCl group (34.55 g). The lowest biomass (25.67 g) occurred in the unprimed control under high salinity (2,000 ppm NaCl). This represents a 39.7% increase in fresh biomass when comparing the 100 ppm KCl + 1,000 ppm NaCl group to the stressed control, suggesting improved water retention and cellular expansion under optimal priming.

Dry weight data followed a similar trend. The maximum dry weight (6.30 g) was observed in plants primed with 100 ppm KCl under 1,000 ppm NaCl, indicating effective carbon assimilation and structural accumulation. The lowest dry weight (4.33 g) was recorded in the 2,000 ppm NaCl control without priming. This 45.5% increase in dry biomass suggests that moderate KCl priming supports not only transient water-based biomass accumulation but also long-term growth by enhancing structural development and resource use efficiency.

These results confirm that KCl osmopriming at moderate levels (50-100 ppm) optimizes shoot-root balance and biomass production under mild to moderate salinity. The benefits include enhanced turgor, leaf area expansion, and shoot mass accumulation, likely mediated by potassium's role in osmoregulation and metabolic stability.

Chlorophyll and proline content

Salinity stress significantly influenced both total chlorophyll and leaf proline content, and these effects were modulated by KCl osmopriming ($P<0.05$). As shown in Table 10, the highest chlorophyll content (7.67 mg/g FW) was recorded in the group treated with 50 ppm KCl under 1,000 ppm NaCl, followed closely by the 100 ppm KCl group under non-saline conditions (7.45 mg/g FW). Conversely, the lowest chlorophyll levels were found in plants exposed to 2,000 ppm NaCl without priming (4.10 mg/g FW), suggesting salt-induced degradation of photosynthetic pigments. Compared to the unprimed group at 1,000 ppm NaCl (6.47 mg/g FW), 50 ppm KCl priming increased chlorophyll content by 18.6%, while 100 ppm KCl resulted in a 15.1% increase. These enhancements reflect improved preservation of photosynthetic structures and pigment biosynthesis pathways under moderate salinity.

The enhancement of chlorophyll content by KCl priming may be attributed to improved nitrogen metabolism, antioxidant defense, and stabilization of chloroplast structures under stress (Chun et al. 2018; Solichatun et al. 2022). Notably, the 50-100 ppm KCl treatments consistently produced higher pigment levels across all salinity conditions, indicating a priming-induced tolerance mechanism that preserves photosynthetic efficiency. This suggests that primed plants maintain better photosynthetic capacity by minimizing oxidative damage and protecting chloroplast membranes, even under osmotic constraints.

Leaf proline content, a well-established osmoprotectant under abiotic stress, exhibited an opposite trend. As shown in Table 11, the highest proline levels (0.29 M) were found in unprimed plants under 2,000 ppm NaCl, suggesting elevated stress perception. In contrast, proline accumulation was lowest (0.11-0.15 M) in plants treated with 50-100 ppm KCl under non-saline or mildly saline conditions. At 1,000 ppm NaCl, 100 ppm KCl priming reduced proline accumulation by 21.7% compared to the unprimed control. This decline suggests lower internal stress perception, possibly due to more stable cellular water potential and ion balance.

Table 8. The shoot-to-root ratio of cayenne pepper plants under different KCl and salinity treatments

Salinity (NaCl)	0 ppm KCl	50 ppm KCl	100 ppm KCl	200 ppm KCl
0 ppm	**1.89 ± 0.08^{a}**	2.35 ± 0.11^{b}	2.94 ± 0.09^{c}	2.49 ± 0.08^{b}
1,000 ppm	2.47 ± 0.10^{b}	2.70 ± 0.09^{c}	**3.35 ± 0.12^{d}**	2.82 ± 0.10^{c}
2,000 ppm	2.16 ± 0.09^{ab}	2.39 ± 0.10^{b}	2.59 ± 0.11^{b}	2.20 ± 0.08^{ab}

Note: Values are means ± SD (n=3). Different letters indicate significant differences at $P<0.05$ (DMRT)

Table 9. Fresh and dry biomass of cayenne pepper under KCl priming and salinity treatments

Salinity (NaCl)	KCl (ppm)	Fresh weight (g)	Dry weight (g)
0 ppm	0	28.13 ± 1.1^{ab}	4.53 ± 0.2^{ab}
	50	34.55 ± 1.3^{c}	5.80 ± 0.2^{c}
	100	32.67 ± 1.2^{bc}	5.63 ± 0.2^{bc}
	200	30.20 ± 1.1^{b}	5.10 ± 0.1^{b}
1,000 ppm	0	30.87 ± 1.2^{b}	5.17 ± 0.2^{b}
	50	32.60 ± 1.3^{bc}	5.83 ± 0.2^{c}
	100	35.87 ± 1.4^{c}	6.30 ± 0.3^{c}
	200	31.73 ± 1.2^{b}	5.37 ± 0.2^{b}
2,000 ppm	0	25.67 ± 1.0^{a}	4.33 ± 0.2^{a}
	50	29.50 ± 1.1^{b}	5.00 ± 0.1^{b}
	100	30.40 ± 1.3^{b}	5.20 ± 0.2^{b}
	200	27.73 ± 1.1^{ab}	4.67 ± 0.1^{ab}

Note: Values are means ± SD (n=3). Different letters indicate significant differences at P<0.05 (DMRT)

Table 10. Total chlorophyll content (mg/g fresh weight) under different KCl and salinity treatments

Salinity (NaCl)	0 ppm KCl	50 ppm KCl	100 ppm KCl	200 ppm KCl
0 ppm	5.10 ± 0.21^{ab}	6.93 ± 0.24^{c}	7.20 ± 0.26^{c}	6.07 ± 0.23^{bc}
1,000 ppm	5.33 ± 0.20^{b}	7.67 ± 0.27^{c}	7.30 ± 0.25^{c}	6.23 ± 0.22^{b}
2,000 ppm	4.10 ± 0.18^{a}	5.83 ± 0.21^{bc}	5.63 ± 0.22^{b}	4.77 ± 0.19^{ab}

Note: Values are means ± SD (n=3). Different letters in a row indicate significant differences at P<0.05 (DMRT)

Table 11. Leaf proline content (M) in cayenne pepper under KCl osmopriming and salinity treatments

Salinity (NaCl)	0 ppm KCl	50 ppm KCl	100 ppm KCl	200 ppm KCl
0 ppm	0.14 ± 0.01^{bc}	0.11 ± 0.01^{b}	0.13 ± 0.01^{b}	0.15 ± 0.01^{bc}
1,000 ppm	0.20 ± 0.01^{c}	0.15 ± 0.01^{bc}	0.13 ± 0.01^{b}	0.17 ± 0.01^{c}
2,000 ppm	0.29 ± 0.02^{a}	0.19 ± 0.01^{c}	0.21 ± 0.01^{c}	0.23 ± 0.01^{c}

Note: Values are means ± SD (n=3). Different letters indicate significant differences at P<0.05 (DMRT)

These results indicate that osmoprimed plants experience lower stress intensity, as reflected in reduced proline biosynthesis, supporting the hypothesis that K^+ application mitigates osmotic and oxidative damage. This aligns with earlier findings that KCl priming reduces reactive oxygen species accumulation and membrane lipid peroxidation, and promotes better osmotic adjustment in solanaceous species (Naz et al. 2014; Costa et al. 2018). The inverse relationship between chlorophyll and proline levels in primed vs. unprimed plants provides physiological evidence of stress alleviation via pre-treatment with KCl.

Taken together, the complementary increase in chlorophyll and reduction in proline in primed plants highlight the efficacy of KCl osmopriming (especially at 50-100 ppm) in enhancing physiological resilience under salt stress. These effects are dose-dependent and more pronounced under moderate salinity, reinforcing the need for optimization of priming strategies in saline agriculture.

Interaction effects of KCl priming and salinity

To further illustrate the combined effects of KCl osmopriming and NaCl-induced salinity, selected parameters were synthesized into a composite interaction profile, highlighting treatment synergies and trade-offs across morphological and physiological traits. The visual summary presented in Figure 2 shows that moderate KCl concentrations (50-100 ppm) under 1,000 ppm NaCl consistently led to superior outcomes across key growth indicators plant height, leaf number, chlorophyll content, and biomass accumulation compared to either control or extreme treatments.

Standardized scores were calculated using min-max normalization for each measured parameter to enable direct comparison across traits with different units (e.g., cm, g, mg/g FW). The transformation scaled all variables between 0 and 1. For proline content, the values were inversely standardized so that lower accumulation—indicative of lower stress—corresponded to a higher score. This approach allowed for the unified visualization of performance across all treatments and traits.

Notably, the 100 ppm KCl + 1,000 ppm NaCl treatment emerged as the most balanced and consistently high-performing across nearly all variables. Meanwhile, 200 ppm KCl under 2,000 ppm NaCl was associated with the lowest values in chlorophyll, biomass, and leaf development. These interaction effects indicate that priming efficiency is context-dependent, where suboptimal or excessive priming concentrations may exacerbate ionic imbalance rather than alleviate stress.

A cluster analysis of treatment responses (data not shown) confirmed that the salinity level was the dominant driver of physiological variation, but priming modulated the magnitude and direction of the response. These results are in line with earlier studies that emphasize the role of priming in adjusting the ionic threshold tolerance of plants through pre-exposure signaling and improved ion homeostasis (Elouaer and Hannachi 2012; Solichatun et al. 2022). The interaction profile supports the conclusion that osmopriming with 50-100 ppm KCl provides a significant protective effect under moderate salt stress (1,000 ppm NaCl), optimizing resource allocation, delaying stress symptoms, and maintaining photosynthetic capacity.

Discussion

The findings of this study highlight the modulatory effect of potassium chloride (KCl) seed osmopriming on the salinity response of *Capsicum frutescens*, with outcomes that varied according to both priming dose and salinity level. While prior studies on *C. annuum* reported significant improvements in seed germination and vegetative traits under salt stress (Aloui et al. 2014; Solichatun et al. 2022), our results suggest that *C. frutescens* responds in a similarly beneficial but more dose-sensitive manner. Priming at 50-100 ppm KCl notably improved shoot height, leaf development, and chlorophyll content, particularly under moderate salinity conditions (1,000 ppm NaCl), whereas priming at 200 ppm under high salinity (2,000 ppm NaCl) negatively impacted growth, possibly due to ionic toxicity. The standardized interaction analysis (Figure 2) also revealed that 100 ppm KCl under 1,000 ppm NaCl consistently produced the most balanced growth and physiological responses, while 200 ppm KCl under high salinity reduced most parameters. These findings have practical implications for agriculture, suggesting that KCl seed osmopriming could be a useful tool to improve plant growth under salinity stress.

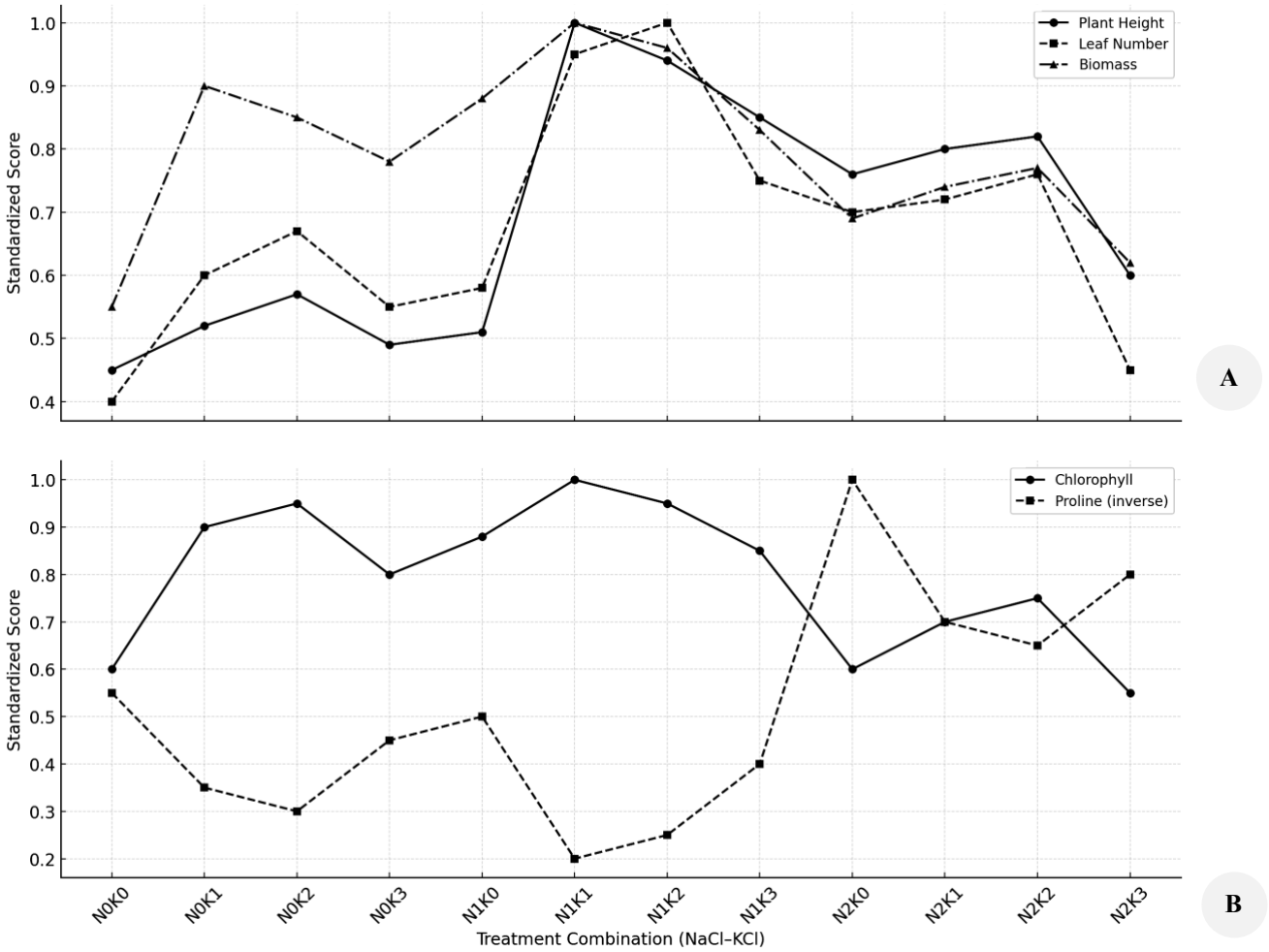

Figure 2. Growth and physiological responses of cayenne pepper (*C. frutescens*) under different KCl priming concentrations and salinity stress levels. A. Min-max standardized scores of growth-related traits (plant height, leaf number, and biomass accumulation) across 12 treatment combinations. B. Standardized physiological traits, including total chlorophyll content and proline accumulation (inversely scaled to reflect lower stress as higher scores). Standardization was applied individually per trait using the formula (x-min)/(max-min). Treatment codes denote salinity level (NaCl) and KCl priming concentration (e.g., N1K2 = 1,000 ppm NaCl + 100 ppm KCl). Each point represents the mean value of three biological replicates. Error bars were omitted to simplify visual comparison of pattern trends; raw variance is provided in Tables 4-11

In contrast to *C. annuum*, where enhanced germination following KCl priming has been frequently reported (Naz et al. 2014), the present study found no significant variation in germination percentage or sprout length across treatments in *C. frutescens*. This suggests a species-specific priming response, potentially related to inherent seed quality or differing physiological sensitivity to osmotic pre-treatment. Nonetheless, KCl priming conferred substantial advantages at post-germination stages, particularly during early vegetative development. The most pronounced improvement was observed in the 100 ppm KCl + 1,000 ppm NaCl treatment, which produced plants averaging nearly 59 cm in height, significantly taller than unprimed controls. Compared to the unprimed group under 1,000 ppm NaCl, shoot height increased by 27.8% and dry weight by 23.4%, indicating improved cell expansion and water relations. This enhancement may reflect improved cell turgor maintenance, membrane stability, and metabolic efficiency facilitated by potassium ions under moderate osmotic stress (Chun et al. 2018; Dong et al. 2020).

Potassium plays a dual role as both an osmotic regulator and a metabolic cofactor. It activates a wide range of enzymes related to energy metabolism, protein synthesis, and antioxidant defenses. The uptake of K^+ during priming may precondition plant metabolism to cope with subsequent salt-induced stress. This "primed state" did not noticeably influence germination metrics but was clearly beneficial for shoot development and leaf expansion. Root growth, however, did not respond significantly to priming or salinity. The absence of root elongation improvement may be due to localized salt accumulation in hydroponic media, which can lead to severe ionic stress in the rhizosphere. Moreover, the increased shoot-to-root ratio in primed plants implies preferential assimilate allocation to above-ground organs, consistent with previous findings in *P. sativum* and *C. annuum* under salt stress (Ghafoor et al. 2004; Costa et al. 2018). This reallocation, reaching up to 28.4% increase in the shoot-to-root ratio at 100 ppm KCl under moderate salinity, enhances light capture and transpiration potential, although possibly at the expense of root buffering capacity.

Leaf traits were among the most responsive indicators. Both leaf number and area increased significantly in primed plants under 1,000 ppm NaCl, particularly at 100 ppm KCl. These traits are critical for light capture, transpiration, and carbon assimilation, and their enhancement suggests better meristematic activity and membrane transporter stability. This supports earlier observations by Solichatun et al. (2022) in *C. annuum* and reinforces the relevance of KCl priming in maintaining photosynthetic structure under moderate stress. However, leaf development declined sharply under high salinity when priming concentrations were excessive (200 ppm), likely due to cumulative ionic imbalance and reduced cellular viability. Leaf area, for example, dropped by over 29.6% in the 200 ppm KCl + 2,000 ppm NaCl group compared to the 50 ppm KCl treatment without salinity.

Biomass production followed a similar trend. Plants treated with 100 ppm KCl under 1,000 ppm NaCl produced the highest fresh (35.87 g) and dry (6.30 g) weights. Compared to the unprimed group under the same salinity, fresh biomass increased by 39.7%, and dry biomass by 45.5%, pointing to better carbon fixation, nutrient use efficiency, and stomatal regulation. Potassium's role in enhancing enzymatic activity, particularly those involved in nitrogen assimilation and photosynthesis, such as Rubisco and nitrate reductase, may explain this biomass advantage (Chun et al. 2018). By contrast, high salinity without priming or with excessive priming led to notable reductions in plant mass, emphasizing the importance of optimizing priming dosage.

Physiological markers further validated the effects of KCl priming. Total chlorophyll content was consistently higher in primed plants, especially at 50-100 ppm. Chlorophyll degradation under salinity is often associated with oxidative stress and chloroplast disruption. Therefore, chlorophyll retention suggests a protective mechanism induced by effective early KCl application, which likely involves enhanced antioxidant activity and membrane integrity preservation (Costa et al. 2018). Potassium is known to support antioxidant enzyme function, which could contribute to maintaining pigment stability under stress. At 1,000 ppm NaCl, 50 ppm KCl priming raised chlorophyll content by 18.6% relative to the non-primed group.

Inversely, proline levels a common stress marker—increased in unprimed plants exposed to high salinity, indicating greater osmotic stress. In primed plants, especially those under moderate or no stress, proline accumulation was significantly lower. Although proline aids in osmotic balance and ROS detoxification, its excessive presence often reflects damage rather than tolerance. At 100 ppm KCl under 1,000 ppm NaCl, proline content dropped by 21.7% compared to the unprimed group, suggesting better stress mitigation. The lower proline content in primed groups thus suggests that these plants experienced less cellular stress and maintained more stable metabolic functions (Naz et al. 2014; Solichatun et al. 2022).

The combined analysis of all parameters reveals that KCl priming, particularly at 100 ppm, was most effective under moderate salinity conditions. Higher concentrations of KCl did not offer additional benefits and, under severe stress, appeared to impair plant performance. This reinforces the non-linear nature of priming responses and the importance of maintaining ion homeostasis. Excess K^+ may interfere with the uptake of other crucial ions like calcium (Ca^{2+}) and magnesium (Mg^{2+}), as also noted by Putri et al. (2017), leading to nutritional imbalances and secondary physiological stress.

Overall, this study supports the use of KCl-based osmopriming as a practical and low-cost strategy to enhance salinity tolerance in *C. frutescens*. KCl application enhances early growth, supports biomass accumulation, stabilizes chlorophyll content, and reduces stress signaling, particularly when used at optimal doses under moderate saline conditions. This is highly relevant for chili cultivation in coastal and degraded lands that are increasingly affected by salinization. Moreover, KCl priming can be readily adopted by smallholder farmers using simple pre-sowing techniques.

Despite these promising results, some limitations must be acknowledged. The study was conducted using a single cultivar under controlled hydroponic conditions, which may not reflect the complexities of field environments. Environmental variability, soil type, and biotic interactions could alter the effectiveness of priming. Additionally, only a limited set of physiological markers chlorophyll and proline were analyzed. Future studies should incorporate more comprehensive biochemical and molecular assessments, including ion profiling, antioxidant enzyme activity, and gene expression analysis, to fully elucidate the tolerance mechanisms induced by priming.

Field trials across multiple agroecological zones are also essential to validate scalability. Evaluating long-term impacts on yield attributes such as fruit number, size, and capsaicin content would further support the integration of osmopriming into practical agricultural systems. In this context, KCl priming represents not only a tool for enhancing stress tolerance but also a gateway to more resilient crop production in salt-affected areas.

REFERENCES

Aisy R, Rachmawati N. 2022. Nutritional and pharmacological potential of chili peppers. Jurnal Hortikultura Indonesia 13 (2): 155-164. DOI: 10.21082/jhi.v13n2.2022.p155-164.

Aloui H, Rejeb MN, Ghnaya T, Abdelly C, Rabhi M. 2014. Salt tolerance of pea seeds subjected to osmopriming and post-priming treatments. Acta Physiol Plant 36: 2151-2157. DOI: 10.1007/s11738-014-1562-1.

Aranega-Bou P, Leyva MD, Finiti I, Garcia-Agustin P, Gonzalez-Bosch C. 2014. Priming of plant resistance by natural compounds. Plant Physiol Biochem 84: 51-61. DOI: 10.1016/j.plaphy.2014.09.027.

Bappenas. 2010. National Action Plan for Climate Change Adaptation (RAN-API). Bappenas Publication, Jakarta. [Indonesian]

Barus RA, Hutapea RK, Sembiring B, Suriani. 2021. Salt stress effect on growth of several chili genotypes. Jurnal Agroekoteknologi 9 (3): 435-441.

Bates LS, Waldren RP, Teare ID. 1973. Rapid determination of free proline for water-stress studies. Plant Soil 39: 205-207. DOI: 10.1007/BF00018060.

Chun SC, Paramasivan M, Chandrasekaran M. 2018. Proline accumulation influenced by osmotic stress in arbuscular mycorrhizal symbiotic plants. Front Microbiol 9: 2525. DOI: 10.3389/fmicb.2018.02525.

Copeland LO, McDonald MB. 2001. Principles of Seed Science and Technology. Springer, New York.

Costa EM, Silva S, Veiga M, Pintado MM. 2018. The role of chitosan in the preservation of agricultural commodities. Post-harvest Biol Technol 143: 1-14. DOI: 10.1016/j.postharvbio.2018.04.001.

Devika OS, Preetha PP, Rajamma MM. 2021. Osmopriming: A novel strategy to improve seed quality. Seed Sci Technol 49 (3): 501-510. DOI: 10.15258/sst.2021.49.3.01

Dong H, Li W, Tang W, Zhang D. 2020. Enhanced photosynthetic performance in cotton under salinity stress by potassium application. Plant Soil 260: 169-179. DOI: 10.1023/A:1026496408367.

Elouaer MA, Hannachi C. 2012. Effect of salt stress on seed germination and antioxidant activities in Triticum durum Desf. Afr J Biotechnol 11 (47): 10709-10715. DOI: 10.5897/AJB11.3039

Ghafoor A, Arshad M, Akhtar J, Qureshi RH. 2004. Salt tolerance of different plant species under field conditions. Soil Environ 23: 50-55.

Hendry GA, Grime JP. Methods In Comparative Plant Ecology: A Laboratory Manual. Springer Science & Business Media, London.

Ibrahim MK. 2016. Improving salinity tolerance in rice through osmopriming. Rice Res 4: 176. DOI: 10.4172/2375-4338.1,000176.

Karolinoerita A, Yusuf S. 2020. Vulnerability of coastal agriculture due to saltwater intrusion. Jurnal Sosek Tan 20 (2): 81-90. DOI: 10.24843/JUST.2020.v20.i02.p02.

Liang X, Zhang L, Natarajan SK, Becker DF. 2013. Proline mechanisms of stress tolerance in plants. Amino Acids 45: 555-564. DOI: 10.1007/s00726-013-1501-y.

Naz A, Khokhar KM, Ali MA. 2014. Role of potassium in alleviating salinity stress in plants. Pak J Bot 46 (4): 1351-1359.

Putri IP, Kartika JG, Rohmah AN, Solichatun. 2017. Pengaruh pemberian kalium terhadap pertumbuhan dan hasil cabai rawit pada kondisi cekaman salinitas. Jurnal Produksi Tanaman 5 (9): 1512-1520. DOI: 10.21176/jpt.2017.5.9.1512. [Indonesian]

Rhomadhon D, Khotimah S. 2015. Pengaruh konsentrasi GA3 terhadap perkecambahan benih cabai. BioEksakta 7 (1): 14-18. DOI: 10.20473/bio.v7i1.2015.14-18. [Indonesian]

Ruan S, Xue Q, Tylkowska K. 2002. Effects of seed priming on germination and health of rice seeds. Seed Sci Technol 30: 451-458. DOI: 10.15258/sst.2002.30.2.18.

Savvides A, Ali S, Tester M, Fotopoulos V. 2016. Chemical priming of plants against multiple abiotic stresses: mission possible? Trends Plant Sci 21 (4): 329-340. DOI: 10.1016/j.tplants.2015.11.003.

Sitompul SM, Guritno B. 1995. Analisa Pertumbuhan Tanaman. Gadjah Mada University Press, Yogyakarta. [Indonesian]

Sobir, Afifah AN, Fadillah R, et al. 2018. Salinity stress on chili growth and physiology. Jurnal Agronomi Indonesia 46 (1): 38-45. DOI: 10.24831/jai.v46i1.19621.

Solichatun, Mulyani S, Pujiasmanto B, Sukartono. 2022. The effect of KCl osmopriming on germination, growth, and antioxidant activity of cayenne pepper under salt stress. Biodiversitas 23 (2): 847-854. DOI: 10.13057/biodiv/d230206

Wahyuni DK, Kartika JG. 2022. Effect of PEG osmopriming on growth of tomato under drought stress. Jurnal Hortikultura Indonesia 13 (3): 178-186. DOI: 10.21082/jhi.v13n3.2022.p178-186.

CELL BIOLOGY & DEVELOPMENT
Volume 9, Number 1, June 2025
Pages: 12-25

E-ISSN: 2580-4499
DOI: 10.13057/cellbioldev/v090102

Ecophysiological effects of mangrove canopy density on surface thermal conditions in a tropical lagoon ecosystem of Segara Anakan, Indonesia

ANISA EKA PUTRI ARYANTO[1], ARDIA CANDRA FAJAR HERBOWO[1], ARUM NUR MUKARROMAH[1], AZKA DITA AULIA[1], ABDUL BILAL ZULFIKAR[2], ARI PITOYO[3], AHMAD DWI SETYAWAN[1,3,♥]

[1]Department of Environmental Science, Faculty of Mathematics and Natural Sciences, Universitas Sebelas Maret. Jl. Ir. Sutami 36A, Surakarta 57126, Central Java, Indonesia. Tel.: +62-271-669376, Fax.: +62-271-663375, ♥email: volatileoils@gmail
[2]Department of Geography Education, Faculty of Teacher Training and Education, Universitas Sebelas Maret. Jl. Ir. Sutami 36A, Surakarta 57126, Central Java, Indonesia
[3]Department of Biology, Faculty of Mathematics and Natural Sciences, Universitas Sebelas Maret. Jl. Ir. Sutami 36A, Surakarta 57126, Central Java, Indonesia
[4]Biodiversity Research Group, Universitas Sebelas Maret. Jl. Ir. Sutami 36A, Surakarta 57126, Central Java, Indonesia

Manuscript received: 17 December 2025. Revision accepted: 7 April 2025.

Abstract. *Aryanto AEP, Herbowo ACF, Mukarromah AN, Aulia AD, Zulfikar AB, Pitoyo A, Setyawan AD. 2025. Ecophysiological effects of mangrove canopy density on surface thermal conditions in a tropical lagoon ecosystem of Segara Anakan, Indonesia. Cell Biol Dev 9: 12-25.* Mangrove forests are ecologically critical coastal ecosystems that regulate local microclimates and buffer against multiple forms of environmental stress. This study investigates the influence of mangrove canopy density on surface thermal dynamics in the climate-sensitive Segara Anakan Lagoon, Cilacap, Indonesia, using satellite-derived indices. Vegetation density was quantified using the Normalized Difference Vegetation Index (NDVI), while Land Surface Temperature (LST) was derived from Landsat 9 thermal imagery. Spatial overlay and statistical correlation of NDVI and LST were employed to delineate thermal stress zones—defined as areas where surface temperatures exceed physiological thresholds for mangrove growth. Results revealed a strong negative correlation between NDVI and LST ($R^2 = 0.68$; Pearson's $r = -0.82$), indicating that denser vegetation corresponds with cooler surface conditions. Zones with NDVI>0.60 typically exhibited temperatures of 23-25°C, while areas with lower canopy density exceeded 25°C. Thermal hotspots were concentrated in southern and central Cilacap, where anthropogenic disturbance has reduced canopy continuity. These findings highlight the ecophysiological importance of maintaining mangrove canopy cover in mitigating thermal stress. The integration of NDVI-LST analysis provides a non-invasive, scalable tool for monitoring vegetation health, supporting targeted restoration, and informing climate adaptation strategies in tropical coastal landscapes.

Keywords: Land surface temperature, mangrove canopy, NDVI, remote sensing, Segara Anakan, thermal stress

INTRODUCTION

Mangrove forests with their unique and complex nature stand out as one of the most ecologically significant vegetation types in tropical coastal zones. They provide crucial ecosystem services such as shoreline stabilization, carbon sequestration, and habitat provision for various biota. These ecosystems are typically located in estuarine and intertidal areas, are the result of a dynamic interaction between freshwater inflows and tidal seawater, creating a productive environment that is both fascinating and crucial for our understanding of coastal ecosystems (Sipayung and Poedjirahajoe 2021). In Indonesia, mangrove forests are widely distributed, and one of the notable mangrove systems is found in the Segara Anakan Lagoon, Cilacap District, Central Java. This region is characterized by brackish water conditions and the convergence of multiple rivers, presenting a complex hydrological and ecological zone that is challenging for further exploration (Ardelia and Fahleny 2023).

The structure and density of mangrove vegetation play a crucial role in regulating microclimatic variables, particularly Land Surface Temperature (LST), which is a key component of local thermal regimes. The dense canopies formed by mangrove trees modulate light interception, air humidity, and evapotranspiration, all of which are physiologically important for plant growth and microclimate regulation (Indrawati et al. 2020; Huang et al. 2024). In high-density stands, shading reduces direct solar radiation and promotes evaporative cooling, which in turn lowers the temperature of the surrounding environment. This significant role of mangroves in regulating microclimatic variables underscores their importance and the need for their conservation. Conversely, mangrove degradation and canopy loss can expose the soil surface, intensify thermal load, and compromise the ecosystem's thermal buffering capacity (Rahaman et al. 2023; Guo et al. 2024).

Recent advances in satellite remote sensing technologies have enabled the simultaneous assessment of vegetation density and surface temperature through vegetation indices such as the Normalized Difference Vegetation Index (NDVI) and thermal infrared data (Malik et al. 2019). NDVI values, derived from the ratio of near-infrared to red reflectance, serve as reliable proxies for plant greenness, biomass, and canopy vigor (Kshetri 2018; Latue et al. 2023). Likewise, thermal bands from sensors such as Landsat's Thermal Infrared Sensor (TIRS) provide high-resolution estimates of LST, allowing researchers to quantify surface thermal

variation across vegetation gradients (Fadlin et al. 2020). In coastal ecosystems, the combination of NDVI and LST provides valuable insight into how vegetation structure mediates land-atmosphere interactions.

Although NDVI and LST are widely used for assessing vegetation-environment interactions, fewer studies have focused specifically on the ecophysiological interpretation of mangrove canopy effects on surface thermal regimes in tropical lagoons. Such interpretation is important because changes in surface temperature may alter photosynthetic performance, respiration rates, and water-use efficiency of mangrove species (Alongi 2018; Fazlioglu et al. 2020). Temperature fluctuations can also affect mangrove metabolic rates and nutrient cycling, leading to downstream impacts on forest productivity and resilience. In extreme cases, prolonged exposure to high temperatures can exceed species-specific thermal tolerances, potentially leading to stress, reduced carbon sequestration, or mortality (Li et al. 2015; Segaran et al. 2023).

In the context of climate change, understanding the relationship between vegetation cover and surface thermal dynamics becomes increasingly urgent. Rising global temperatures, coupled with sea level rise and altered precipitation patterns, may compromise the ecological stability of mangrove forests (de Lacerda et al. 2019). In Southeast Asia, mangroves already face pressures from land conversion, aquaculture, and coastal development, which reduce canopy density and exacerbate thermal stress on exposed surfaces (Al Kafy et al. 2021). Mangrove canopy loss not only accelerates surface warming but also limits the forest's ability to moderate air temperatures, store carbon, and regulate favorable conditions for seedling establishment.

In Indonesia, this challenge is addressed by Presidential Regulation No. 73 of 2020 through the national mangrove rehabilitation program led by the Peatland and Mangrove Restoration Agency (BRGM). This policy underscores the need for scalable monitoring tools, where satellite-based indices such as NDVI and LST can help identify canopy degradation and thermal risk zones in support of targeted restoration. Despite their potential, integrated analyses of NDVI and LST in mangrove systems remain limited in Indonesian contexts, particularly in lagoonal environments.

Segara Anakan provides a critical case study for exploring how mangrove canopy structure influences surface thermal conditions under tropical lagoon settings. With large expanses of both intact and degraded mangrove stands, the region allows for spatial comparisons of canopy density and its thermal effects. By examining these patterns, researchers can infer the potential physiological stress gradients experienced by mangrove trees and anticipate changes in ecosystem function. Moreover, such spatial data can inform restoration efforts by identifying priority areas for replanting or protection based on thermal vulnerability.

This study aims to assess the ecophysiological implications of mangrove canopy density on land surface temperature in the Segara Anakan Lagoon. Specifically, it seeks to (i) map vegetation density and surface temperature using remote sensing tools, (ii) analyze the spatial correlation between canopy density and surface thermal gradients, and (iii) discuss the physiological significance of observed patterns for mangrove species. The novelty of this study lies in its integration of satellite-based thermal data with ecophysiological reasoning, highlighting how vegetation structure mediates environmental temperature in tropical coastal forests.

MATERIALS AND METHODS

Study area

The study was conducted in the Segara Anakan Lagoon, located in Cilacap District, Central Java, Indonesia. This lagoon is one of the largest and most dynamic estuarine ecosystems on the southern coast of Java Island. Administratively, the mangrove forest area around Segara Anakan spans several sub-districts, including Kalipucang, Patimuan, Kampung Laut, South Cilacap, and Central Cilacap.

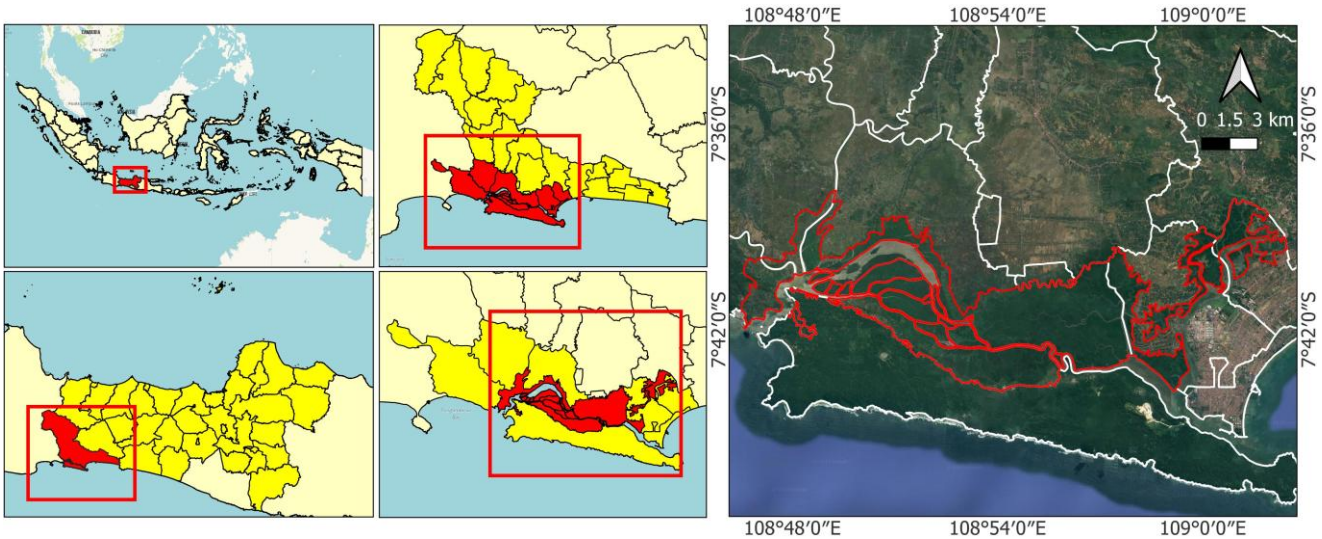

Figure 1. Study area map showing the mangrove region around Segara Anakan Lagoon, Cilacap District, Central Java, Indonesia

Table 1. Geographic coordinates and ecological descriptions of the observed mangrove sub-regions in Segara Anakan Lagoon, Cilacap District, Central Java, Indonesia

Sub-district	Coordinates (Lat, Long)	Key features	Dominant vegetation
Kalipucang	7°38′S, 108°52′E	Fringing mangrove, adjacent to river mouths	*Rhizophora apiculata* Blume
Patimuan	7°40′S, 108°50′E	Mixed mangrove with sediment-rich tidal flats	*Sonneratia alba* Sm.
Kampung Laut	7°43′S, 108°48′E	Dense canopy mangrove, community-managed area	*Avicennia marina* (Forssk.) Vierh.
South Cilacap	7°44′S, 109°00′E	Fragmented mangrove interspersed with settlements	*Bruguiera gymnorhiza* (L.) Lam.
Central Cilacap	7°45′S, 109°02′E	Urban-influenced coastal vegetation	*Avicennia officinalis* L.

Table 2. Summary of Landsat 9 satellite imagery used in the study

Parameter	Description
Satellite / Sensor	Landsat 9 / OLI (Optical), TIRS (Thermal)
Acquisition date	July 2023 (Dry season, minimal cloud cover)
Bands for NDVI	Band 4 (Red), Band 5 (Near Infrared, NIR)
Bands for LST	Band 10 and Band 11 (Thermal Infrared)
Spatial resolution	30 m (Optical and thermal, resampled)
Image pre-processing steps	Radiometric correction, atmospheric correction, and cloud masking
Processing software	QGIS 3.28, ENVI 5.6, Semi-Automatic Classification Plugin

Geographically, the study area lies between latitudes 7°35'-7°50' South and longitudes 108°45'-109°03' East. The region encompasses a complex mosaic of tidal channels, mudflats, and mangrove stands, where the influence of riverine sedimentation and tidal inundation creates favorable conditions for mangrove growth (Hilmi et al. 2022). These environmental gradients contribute to the spatial heterogeneity of canopy structure, vegetation density, and surface temperature observed across the lagoon.

The climate in the study region is tropical monsoonal, with distinct wet and dry seasons. Annual rainfall exceeds 3,000 mm, and the temperature ranges from 25°C to 33°C throughout the year. The mangrove vegetation is dominated by typical Southeast Asian species such as *Rhizophora apiculata*, *Avicennia marina*, and *Sonneratia alba*, which are adapted to saline soils and tidal flooding.

Due to its ecological significance, the Segara Anakan Lagoon has been subject to various conservation, mapping, and monitoring efforts. However, increasing anthropogenic pressure from aquaculture, land reclamation, and sedimentation from upstream rivers has resulted in degradation of some mangrove areas, making it a suitable site for studying vegetation-climate interactions. Figure 1 shows the geographical location and administrative boundaries of the Segara Anakan mangrove region used in this study. Table 1 summarizes the detailed descriptions of the five observed subregions.

Data sources and satellite imagery

This study employed multi-spectral and thermal infrared satellite imagery from the Landsat 9 Operational Land Imager (OLI) and Thermal Infrared Sensor (TIRS) sensors to obtain data on vegetation cover and land surface temperature. Landsat 9 provides free and regularly updated Earth observation data with a spatial resolution of 30 meters for optical bands and 100 meters (resampled to 30 m) for thermal bands, making it suitable for regional-scale environmental analysis (Fadlin et al. 2020).

The imagery used in this study was acquired during the dry season to minimize the influence of cloud cover and seasonal hydrological variability. Dry season imagery ensures clearer spectral readings, especially in mangrove ecosystems where tidal inundation and moisture fluctuations can affect reflectance values. The date of acquisition was selected based on minimal cloud cover (<10%) and data quality checks using pre-processed metadata.

Two sets of spectral data were used for analysis: (i) bands 4 (Red) and 5 (Near-Infrared, NIR) for the calculation of the Normalized Difference Vegetation Index (NDVI), and (ii) bands 10 and 11 (Thermal Infrared) for Land Surface Temperature (LST) estimation. These bands were chosen based on their proven applicability for vegetation and thermal studies in tropical and coastal environments (Kshetri 2018; Malik et al. 2019).

Data pre-processing included radiometric calibration, atmospheric correction, and cloud masking using standardized tools in spatial analysis software. For NDVI calculations, Top-of-Atmosphere (TOA) reflectance values were used, while surface radiance data were extracted from thermal bands for LST computation. All processing steps were conducted using QGIS (version 3.28) and ENVI, complemented by the Semi-Automatic Classification Plugin and raster calculator functions (Table 2).

The spatial extent for image clipping and analysis was defined by the mapped boundary of the Segara Anakan mangrove zone as shown in Figure 1. The zone was digitized from administrative maps and validated using existing shapefiles from the National Mangrove Mapping Project (Hilmi et al. 2022). The final analysis included all terrestrial mangrove areas, excluding open water bodies and urban areas where mangrove vegetation was absent.

NDVI calculation and vegetation density classification

Vegetation density in the Segara Anakan mangrove area was assessed using the Normalized Difference Vegetation Index (NDVI), which is a widely applied spectral index for evaluating vegetation health, canopy cover, and biomass. NDVI is computed from the reflectance values of the Red (R) and Near-Infrared (NIR) bands of satellite imagery, based on the principle that healthy vegetation absorbs red light for photosynthesis and reflects near-infrared light (Kshetri 2018; Malik et al. 2019).

The NDVI value was calculated using the following formula:

$$\text{NDVI} = \frac{(NIR - Red)}{(NIR + Red)}$$

Where:
NIR : Reflectance in near-infrared (Band 5-Landsat 9)
Red : Reflectance in red spectrum (Band 4-Landsat 9)

The resulting NDVI values range from -1 to +1, where higher values (typically >0.6) indicate dense and healthy vegetation, and lower values (<0.2) suggest sparse or degraded cover. Areas with values near zero represent barren land or built-up areas, while negative values indicate water bodies (Latue et al. 2023). For analysis, NDVI values were reclassified into five vegetation density categories based on thresholds modified from previous mangrove classification studies in Indonesia (Hilmi et al. 2022; Mahardianti et al. 2024) (Table 3). The NDVI calculation was performed using raster calculator tools in QGIS and further processed through zonal statistics to determine the total area of each density class. Only vegetated zones within the mangrove polygon boundary were included in this analysis. Open water, exposed mudflats, and anthropogenic structures were masked out during pre-processing to avoid classification errors. The spatial distribution of vegetation density was then visualized through a false-color composite NDVI map, which served as a base for subsequent correlation analysis with land surface temperature (Figure 2).

To address the lack of field-based validation, NDVI classification results were visually compared with high-resolution Google Earth imagery from 2019, focusing on known vegetated and degraded zones within the Segara Anakan Lagoon. This approach provided a basic cross-reference to assess the plausibility of NDVI class boundaries. While this method does not replace quantitative accuracy assessment, it offers a practical means of validating vegetation density interpretation in the absence of comprehensive ground-truth data. The authors acknowledge this as a methodological limitation and recommend future studies incorporate field sampling or very high-resolution imagery for more rigorous classification accuracy assessment.

LST calculation and surface temperature mapping

Land Surface Temperature (LST) was derived from thermal infrared data using the Thermal Infrared Sensor (TIRS) bands of Landsat 9. The thermal bands (Band 10 and Band 11) are sensitive to emitted longwave radiation and are commonly used to estimate surface temperatures, particularly in studies related to vegetation-climate interactions (Fadlin et al. 2020; Mahardianti et al. 2024).

The LST estimation process involved several key steps: (i) conversion of Digital Numbers (DN) to Top-of-Atmosphere (TOA) radiance, (ii) calculation of brightness temperature, (iii) correction for Land Surface Emissivity (LSE), and (iv) transformation to actual surface temperature in degrees Celsius. Emissivity values were estimated based on the Proportion of Vegetation (PV), which was inferred from NDVI values following the method of Malik et al. (2019).

Table 3. NDVI-based classification of vegetation density in Segara Anakan

NDVI range	Vegetation density class	Description
<0.00	Water bodies	Non-vegetated, permanently inundated areas
0.00-0.20	Low density	Degraded mangrove or early regrowth
0.21-0.40	Medium density	Moderately developed canopy
0.41-0.60	High density	Well-established, continuous canopy cover
>0.60	Very high density	Dense mangrove stands with full canopy

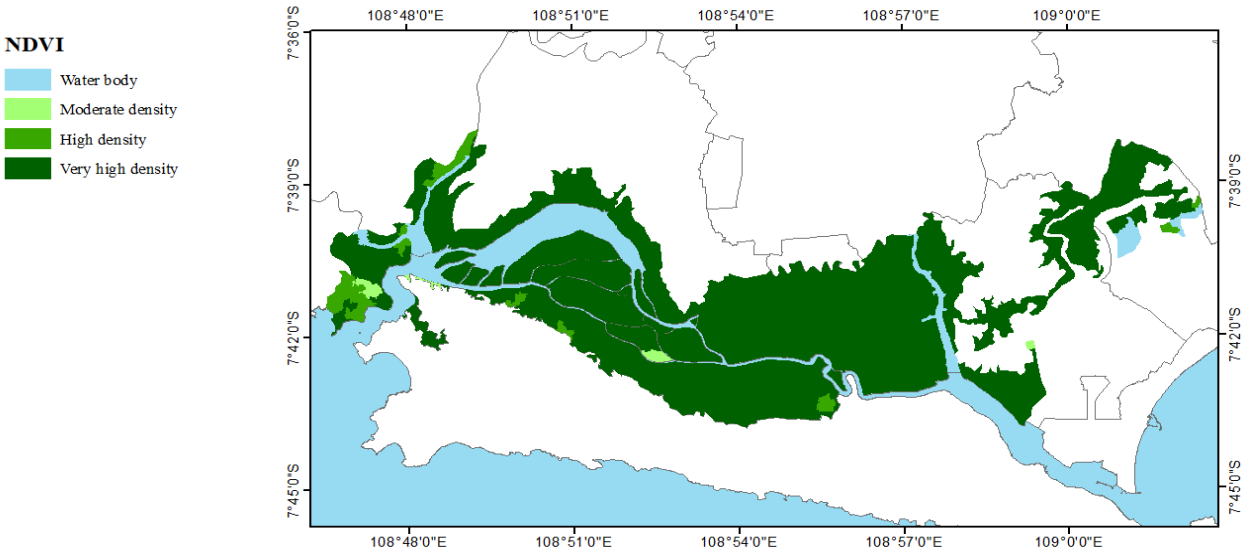

Figure 2. NDVI-based mangrove vegetation density map of Segara Anakan, classified into five density categories

The key formulas used in this process are summarized:
TOA Radiance (Lλ):

$$L_\lambda = M_L \times Q_{cal} + A_L$$

Where:
M_L: Band-specific multiplicative rescaling factor
A_L : Band-specific additive rescaling factor
Q_{cal} : Quantized calibrated pixel values (DN)

Brightness Temperature (BT):

$$BT = \frac{K_2}{\ln\left(\frac{K_1}{L_\lambda} + 1\right)}$$

Where:
K1 and K2 : Band-specific thermal conversion constants

Proportion of Vegetation (PV):

$$PV = \left(\frac{NDVI - NDVI_{min}}{NDVI_{max} - NDVI_{min}}\right)^2$$

Land Surface Emissivity (LSE or ε):

$$\varepsilon = 0.004 \times PV + 0.986$$

LST in Kelvin and conversion to Celsius:

$$LST = \frac{BT}{1 + \left(\frac{\lambda \times BT}{\rho}\right)\ln(\varepsilon)}$$

$$LST(^\circ C) = LST(K) - 273.15$$

Where:
λ= Wavelength of emitted radiance (~11.5 µm)
ρ=h·c/σ ≈ 1.438 × 10^{-2} m·K
h : Planck's constant
c: speed of light
σ: Boltzmann constant

LST values were calculated per pixel and spatially mapped using GIS-based tools. Water bodies and non-vegetated regions were masked using NDVI thresholds to isolate surface temperature data relevant to mangrove vegetated areas.

The final LST raster was classified into six temperature classes to facilitate comparison across vegetation density gradients and to identify potential thermal hotspots or cool zones. Classification thresholds were set based on the natural breaks in the temperature (Table 4).

The LST classification map shown in Figure 3 visualizes the spatial distribution of surface temperature. This map was used to assess correlations with NDVI classes and interpret ecophysiological implications related to thermal stress.

Table 4. Classification scheme for surface temperature in the study area

Temperature range (°C)	Class	Description
13-18	Very low	Shaded areas, high canopy cover
18.1-21	Low	Dense canopy or water-adjacent zones
21.1-23	Moderate-Low	Stable vegetated surfaces
23.1-24	Moderate	Transitional vegetated-open zones
24.1-25	High	Sparse canopy or disturbed vegetated area
>25	Very high	Bare land or mangrove degradation area

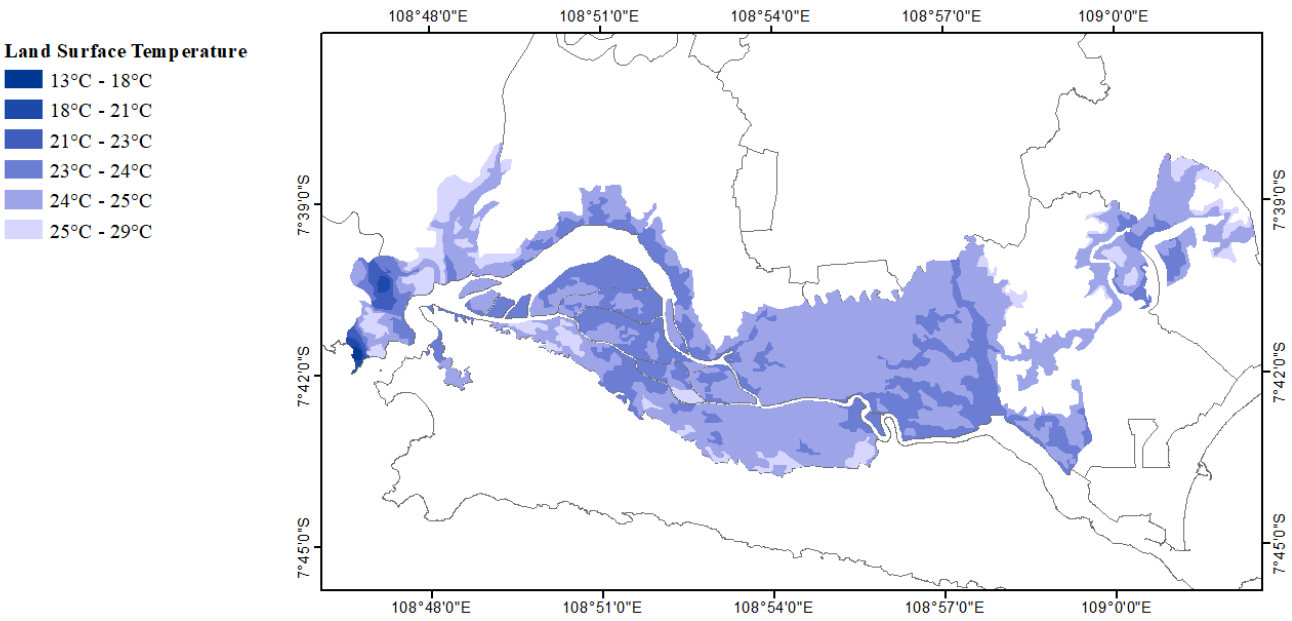

Figure 3. Classified land surface temperature map of Segara Anakan, derived from Landsat 9 thermal bands

Sampling strategy and statistical analysis

To ensure spatially representative and statistically valid results, a stratified random sampling approach based on vegetation density zones derived from the NDVI classification was adopted. This method divides the study area into defined strata—such as water bodies and low, medium, high, and very high vegetation density—and allows for proportionate random sampling within each stratum (Arieska and Herdiani 2018). This strategy enhances analytical robustness by capturing variability across different vegetation conditions in the mangrove ecosystem, significantly enhancing the analytical robustness of the study and providing a comprehensive understanding of the ecosystem.

The number of sampling units (pixels) required from each stratum was determined using the Slovin formula, which is commonly used to calculate sample size when population size is known and a specific margin of error is desired (Madjina et al. 2024):

$$n = \frac{N}{1 + Ne^2}$$

Where:

n : Required sample size

N : Total number of observation units (NDVI pixels)

e : Margin of error (set at 5% in this study)

Using this formula, the total number of pixels to be sampled was computed, then allocated proportionally across strata based on their area coverage (as shown in Table 3). Within each stratum, pixel locations were selected randomly using GIS-based random sampling tools to ensure unbiased representation.

Once sample pixels were selected, NDVI and LST values were extracted for each location and exported for statistical analysis. A linear regression analysis was conducted to test the hypothesis that vegetation density (as indicated by NDVI) has a negative correlation with Land Surface Temperature (LST). This test was chosen due to the continuous and normally distributed nature of both variables and the established theoretical expectation of inverse association (Pramudiyasari et al. 2021; Fitriani et al. 2023).

The statistical model used was:

$$LST = \beta_0 + \beta_1 \cdot NDVI + \varepsilon$$

Where:

LST : Land Surface Temperature (°C)

NDVI : Normalized Difference Vegetation Index

β : Intercept

β1: Regression coefficient

ε: Error term

The coefficient of determination (R^2), p-value, and regression slope were used to evaluate the strength and significance of the relationship. In addition, Pearson's correlation coefficient (r) was calculated to further describe the direction and magnitude of association between NDVI and LST values.

All statistical analyses were conducted using IBM SPSS Statistics and validated using R (version 4.2) for cross-verification. Prior to model fitting, data were tested for normality, linearity, and homoscedasticity to satisfy the assumptions of linear regression. Outliers and anomalies were addressed through residual diagnostics and visual inspection of scatterplots.

Data interpretation and ecophysiological inference

The integration of spatial analysis and statistical modeling in this study aimed not only to quantify the relationship between vegetation density and Land Surface Temperature (LST), but also to provide a physiologically meaningful interpretation of the results. Specifically, NDVI was interpreted as a proxy for canopy vigor, Leaf Area Index (LAI), and photosynthetic potential, while LST served as an indicator of thermal stress in the mangrove ecosystem (Alongi 2018; Fazlioglu et al. 2020).

High NDVI values are commonly associated with dense and healthy mangrove canopies, which exert a cooling influence on surface temperatures through shading and evapotranspiration. These processes reduce incoming solar radiation at the ground level and enhance latent heat flux, both of which contribute to lower LST (Indrawati et al. 2020; Neinavaz et al. 2020). In contrast, areas with low NDVI—typically reflecting sparse vegetation or disturbed zones—exhibit reduced evapotranspiration rates and greater exposure to solar radiation, resulting in elevated LST values.

By statistically correlating NDVI and LST values, it is possible to infer the degree to which canopy structure modulates microclimatic conditions, particularly in terms of thermal buffering. This is especially relevant in tropical lagoon ecosystems like Segara Anakan, where mangroves are exposed to intense solar radiation and fluctuating tidal moisture regimes. A strong negative correlation between NDVI and LST would support the hypothesis that vegetation density plays a vital role in mitigating surface heat.

Beyond physical interpretation, these patterns also carry ecophysiological significance. Lower surface temperatures in densely vegetated mangrove zones may promote optimal conditions for photosynthesis, reduce transpiration-driven water loss, and protect plants from thermal damage (Saintilan et al. 2014; Segaran et al. 2023). Inversely, higher LST values may induce physiological stress, alter stomatal behavior, and increase respiration rates, potentially reducing net primary productivity in vulnerable stands (de Lacerda et al. 2019).

These implications are particularly important in the context of climate change, where high surface and ambient temperatures may push mangrove species beyond their physiological tolerance limits. Therefore, the spatial interaction between NDVI and LST revealed in this study not only reflects surface conditions but also serves as an indirect indicator of plant physiological health and ecosystem stability.

In summary, this methodological framework—linking remote sensing-derived vegetation indices and thermal data—provides a valuable tool for assessing ecophysiological conditions in mangrove landscapes. It can be extended to support long-term monitoring, restoration planning, and vulnerability assessment under scenarios of global warming and anthropogenic disturbance.

RESULTS AND DISCUSSIONS

NDVI-derived mangrove vegetation density

The spatial distribution of mangrove vegetation in Segara Anakan was assessed using the Normalized Difference Vegetation Index (NDVI), which effectively captures canopy density and greenness. NDVI values in the study area ranged from below 0.00 (water bodies) to above 0.60 (very dense vegetation), reflecting varying levels of canopy closure across the lagoon landscape.

Based on the NDVI classification thresholds established in the methodology (Table 3), five distinct vegetation density classes were identified: water bodies, low, medium, high, and very high vegetation density. The reclassified NDVI map revealed that the majority of the mangrove area in Segara Anakan fell into the "Very High Density" category.

Table 5 summarizes the areal coverage of each NDVI class, while Figure 2 visualizes the spatial pattern of mangrove vegetation density. Table 5 shows that approximately 84.1% of the mangrove zone exhibited NDVI values >0.60, while 8.5% fell within the Low Density class (NDVI 0.00-0.20), indicating sparse or regenerating canopy zones. This revision aligns the vegetation classification with the observed extent of thermal stress zones, strengthening the spatial interpretation of canopy-related microclimatic variation.

The map vividly demonstrates the significance of the very high-density vegetation zone forming a contiguous green belt along the inner lagoon and estuarine margins. This belt, particularly concentrated in Kampung Laut and Patimuan sub-districts, plays a crucial role in the health and stability of the mangrove ecosystem. Areas of medium or high density, while more fragmented, also contribute to the overall balance, often occurring near anthropogenic edges or in recently disturbed sites.

The dominance of very high NDVI values across the landscape not only suggests favorable growth conditions but also hints at the potential for high photosynthetic productivity in most parts of the mangrove forest. The spatial presence of medium-density patches, while indicating the existence of transitional or regenerating stands, also presents an opportunity for further growth and regeneration, even in the face of thermal stress or anthropogenic pressure.

Land surface temperature distribution

Land Surface Temperature (LST) across the Segara Anakan mangrove landscape was extracted from Landsat 9 thermal bands and classified into six categories to represent varying degrees of surface heat intensity. The temperature values ranged from 13°C to just under 29°C, with most areas concentrated in the moderate to high temperature range. The LST classification was based on the natural breaks observed in the temperature histogram and is summarized in Table 6. The corresponding LST distribution map is presented in Figure 3.

As shown in Table 6, the largest portion of the area (~61.5%) falls within the 24.1-25°C class, while ~27.7% lies in the 23.1-24°C range. These two classes combined account for nearly 90% of the total study area, indicating a relatively consistent thermal regime across most of the vegetated surface.

The highest temperature zones (>25°C), which represent 998 ha or 9.5% of the area, are spatially concentrated near degraded or edge habitats. Conversely, zones with lower surface temperatures (<23°C) comprise only a minor fraction of the landscape (1.4%), typically corresponding to areas with dense vegetation or persistent shading.

The overall distribution suggests a strong moderation of surface temperature by vegetation cover, but also highlights localized warming in areas with reduced canopy or altered land cover. These thermal gradients provide the basis for further analysis of vegetation-temperature interactions in the subsequent sections.

Spatial overlay of vegetation density and surface temperature

To examine the spatial correspondence between mangrove vegetation density and Land Surface Temperature (LST), an overlay analysis was performed by intersecting the NDVI-based vegetation classification map with the LST classification map. This approach allowed the identification of spatial patterns where canopy density and thermal characteristics co-occur, revealing zones of thermal resilience or vulnerability across the mangrove landscape.

Table 5. Areal distribution of mangrove vegetation density classes in Segara Anakan based on NDVI values (revised)

Vegetation density class	NDVI range	Area (ha)	Proportion of total area (%)
Water bodies	<0.00	384	3.65
Low density	0.00-0.20	894	8.51
Medium density	0.21-0.40	48	0.46
High density	0.41-0.60	348	3.31
Very high density	>0.60	8,836	84.08
Total	—	10,510	100.00

Table 6. Areal distribution of classified surface temperature zones in Segara Anakan

Temperature class	Temperature range (°C)	Area (ha)	Proportion of total area (%)
Very low	13-18	10	0.10
Low	18.1-21	41	0.39
Moderate-Low	21.1-23	96	0.91
Moderate	23.1-24	2,906	27.65
High	24.1-25	6,459	61.45
Very high	>25	998	9.50
Total	—	10,510	100.00

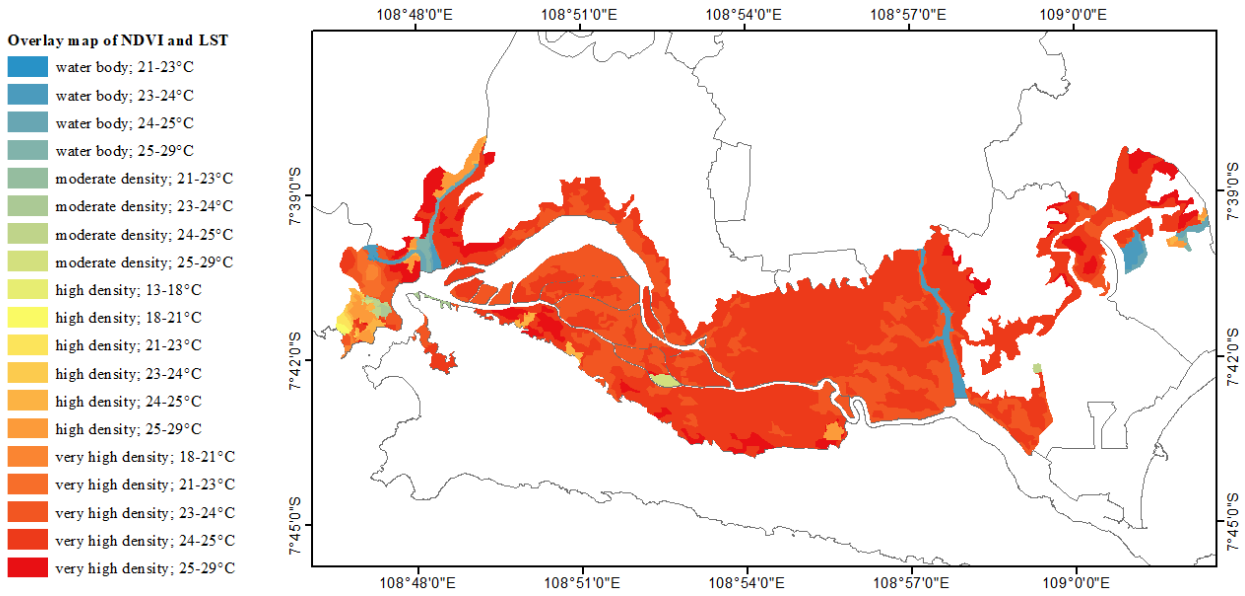

Figure 4. Overlay map of vegetation density (NDVI) and surface temperature (LST) classes in the Segara Anakan mangrove area

Table 7. Overlay table

Overlay	Area (ha)	%
Water body; 21-23°C	2.23	0.02%
Water body; 23-24°C	222.59	2.11%
Water body; 24-25°C	120.24	1.14%
Water body; 25-29°C	42.10	0.40%
Moderate density; 21-23°C	0.10	0.00%
Moderate density; 23-24°C	25.12	0.24%
Moderate density; 24-25°C	25.74	0.24%
Moderate density; 25-29°C	32.79	0.31%
Very high density; 23-24°C	9.06	0.09%
High density; 13-18°C	0.99	0.01%
High density; 18-21°C	11.01	0.10%
High density; 21-23°C	15.74	0.15%
High density; 23-24°C	10.71	0.10%
High density; 24-25°C	105.78	1.00%
High density; 25-29°C	203.65	1.93%
Very high density; 18-21°C	29.96	0.28%
Very high density; 21-23°C	78.11	0.74%
Very high density; 23-24°C	2,647.82	25.10%
Very high density; 24-25°C	6,246.12	59.21%
Very high density; 25-29°C	719.42	6.82%

Figure 4 displays the result of the spatial overlay, highlighting the interaction between vegetation density (five NDVI classes) and surface temperature (six LST classes). The spatial overlay facilitated pixel-wise analysis and visual differentiation of cool-dense zones (e.g., very high NDVI + moderate LST) from hot-sparse zones (e.g., medium NDVI + very high LST). Table 7 summarizes the area coverage of each NDVI-LST class combination. The data show that areas with very high vegetation density (NDVI>0.60) are predominantly associated with moderate (23-24 °C) and high (24-25°C) temperature classes, covering 25.10% and 59.21% of the landscape, respectively. This pattern indicates that dense mangrove canopy helps buffer surface temperature, likely through shading, evapotranspiration, and humidity retention, although the thermal reduction effect may be constrained under intense tropical solar radiation.

In contrast, zones with moderate vegetation density (NDVI 0.21-0.40), though limited in area, tend to align with higher LST categories, including the very high temperature class (>25°C). These transitional areas are commonly found near settlements, along tidal creek margins, or in recently disturbed patches, and appear more susceptible to heat accumulation due to reduced canopy cover.

Water bodies (NDVI<0) consistently register lower LST values (13-21°C), reflecting the high specific heat capacity and evaporative potential of aquatic surfaces. These features act as natural thermal sinks and contribute to local microclimate stabilization.

While the overall pattern confirms a negative spatial correlation between vegetation density and surface temperature, some anomalies were detected. A small proportion of pixels with very high NDVI values coincided with unexpectedly elevated LST (25-29°C), particularly in open or exposed zones. These exceptions may result from local geomorphological variations, surface albedo differences, or anthropogenic disturbances—such as vegetation clearance or infrastructure intrusion—that are not captured by NDVI classification alone.

In summary, the spatial overlay supports the hypothesis that intact mangrove canopy plays a critical role in mitigating surface thermal stress. Areas with continuous vegetation cover demonstrate reduced temperature variability, whereas fragmented or low-density zones exhibit elevated thermal exposure. This spatial insight provides a strong visual and quantitative foundation for the correlation analysis discussed in the subsequent section.

Table 8. Linear regression results: NDVI as predictor of LST

Parameter	Value
Regression coefficient (β_1)	-6.82
Intercept (β_0)	27.44
Coefficient of determination (R^2)	0.68
p-value	< 0.001
Pearson's r	-0.82

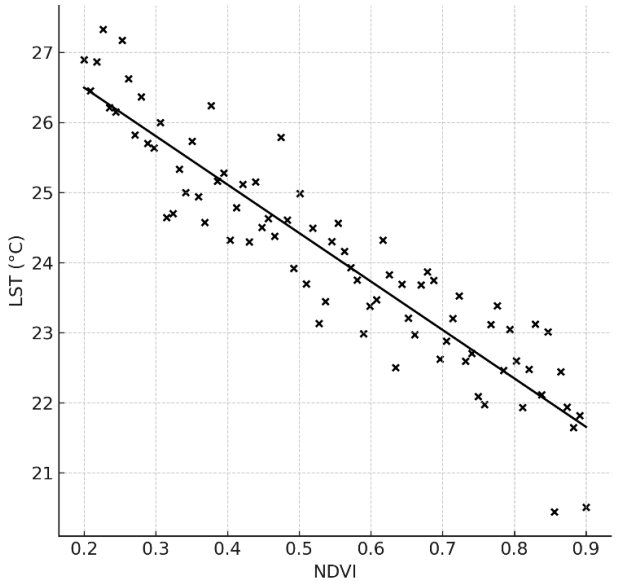

Figure 5. Scatterplot and linear regression line showing the relationship between NDVI and LST in Segara Anakan

Statistical correlation between NDVI and LST

To quantitatively assess the relationship between vegetation density and Land Surface Temperature (LST), a linear regression analysis was conducted using NDVI as the independent variable and LST as the dependent variable. This analysis aimed to validate the spatial trend observed in previous sections, where denser vegetation appears to correlate with lower surface temperatures across the Segara Anakan mangrove ecosystem.

A total of 250 stratified random sample points were extracted from the NDVI-LST overlay map, ensuring balanced representation across vegetation and temperature classes. The scatterplot of NDVI versus LST (Figure 5) shows a strong negative linear trend, indicating that increases in NDVI values are associated with decreases in surface temperature.

The results of the linear regression analysis are presented in Table 8. The model yielded a negative regression coefficient ($\beta_1 = -6.82$), indicating that for every unit increase in NDVI, LST decreases by approximately 6.82°C. The regression model explains 68% of the total variance in surface temperature ($R^2 = 0.68$), and the association is statistically significant ($p<0.001$). Pearson's correlation coefficient further confirms a strong inverse relationship ($r = -0.82$).

These results support the hypothesis that vegetation density, as indicated by NDVI, plays a critical role in modulating surface thermal conditions. Areas with low or medium NDVI tend to accumulate more heat due to reduced shading and evapotranspiration, while densely vegetated mangrove zones act as thermal buffers by lowering surface temperatures and stabilizing microclimates.

The statistical strength and ecological relevance of this relationship emphasize the importance of preserving mangrove canopy cover to reduce localized thermal stress and enhance ecosystem resilience. Further ecological interpretations and conservation implications of these findings are discussed in the next section.

Identification of thermal stress zones

Based on the spatial overlay and regression results, specific zones within the Segara Anakan mangrove landscape were identified as areas of potential thermal stress. These zones are defined by the co-occurrence of low to medium NDVI values (≤0.40) and high to very high land surface temperature (LST≥25°C), indicating insufficient canopy coverage and increased surface heating.

Figure 6 presents the spatial distribution of these zones, delineating thermally vulnerable patches where mangrove vegetation may be exposed to ecophysiological strain. These hotspots correspond spatially with areas classified as Low Density (NDVI 0.00-0.20), reinforcing their role as loci of microclimatic instability and physiological stress.

The overlay analysis identified approximately 927 hectares—or 8.8% of the total mangrove area—as falling within thermal stress zones. These areas are not evenly distributed, with the majority located in South Cilacap and Central Cilacap sub-districts, regions historically subjected to intense anthropogenic pressures such as aquaculture expansion, unregulated shoreline alteration, and resource extraction (Table 9).

To complement the tabular data, Figure 7 provides a visual summary of thermal stress distribution across sub-districts, illustrating both the absolute area and relative proportion of vulnerable mangrove zones.

Table 9. Thermal stress zone extent by sub-district

Sub-district	Thermal stress area (ha)	Percentage of sub-district mangrove area (%)
Kalipucang	42	3.7
Patimuan	65	5.2
Kampung Laut	71	4.6
South Cilacap	356	18.9
Central Cilacap	393	21.4
Total	927	8.8

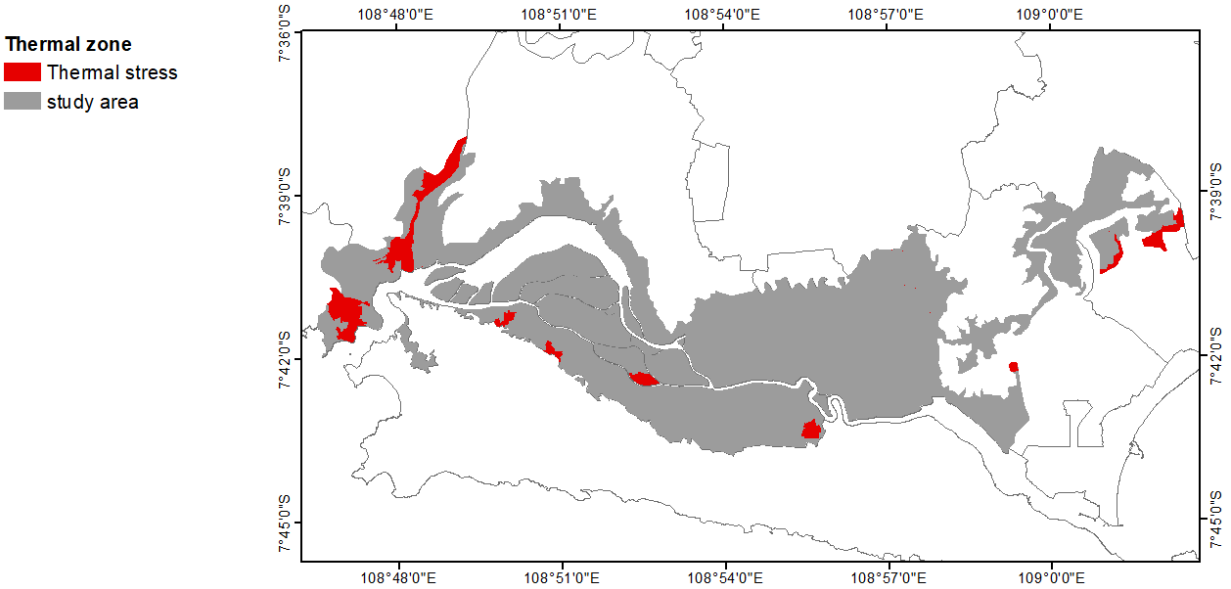

Figure 6. Spatial distribution of potential thermal stress zones in the Segara Anakan mangrove area, based on integrated NDVI-LST thresholds

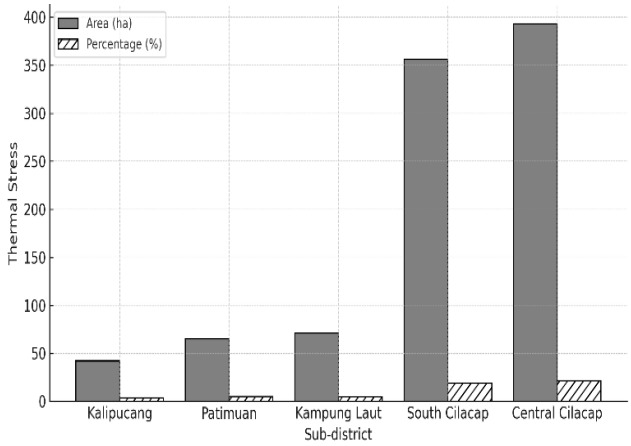

Figure 7. Thermal stress zones in Segara Anakan by sub-district, represented in both absolute area (hectares) and relative percentage of mangrove coverage. Gray bars denote area (ha), while hatched bars indicate percentage (%)

These findings underscore the uneven vulnerability of the Segara Anakan mangrove system. While high canopy density dominates the region, marginal and fragmented stands remain susceptible to thermal stress, particularly during dry seasons or under projected climate change scenarios. These zones are ecophysiologically vulnerable due to increased evapotranspiration demands, reduced stomatal efficiency, and impaired seedling establishment.

Identifying these thermal hotspots is essential for informing spatially targeted mangrove management strategies. Interventions such as canopy gap restoration, enrichment planting, and shoreline rehabilitation in these zones could significantly enhance the thermal resilience and long-term ecological functionality of the mangrove ecosystem.

Discussion

Influence of vegetation density on surface temperature

The results of this study demonstrate a strong and consistent negative correlation between vegetation density, as measured by NDVI, and Land Surface Temperature (LST) across the Segara Anakan mangrove ecosystem. Areas with very high NDVI values (>0.60), which reflect dense mangrove canopy cover, were predominantly associated with moderate surface temperatures (23-25°C), while areas with medium NDVI values exhibited higher LST (>25°C). This inverse relationship is supported by both visual spatial analysis (overlay maps) and quantitative regression results, with Pearson's r = -0.82 and R^2 = 0.68, indicating that vegetation density accounts for a substantial proportion of surface thermal variation.

The underlying mechanism of this relationship lies in the physical properties of dense mangrove canopies, which influence microclimatic conditions through shading and evapotranspiration. Dense canopy structures intercept a significant fraction of incoming solar radiation, thereby reducing the amount of energy that reaches and is absorbed by the soil or surface beneath (Indrawati et al. 2020). This interception function effectively lowers the ground-level radiant energy load and limits heat accumulation, resulting in cooler surface conditions.

In addition to shading, mangrove vegetation contributes to surface cooling via evapotranspiration, a process in which water is transferred from soil and plant tissues to the atmosphere. Through this process, latent heat is consumed, which further decreases the surrounding air and surface temperature (Neinavaz et al. 2020; Fitriani et al. 2023). In regions with high NDVI values, evapotranspiration rates tend to be higher due to greater leaf area and stomatal activity, both of which enhance the cooling capacity of the ecosystem.

This thermoregulatory function of mangrove vegetation has been documented in various coastal and estuarine environments globally. This research has significant practical implications, as it provides a scientific basis for the conservation and restoration of mangrove ecosystems. Forested zones consistently exhibit lower surface temperatures than adjacent deforested or degraded areas (Al Kafy et al. 2021; Guo et al. 2024); a pattern observed in the context of Segara Anakan. This research underscores the pivotal role of vegetation cover in maintaining surface temperature stability in tropical lagoon ecosystems, a finding that can guide real-world conservation efforts.

Interestingly, a few areas with very high NDVI values were also associated with relatively elevated LST levels. These localized anomalies may be attributed to factors such as slope orientation, soil albedo, or anthropogenic disturbance (e.g., recent clearing or infrastructure development), which could override the cooling effects of dense canopy cover. Such deviations highlight the complexity of surface energy dynamics and the need for fine-scale spatial analysis.

The absence of low-density vegetation zones (NDVI<0.2) in this study is notable. It suggests that either such areas are minimal in extent or have transitioned into non-vegetated categories such as exposed soil, settlements, or open water. These surfaces, lacking both canopy and evapotranspiration potential, tend to exhibit elevated LST values due to unmitigated solar absorption.

In summary, the findings confirm that mangrove canopy density exerts a significant biophysical influence on surface thermal dynamics, functioning as a natural buffer against heat accumulation. Preserving and enhancing vegetation density, particularly in edge and transition zones, is thus essential not only for ecological integrity but also for regulating microclimatic stability in tropical coastal environments.

Ecophysiological implications of thermal variation

Beyond its physical effects on microclimate, surface temperature variation has important ecophysiological consequences for mangrove species, particularly in zones exposed to persistent thermal stress. As observed in this study, areas with reduced vegetation density were consistently associated with elevated surface temperatures (>25°C), a threshold that may exceed the physiological tolerance range of several dominant mangrove taxa (Fazlioglu et al. 2020; Segaran et al. 2023).

High temperatures can affect mangrove physiology by altering key processes such as photosynthesis, respiration, and stomatal regulation. Elevated leaf temperatures disrupt enzymatic processes involved in carbon fixation, leading to reduced photosynthetic efficiency. At the same time, thermal stress increases respiration rates, which in turn causes a net carbon loss that compromises plant growth and biomass accumulation (Alongi 2018).

Moreover, higher temperatures increase Vapor Pressure Deficit (VPD), intensifying water loss through transpiration and imposing greater demands on plant water-use efficiency. In mangrove species, particularly those in fringe and degraded zones with limited freshwater availability, this condition may lead to osmotic imbalance, cellular dehydration, and reduced turgor pressure, ultimately lowering survival probability under prolonged heat stress (Field 1995; de Lacerda et al. 2019). Such stress is often compounded by concurrent salinity pressure, further narrowing the physiological buffer range available to these species.

Thermal variation also indirectly affects nutrient cycling and microbial activity in mangrove soils, which are tightly linked to vegetation productivity and resilience. High temperatures can shift microbial community composition, affect litter decomposition rates, and alter nitrogen and phosphorus availability, thereby impacting root function and nutrient uptake (Segaran et al. 2023). Such changes may have cascading effects on seedling establishment, canopy regeneration, and overall forest structure.

In this context, the spatial pattern of thermal stress zones mapped in Segara Anakan may signal early stages of physiological degradation or delayed regeneration, particularly in areas with a history of disturbance or incomplete canopy recovery. The dense canopy areas in Segara Anakan that maintain moderate surface temperatures are likely to provide a more stable physiological environment for mangrove trees, promoting sustained gas exchange, efficient water use, and optimal metabolic function. In contrast, thermally stressed zones—identified in this study as areas with medium NDVI and very high LST—represent ecophysiological risk zones where productivity and long-term viability may be impaired.

Therefore, understanding the thermal landscape of mangrove ecosystems is not merely a climatological concern but a direct proxy for plant health and ecological function. The integration of NDVI and LST provides a non-destructive, scalable approach to assess ecophysiological conditions across large spatial extents, especially in resource-limited or monitoring-deficient mangrove regions. By identifying biophysically stressed zones early, managers can intervene proactively to prevent irreversible degradation and guide strategic restoration planning.

Spatial vulnerability and restoration priorities

The spatial overlay of vegetation density and surface temperature has enabled the identification of thermally vulnerable zones within the Segara Anakan mangrove ecosystem. These zones are characterized by medium NDVI values (0.21-0.40) and elevated LST (>25 °C), suggesting patches of fragmented canopy or incomplete regeneration under disproportionate thermal load. Such areas, though limited in extent (~8.8% of the total study area), represent ecologically significant targets for restoration due to their susceptibility to stress and their capacity to serve as critical thermal buffers if rehabilitated.

Sub-districts such as South Cilacap and Central Cilacap exhibited the highest concentrations of thermal stress zones, likely due to their proximity to urban development, infrastructure, and altered hydrological regimes. These peripheral and transitional areas often experience higher anthropogenic pressure, including logging, aquaculture, and land conversion, which reduce canopy density and

expose the substrate to solar heating (Al Kafy et al. 2021; Rahaman et al. 2023).

Prioritizing these thermally stressed areas for restoration offers dual benefits: improving local microclimate stability and enhancing the physiological resilience of mangrove stands. Reforestation with native, heat-tolerant species such as *Avicennia marina* or *Sonneratia alba* could accelerate canopy closure, increase evapotranspiration capacity, and reduce surface temperatures over time. Such actions would not only restore vegetation structure but also mitigate further degradation driven by climate-induced warming.

Furthermore, spatially explicit restoration planning allows for efficient resource allocation by focusing efforts on the most vulnerable zones rather than uniform interventions across the landscape. This targeted strategy aligns with adaptive ecosystem-based management approaches and supports Indonesia's national agenda for coastal resilience and blue carbon conservation (Hilmi et al. 2022).

Integrating thermal vulnerability mapping into mangrove rehabilitation programs also provides a science-based rationale for monitoring the effectiveness of restoration efforts over time. Changes in NDVI and LST can serve as measurable indicators of ecological recovery and ecosystem service enhancement, particularly in terms of temperature regulation, carbon storage, and habitat stabilization.

Identifying and mapping spatial thermal vulnerability in Segara Anakan thus provides not only a diagnostic tool but also an operational pathway for planning ecologically and physiologically grounded restoration. These thermally exposed areas should be recognized as conservation priorities to prevent further canopy loss and to maintain the functional integrity of coastal vegetation under increasing climate pressures.

Integrating remote sensing for ecophysiological monitoring

Remote sensing has emerged as a valuable tool in assessing vegetation health and environmental stress, particularly in complex and inaccessible ecosystems such as mangrove forests. In this study, the integration of NDVI and LST metrics derived from Landsat 9 imagery enabled a spatially explicit, landscape-level assessment of vegetation structure and surface thermal dynamics in Segara Anakan. This approach provides an indirect but powerful means of inferring ecophysiological conditions without destructive sampling or intensive ground measurements.

NDVI serves as a reliable proxy for canopy greenness, biomass, and photosynthetic activity, while LST reflects the surface energy balance influenced by vegetation cover, moisture, and solar radiation. The strong inverse relationship between these two indices, confirmed through regression analysis, validates their combined use in identifying areas of physiological stress and microclimatic regulation (Malik et al. 2019; Pramudiyasari et al. 2021). This relationship is particularly valuable in tropical estuarine systems where direct physiological measurements are logistically challenging.

The spatial resolution and repeatability of satellite data make it well-suited for long-term monitoring, allowing researchers and managers to detect changes in canopy condition and thermal exposure over time. For example, declines in NDVI coupled with rising LST may signal degradation, canopy loss, or reduced evapotranspiration—conditions that warrant ecological intervention. Conversely, increasing NDVI and cooling trends may indicate successful restoration or natural regeneration. This capacity to detect directional trends enables remote sensing to function as an early-warning system for ecosystem stress.

Despite its strengths, remote sensing also presents limitations in ecophysiological interpretation. While NDVI and LST provide valuable surrogates, they do not directly measure physiological parameters such as chlorophyll fluorescence, stomatal conductance, or sap flow. Thus, field validation and integration with ground-based measurements remain essential, especially for species-specific assessments or detecting early sublethal stress. A hybrid monitoring approach that combines satellite-derived indices with in situ ecological data would enhance diagnostic precision.

Moreover, satellite data may be affected by atmospheric interference, cloud cover, and sensor calibration differences, which require careful pre-processing and quality control. In coastal environments, the presence of mixed pixels (e.g., water-land interface) may also reduce classification accuracy and necessitate masking techniques or higher-resolution imagery. The dynamic tidal regime in estuarine zones further complicates classification and calls for temporal filtering or multi-date compositing.

Nonetheless, the synergy between NDVI and LST represents a practical and scalable framework for ecophysiological monitoring in mangrove systems. By capturing vegetation-temperature interactions, this method contributes to a better understanding of forest health dynamics, supports restoration planning, and informs adaptive management in the face of climate variability. As climate impacts intensify, such integrative remote sensing approaches will be indispensable in guiding evidence-based interventions for coastal ecosystem resilience.

Broader implications under climate change

The findings of this study offer important insights into the role of mangrove canopy structure in mitigating thermal stress, which is directly relevant to broader climate change dynamics in tropical coastal ecosystems. As global temperatures continue to rise and sea levels increase, mangrove forests face heightened exposure to thermal extremes, salinity fluctuations, and hydrological instability (Saintilan et al. 2014; de Lacerda et al. 2019).

Surface warming threatens the physiological performance of mangrove species and undermines their capacity to deliver key services such as carbon sequestration, shoreline protection, and fisheries support. Elevated LST can impair photosynthetic function, increase respiration rates, and reduce the net primary productivity of mangrove stands, thereby weakening their ability to act as carbon sinks and climate buffers (Alongi 2018; Fazlioglu et al. 2020). Such disruptions not only affect individual tree health but can scale up to compromise ecosystem service delivery.

Moreover, increased thermal exposure may exacerbate the vulnerability of mangroves to other climate-related stressors, including more frequent droughts, intensified

storms, and saltwater intrusion. These compound threats can lead to shifts in species composition, migration of physiological limits, and in some cases, collapse of fringe mangrove belts—especially in areas where anthropogenic disturbance has already fragmented canopy cover (Field 1995; Li et al. 2015). The interaction between climate forcing and local degradation accelerates ecological decline, often beyond natural recovery thresholds.

The identification of thermally vulnerable zones in Segara Anakan highlights the importance of spatially targeted adaptation strategies. Maintaining dense vegetation cover in key buffer zones may offer a low-cost, ecosystem-based solution to limit microclimatic instability and support resilience under future warming scenarios. Restoration programs that prioritize degraded hotspots, as revealed through NDVI-LST analysis, can enhance thermal regulation and promote landscape-scale ecosystem stability. This highlights the operational utility of spatial diagnostics in directing resource-efficient adaptation measures.

In a policy context, integrating remote sensing indicators like NDVI and LST into climate vulnerability assessments can strengthen early warning systems and inform national strategies such as Indonesia's National Adaptation Plan (NAP) or REDD+ initiatives. Furthermore, these findings align with global conservation frameworks such as the UN Decade on Ecosystem Restoration, which emphasizes the importance of nature-based solutions to climate resilience. Such alignment reinforces the relevance of local-scale evidence to international climate agendas.

The spatial coupling of vegetation density and surface temperature thus functions not only as an ecological diagnostic tool but also as a foundation for implementing adaptive, climate-informed mangrove management. By understanding how canopy structure modulates thermal stress, stakeholders can implement more responsive and science-based actions to sustain coastal forest health in a warming world.

In conclusion, this study demonstrates that mangrove canopy density exerts a critical influence on surface temperature regulation within the Segara Anakan estuarine ecosystem. A strong inverse relationship between NDVI and LST—where high NDVI values correspond with cooler surface temperatures—highlights the thermoregulatory function of dense vegetation. Areas with low to medium NDVI values (≤0.40) exhibited disproportionately high LST (>25 °C), with the majority of thermally stressed zones corresponding to the Low Density class. This reinforces the need to monitor and restore sparse canopy areas as part of climate-sensitive mangrove management. The spatial overlay of NDVI and LST enabled the identification of ecophysiologically vulnerable hotspots, primarily concentrated in South and Central Cilacap sub-districts. These findings support the strategic use of satellite-derived indicators for targeting mangrove restoration and adaptive management. NDVI-LST integration offers a scalable and non-destructive tool to monitor degradation risks and climate sensitivity, reinforcing the importance of preserving canopy continuity. Strengthening mangrove cover is vital not only for biodiversity and carbon sequestration, but also for mitigating surface heat extremes and sustaining ecosystem services in the face of climate change.

ACKNOWLEDGEMENTS

We would like to thank all colleagues and local stakeholders who supported field access, satellite data processing, and spatial analysis for this research. We are also grateful to anonymous reviewers for their constructive feedback.

REFERENCES

Al Kafy A, Al Rakib A, Akter KS, Rahaman ZA, Al Faisal A, Mallik S, Nasher NMR, Hossain MI, Ali MY. 2021. Monitoring the effects of vegetation cover losses on land surface temperature dynamics using geospatial approach in Rajshahi City, Bangladesh. Environ Chall 4: 100187. DOI: 10.1016/j.envc.2021.100187.

Alongi DM. 2018. Impact of global change on nutrient dynamics in mangrove forests. Forests 9 (10): 596. DOI: 10.3390/f9100596.

Ardelia V, Fahleny R. 2023. Kebiasaan makan ikan kiper (*Scatophagus argus*) di Segara Anakan Cilacap. Jurnal Perikanan Perairan Umum 1 (2): 105-111. [Indonesian]

Arieska PK, Herdiani N. 2018. Pemilihan teknik sampling berdasarkan perhitungan efisiensi relatif. Jurnal Statistika 6 (2): 166-171. DOI: 10.26714/jsunimus.6.2.2018.%25p. [Indonesian]

de Lacerda LD, Borges R, Ferreira AC. 2019. Neotropical mangroves: Conservation and sustainable use in a scenario of global climate change. Aquat Conserv: Mar Freshw Ecosyst 29 (8): 1347-1364. DOI: 10.1002/aqc.3119.

Fadlin F, Kurniadin N, Prasetya AS. 2020. Analisis indeks kekritisan lingkungan di Kota Makassar menggunakan citra satelit Landsat 8 OLI/TIRS. Elipsoida 3: 55-63. DOI: 10.14710/elipsoida.2020.6232. [Indonesian]

Fazlioglu F, Wan JSH, Chen L. 2020. Latitudinal shifts in mangrove species worldwide: Evidence from historical occurrence records. Hydrobiologia 847: 4111-4123. DOI: 10.1007/s10750-020-04403-x.

Field CD. 1995. Impact of expected climate change on mangroves. Hydrobiologia 295: 75-81. DOI: 10.1007/BF00029113.

Fitriani V, La Gandri, Indriyani L, Bana S, De Ahmaliun L. 2023. Analisis hubungan Land Surface Temperature (LST) dan Indeks Kerapatan Vegetasi (NDVI) DAS Wanggu, Sulawesi Tenggara. Jurnal Ilmu-Ilmu Kehutanan 7: 49-57. DOI: 10.31258/jiik.7.1.49-57. [Indonesian]

Guo H, Zhu W, Xiao C, Zhao C, Chen L. 2024. High-precision estimation of pan-Arctic soil surface temperature from MODIS LST by incorporating multiple environmental factors and monthly-based modeling. Intl J Appl Earth Obs Geoinf 133: 104114. DOI: 10.1016/j.jag.2024.104114.

Hilmi E, Sari LK, Mahdiana A, Junaidi T, Muslih M, Samudra SR, Prayogo NA, Baedowi M, Cahyo TN, Putra RRD, Sari FA. 2022. Mapping of mangrove ecosystem in Segara Anakan Lagoon using normalized different vegetation index and dominant vegetation index. Omni-Akuatika 18 (2): 165-178. DOI: 10.20884/1.oa.2022.18.2.926.

Huang Q, Zhang Y, Li C, Ma N. 2024. Quantifying propagation effects of climate and vegetation changes on evapotranspiration and streamflow signatures in Yarlung Tsangpo River Basin. J Hydrol Reg Stud 56: 102015. DOI: 10.1016/j.ejrh.2024.102015.

Indrawati DM, Suharyadi S, Widayani P. 2020. Analisis pengaruh kerapatan vegetasi terhadap suhu permukaan dan keterkaitannya dengan fenomena UHI. Media Komunikasi Geografi 21 (1): 99-109. DOI: 10.23887/mkg.v21i1.24429. [Indonesian]

Kshetri TB. 2018. NDVI, NDBI & NDWI calculation using Landsat 7, 8. GeoWorld 2: 32-34.

Latue PC, Rakuasa H, Sihasale DA. 2023. Analisis kerapatan vegetasi Kota Ambon menggunakan data citra satelit Sentinel-2 dengan metode MSARVI berbasis machine learning pada Google Earth Engine. Sudo Jurnal Teknik Informatika 2: 68-77. DOI: 10.56211/sudo.v2i2.270. [Indonesian]

Latue PC, Rakuasa H, Somae G, Muin A. 2023. Analisis perubahan suhu permukaan daratan di Kabupaten Seram bagian barat menggunakan

platform berbasis Cloud Google Earth Engine. Sudo Jurnal Teknik Informatika 2 (2): 45-51. DOI: 10.56211/sudo.v2i2.261. [Indonesian]

Li S, Meng X, Ge Z, Zhang L. 2015. Vulnerability assessment of the coastal mangrove ecosystems in Guangxi, China, to sea-level rise. Reg Environ Change 15: 265-275. DOI: 10.1007/s10113-014-0639-3.

Madjina NI, Pratiko B, Tripena A. 2024. Penentuan ukuran sampel menggunakan rumus Bernoulli dan Slovin: Konsep dan aplikasinya. Jurnal Ilmiah Matematika dan Pendidikan Matematika 16 (1): 73-84. DOI: 10.20884/1.jmp.2024.16.1.11230. [Indonesian]

Mahardianti MA, Prabawa SE, Effendi AF. 2024. Studi perubahan indeks kerapatan vegetasi terhadap suhu permukaan tanah dan indeks kualitas udara dengan pemanfaatan citra satelit Landsat 8 di Kabupaten Gresik. Geoid 19 (3): 386-404. [Indonesian]

Malik MS, Shukla JP, Mishra S. 2019. Relationship of LST, NDBI and NDVI using Landsat-8 data in Kandaihimmat watershed, Hoshangabad, India. Indian J Geo-Marine Sci 48 (1): 25-31.

Neinavaz E, Skidmore AK, Darvishzadeh R. 2020. Effects of prediction accuracy of the proportion of vegetation cover on land surface emissivity and temperature using the NDVI threshold method. Intl J Appl Earth Obs Geoinf 85: 101984. DOI: 10.1016/j.jag.2019.101984.

Pramudiyasari T, Tambunan MP, Tambunan RP, Manessa MDM. 2021. Analisis LST, NDVI menggunakan satelit Landsat 8 serta trend suhu udara di Kabupaten Majalengka. Jurnal Geosaintek 7 (3): 119-124. DOI: 10.12962/j25023659.v7i3.9043. [Indonesian]

Rahaman SN, Ahmed SMM, Zeyad M, Zim AH. 2023. Effect of vegetation and land surface temperature on NO_2 concentration: A Google Earth Engine-based remote sensing approach. Urban Clim 47: 101336. DOI: 10.1016/j.uclim.2022.101336.

Saintilan N, Wilson NC, Rogers K, Rajkaran A, Krauss KW. 2014. Mangrove expansion and salt marsh decline at mangrove poleward limits. Glob Change Biol 20 (1): 147-157. DOI: 10.1111/gcb.12341.

Segaran TC, Azra MN, Lananan F, Burlakovs J, Vincevica-Gaile Z, Rudovica V, Grinfelde I, Abd Rahim NH, Satyanarayana B. 2023. Mapping the link between climate change and mangrove forest: A global overview of the literature. Forests 14 (2): 421. DOI: 10.3390/f14020421.

Sipayung RH, Poedjirahajoe E. 2021. Pengaruh karakteristik habitat mangrove terhadap kepadatan kepiting (*Scylla serrata*) di pantai utara Kabupaten Demak, Jawa Tengah. Jurnal Tambora 5 (2): 21-30. DOI: 10.36761/jt.v5i2.1113. [Indonesian]

CELL BIOLOGY & DEVELOPMENT
Volume 9, Number 1, June 2025 E-ISSN: 2580-4499
Pages: 26-36 DOI: 10.13057/cellbioldev/v090103

Enhancing growth and flavonoid content of *Eleutherine palmifolia* using chitosan and NPK fertilizer under greenhouse conditions

FAIZA AULIA ROCHMA, WIDYA MUDYANTINI♥, SOLICHATUN
Department of Biology, Faculty of Mathematics and Natural Sciences, Universitas Sebelas Maret. Jl. Ir. Sutami 36A Surakarta 57 126, Central Java, Indonesia. Tel.: +62-271-669376, ♥email: widyamudyantini@yahoo.com

Manuscript received: 26 July 2024. Revision accepted: 26 April 2025.

Abstract. *Rochma FA, Mudyantini W, Solichatun. 2025. Enhancing growth and flavonoid content of* Eleutherine palmifolia *using chitosan and NPK fertilizer under greenhouse conditions. Cell Biol Dev 9: 26-36.* This study evaluated the effects of chitosan and NPK fertilizer on the growth performance, physiological traits, and flavonoid content of *Eleutherine palmifolia*, a medicinal plant widely used in Indonesia. A factorial experiment was conducted under greenhouse conditions using three chitosan concentrations (0, 0.3%, and 0.6%) and three levels of NPK fertilizer (0, 100, and 200 kg/ha). The combination of 0.6% chitosan and 200 kg/ha NPK significantly enhanced leaf number, leaf size, shoot biomass, chlorophyll and carotenoid contents, as well as flavonoid concentration in the tubers. While flowering occurred in selected treatments, overall reproductive development remained limited during the 11-week cultivation period. Notably, the highest total flavonoid content in tuber extracts (6.30 mg QE/g) was recorded under the same treatment, highlighting the potential role of chitosan as a biostimulant and elicitor of secondary metabolites. Although some parameters showed non-significant interaction effects, consistent positive trends support the hypothesis that chitosan improves nutrient uptake and physiological vigor, particularly when combined with adequate macronutrients. This study emphasizes the potential of integrating biostimulant and fertilizer treatments to enhance both agronomic performance and phytochemical accumulation in *E. palmifolia*. These findings provide a foundation for sustainable cultivation practices aimed at increasing the functional quality of this underutilized medicinal plant for future pharmaceutical or nutraceutical applications.

Keywords: Biostimulant, chitosan, *Eleutherine palmifolia*, flavonoids, NPK fertilizer

INTRODUCTION

Eleutherine palmifolia (L.) Merr., commonly known as Dayak onion, is a traditional medicinal plant in the Iridaceae family, extensively utilized by the Dayak ethnic group in Kalimantan, Indonesia. This species is widely applied in folk medicine for treating various ailments, including cardiovascular diseases, tumors, and inflammatory conditions (Kuntorini and Nugroho 2010; Paramita and Nuryanto 2018). Its pharmacological value is attributed to a diverse phytochemical profile, comprising flavonoids, alkaloids, saponins, tannins, and other secondary metabolites (Tamal and Aryanto 2020). Notably, its tubers and leaves exhibit high flavonoid levels, with values reported up to 116.56 mg QE/g extract (Yuswi 2017), which contribute to antioxidant, anti-inflammatory, antihypertensive, and antimicrobia effects (Ferreyra et al. 2012; Ibrahim 2012; Prayitno and Murtini 2018).

Despite this therapeutic potential and rising public interest, large-scale cultivation of *E. palmifolia* remains underdeveloped in Indonesia. The mismatch between demand and supply is mainly due to the absence of standardized cultivation protocols that optimize both biomass production and the accumulation of bioactive compounds (Sari et al. 2020; Atikah et al. 2021). Hence, targeted agronomic interventions are urgently needed to enhance both yield and quality. One promising strategy is the application of biostimulants, such as chitosan, in conjunction with essential macronutrient fertilizers like NPK.

Biostimulants are non-nutritional substances that promote plant growth, improve physiological responses, and enhance stress tolerance. Among them, chitosan, a biopolymer derived from the deacetylation of chitin has garnered significant attention due to its multifunctional properties. It can enhance nutrient uptake, induce systemic resistance, and stimulate secondary metabolite production (Saharan and Pal 2016; Lalla 2022). Chitosan has also been shown to promote the biosynthesis of endogenous hormones such as auxins and gibberellins, which are crucial for vegetative growth and metabolic coordination (Moza et al. 2017; Ingle et al. 2022). Furthermore, it acts as a metabolic elicitor by activating defense-related pathways and increasing flavonoid and phenolic compound accumulation (Chadchawan et al. 2015; Singh and Singla 2020). Supporting this, Suci (2020) demonstrated increased flavonoid synthesis in *Schleichera oleosa* callus cultures, while Nuraini et al. (2017) reported higher tuber weights in potatoes following chitosan treatment at 0.3-0.6%.

In parallel, macronutrient fertilization is a cornerstone of plant productivity. NPK fertilizers, which supply nitrogen (N), phosphorus (P), and potassium (K), are essential for protein synthesis, energy metabolism, and osmotic regulation, respectively (Manurund and Zahrah 2018; Mutua et al. 2021). Beyond vegetative growth, these nutrients also modulate key secondary metabolic pathways. Specifically,

phosphorus and potassium have been linked to enhanced flavonoid and carotenoid biosynthesis (Fanciullino et al. 2014; Cocozza et al. 2020). In *E. palmifolia*, Rosmawaty et al. (2019) reported improved tuber yield and flavonoid concentration following NPK application, while Sumarni et al. (2012) found similar effects in *Allium ascalonicum*, a crop with comparable morphology and organ use.

The interaction between chitosan and NPK has recently emerged as an important area of research in plant physiology. Chitosan is known to facilitate nutrient assimilation by reducing leaching, enhancing root absorption, and serving as a slow-release carrier when formulated in nano-size particles (Duhan et al. 2017; Perez-de-Luque 2017). Studies on crops like cucumber and wheat have shown that chitosan-NPK combinations improve nutrient use efficiency, biomass production, and metabolic output (Abdel-Aziz et al. 2016; Modi et al. 2021). These findings suggest that an integrated chitosan-NPK strategy may be highly beneficial for medicinal plants, including *E. palmifolia*.

However, research on the agronomic responses of *E. palmifolia* to chitosan and NPK particularly in combination —remains limited. Although the phytochemistry and medicinal benefits of the plant are well documented, there is a lack of experimental data evaluating cultivation strategies that simultaneously enhance both vegetative traits and secondary metabolite accumulation.

This study was therefore conducted to investigate the separate and combined effects of chitosan and NPK fertilizer on the growth performance and flavonoid content of *E. palmifolia*. The central hypothesis is that both treatments will enhance vegetative growth and secondary metabolism, and that their interaction will yield synergistic effects. The outcomes of this research are expected to contribute to the development of sustainable and efficient cultivation practices for this underutilized yet valuable medicinal crop.

MATERIALS AND METHODS

Study site and duration

The experiment was conducted at the Integrated Greenhouse Facility of Universitas Sebelas Maret, Surakarta, Central Java, Indonesia (7°33′20″S, 110°50′30″E; ~95 m above sea level). The greenhouse provides a semi-controlled environment with partial exposure to natural sunlight, suitable for experimental cultivation of medicinal plants under tropical monsoon conditions. The site experiences an average daily temperature of 27-32°C and relative humidity ranging from 60% to 85%.

The study was carried out over an 11-week period, from May to July 2023, covering the vegetative and early generative stages of *E. palmifolia*. Daily maintenance activities, including irrigation, random repositioning of plant bags, and basic environmental monitoring, were consistently implemented.

Treatment applications including chitosan and NPK fertilizer were administered during the early vegetative phase, specifically at 2 and 6 weeks after planting (WAP), as described in Section 2.4. Harvest and final observations were conducted at the end of the 11th week.

Plant material and growth medium

Uniform tubers of *E. palmifolia* were used as planting material in this experiment. The tubers were sourced from Pasir Besar Village, South Pontianak District, West Kalimantan, Indonesia. To minimize initial growth variation, only healthy, disease-free tubers of uniform physiological age and weighing between 7 and 12 g were selected.

The planting medium consisted of a homogeneous mixture of topsoil, manure, and rice husk in a 2:1:1 (v/v/v) ratio. This substrate was selected to provide adequate drainage, sufficient organic matter, and balanced nutrient availability. The mixture was thoroughly blended and packed into polyethylene planting bags (25 × 25 cm), each containing approximately 3.5 kg of growing media.

Prior to transplanting, the field capacity of the planting medium was determined using the gravimetric method described by Patoni (2000). The calculation was based on the difference in weight before and after full saturation:

$$\text{Field Capacity} = (W_{\text{wet}} - W_{\text{dry}})$$

Where:

Wwet : the weight of the polybag at saturation

Wdry : the weight before watering.

All tubers were directly transplanted into polybags and arranged randomly within the greenhouse. Plants were irrigated every two days using a volume of water adjusted to maintain field capacity. To reduce microclimatic variability, the position of each polybag was rotated weekly throughout the 11-week cultivation period.

Chitosan and NPK fertilizer preparation

Chitosan used in this study was obtained from E. Merck (Germany) with a degree of deacetylation of 95%. Two concentrations were prepared: 0.3% and 0.6% (w/v), by dissolving 0.3 g or 0.6 g of chitosan powder in 100 mL of 1% (v/v) acetic acid. The mixtures were stirred continuously at room temperature until fully dissolved, yielding homogeneous solutions. Prepared chitosan solutions were stored at room temperature and used within 24 hours to preserve their physicochemical stability and bioactivity.

NPK compound fertilizer with a nutrient composition of 16:16:16 (N:P:K) was commercially obtained under the brand name *Mutiara*. Fertilizer application rates were based on field-equivalent doses of 0 kg/ha (control), 100 kg/ha, and 200 kg/ha, which were converted to 0.104 g and 0.208 g per polybag, respectively. The appropriate amount of fertilizer was dissolved in distilled water immediately before application.

For combined treatments, chitosan and NPK solutions were mixed just before use to ensure physical compatibility and uniform delivery. All treatments including chitosan-only, NPK-only, and chitosan + NPK combinations—were applied twice during the vegetative stage, at 2 and 6 weeks after planting (WAP). Each plant received 100 mL of the respective solution per application, applied directly to the soil surface near the root zone to optimize nutrient and elicitor uptake. Control plants were treated with 100 mL of distilled water on the same schedule.

Experimental design and treatment application

The experiment was conducted using a Completely Randomized Design (CRD) with a factorial arrangement involving two factors: chitosan concentration and NPK fertilizer dose. Each factor consisted of three levels chitosan at 0% (control), 0.3%, and 0.6%; and NPK fertilizer at 0, 100, and 200 kg/ha (equivalent to 0, 0.104, and 0.208 g per polybag, respectively). The combination of these factors resulted in nine treatment groups, each replicated five times, yielding a total of 45 experimental units.

Uniform tubers of *E. palmifolia* were transplanted into polybags containing the pre-prepared soil medium. The polybags were arranged randomly in the greenhouse and re-randomized weekly to reduce the effect of microclimatic heterogeneity.

Treatment solutions were applied via root-zone drenching using 100 mL per plant. Applications were conducted twice, at 2 and 6 weeks after planting (WAP), during the vegetative growth phase. For combined treatments, chitosan and NPK solutions were mixed immediately prior to application to ensure homogeneity. Control plants received the same volume (100 mL) of distilled water on the same schedule.

Irrigation was provided every two days, with water volumes adjusted to maintain substrate moisture near field capacity. All other cultivation practices, including weeding and environmental maintenance, were applied uniformly across treatments. At harvest (week 11), data collection was performed on morphological, physiological, and biochemical parameters, as detailed in subsequent sections.

Growth and morphological measurements

The growth performance of *E. palmifolia* was evaluated using a set of morphological parameters measured at the end of the 11-week cultivation period. The assessed variables included number of leaves, leaf length, leaf width, and number of flowers per plant, serving as indicators of vegetative vigor and transition toward the generative phase. Leaf and flower counts were recorded manually, while leaf length and width were measured using a ruler, focusing on the longest and widest fully expanded leaves on each plant.

To complement aboveground measurements, fresh and dry biomass of both leaves and tubers were also recorded. Fresh weights were determined immediately after harvest using a calibrated analytical balance. For dry weight measurement, samples were oven-dried at 50°C for 72 hours or until constant weight was achieved. The difference between fresh and dry weights was used to calculate relative water content and to evaluate biomass allocation between shoot and root organs.

All measurements were conducted on individual plants within each replicate, and mean values were calculated per treatment group. These morphological assessments provided a comprehensive understanding of vegetative growth, early flowering tendencies, and biomass accumulation of *E. palmifolia* under different combinations of chitosan and NPK fertilizer treatments.

Chlorophyll and carotenoid analysis

Leaf pigment analysis was performed to quantify total chlorophyll and carotenoid contents in *E. palmifolia*. Chlorophyll extraction followed the acetone-based spectrophotometric method described by Hendry and Grime (1993). A total of 0.1 g of fresh leaf tissue was homogenized in 10 mL of 80% acetone using a mortar and pestle. The resulting homogenate was filtered through Whatman No. 42 filter paper, and the filtrate was collected in clean test tubes for analysis.

Spectrophotometric absorbance was measured at 645 nm, 663 nm, and 480 nm using a UV-Vis spectrophotometer (Perkin Elmer Lambda 25 series). An 80% acetone solution was used as the blank. Chlorophyll a, chlorophyll b, and total chlorophyll contents (expressed in mg/g fresh weight) were calculated using standard equations:

$$\text{Chlorophyll a} = [12.7 \times A_{663} - 2.69 \times A_{645}] \times \frac{V}{1000 \times W}$$

$$\text{Chlorophyll b} = [22.9 \times A_{645} - 4.68 \times A_{663}] \times \frac{V}{1000 \times W}$$

$$\text{Total chlorophyll} = [8.02 \times A_{663} + 20.2 \times A_{645}] \times \frac{V}{1000 \times W}$$

$$\text{Carotenoids } (\mu\text{mol/g}) = \frac{(A_{480} + A_{645} - A_{663}) \times V}{1000 \times W}$$

Where:

A_λ : absorbance at wavelength λ

V : volume of extract (mL)

W : fresh weight of sample (g)

These analyses provided quantitative estimates of photosynthetic pigment concentrations, offering insights into the physiological status of plants in response to different chitosan and NPK fertilizer treatments.

Flavonoid content determination

Total flavonoid content in tubers of *E. palmifolia* was quantified using a colorimetric method based on aluminum chloride ($AlCl_3$) complexation, following the protocol of Stankovic (2011). Approximately 1.0 g of oven-dried tuber powder was extracted by maceration in 10 mL of 96% ethanol (p.a. grade) for 24 hours at room temperature. The resulting extract was filtered through Whatman No. 42 filter paper, and the residue was subjected to a second maceration with another 10 mL of ethanol for 2 hours, until the filtrate became colorless. Both filtrates were pooled and evaporated at room temperature to yield the crude ethanol extract.

For analysis, a 1 mL aliquot of the extract was mixed with 1 mL of 2% (w/v) $AlCl_3$ and 1 mL of 120 mM potassium acetate. The mixture was incubated at room temperature for 60 minutes, after which the absorbance was measured at 435 nm using a UV-Vis spectrophotometer. Flavonoid concentration was determined from a quercetin standard calibration curve prepared at 6, 8, 10, 12, and 14 ppm, with all standards undergoing the same treatment as the sample.

The total flavonoid content was expressed as milligrams of quercetin equivalent per gram of dry tuber (mg QE/g), using the following formula:

$$\text{Flavonoid content} = \frac{C \times V \times fp}{m}$$

Where:

C : concentration of quercetin (mg/mL) based on absorbance

V : total volume of extract (mL)

fp : dilution factor

m : dry weight of the sample (g)

This method enabled reliable estimation of flavonoid accumulation as influenced by the chitosan and NPK fertilizer treatments.

Data analysis

All quantitative data derived from morphological, physiological, and biochemical observations were processed and analyzed using IBM SPSS Statistics version 26. A Two-Way Analysis of Variance (ANOVA) was conducted to assess the main effects and interaction between chitosan concentration and NPK fertilizer dosage for each measured parameter. When the ANOVA indicated statistically significant differences ($p<0.05$), Duncan's Multiple Range Test (DMRT) was applied at a 5% significance level to determine pairwise differences among treatment means.

Prior to analysis, data were tested for normality and homogeneity of variance to meet the assumptions of parametric tests. Results are expressed as mean ± Standard Deviation (SD), and statistically significant differences among treatments are denoted by different superscript letters in tables or figure legends, where appropriate.

RESULTS AND DISCUSSION

Effect of chitosan and NPK fertilizer on leaf number

The application of chitosan and NPK fertilizer influenced the number of leaves produced by *E. palmifolia* at harvest. As shown in Table 1, plants treated with higher levels of NPK generally produced more leaves compared to the untreated control. The highest leaf number was observed in the treatment combination of 0% chitosan and 200 kg/ha NPK (K0N2), averaging 18.60 ± 5.90 leaves per plant. Conversely, the lowest value was recorded in the 0.3% chitosan and 0 kg/ha NPK treatment (K1N0), with only 7.80 ± 2.28 leaves per plant.

Although the interaction between chitosan and NPK was statistically significant ($p<0.05$), differences in leaf number across treatment combinations were not consistently significant, as indicated by overlapping superscript letters. While chitosan at 0.3% tended to reduce leaf number in the absence of fertilizer, the application of NPK improved leaf production across all chitosan levels. Treatment with 0.6% chitosan generally resulted in higher leaf numbers under increased NPK levels, particularly in K2N2 (16.40 ± 5.88), although this was slightly lower than the value observed in K0N2.

These trends suggest a modest but observable dose-dependent interaction between biostimulant and fertilizer application. Chitosan is known to enhance nitrogen metabolism by activating enzymes such as nitrate reductase and glutamine synthetase, which play critical roles in vegetative development (Gornik et al. 2008). Simultaneously, NPK fertilizer supplies essential macronutrients that promote meristematic activity and cell expansion in developing leaves (Parvin et al. 2019). Together, these results indicate that the combined use of chitosan and NPK fertilizer can support improved vegetative growth in *E. palmifolia*, although the magnitude of response is influenced by the specific treatment combination.

Leaf length response to treatment combinations

The leaf length of *E. palmifolia* varied in response to different combinations of chitosan and NPK fertilizer. As shown in Table 2, the longest average leaf length (51.04 ± 2.05 cm) was recorded in the K1N2 treatment (0.3% chitosan with 200 kg/ha NPK), whereas the shortest leaves were observed in K0N1 (0% chitosan with 100 kg/ha NPK), with a mean of 33.50 ± 8.12 cm.

Statistical analysis indicated a significant interaction between chitosan and NPK treatments ($p<0.05$), suggesting that the impact of chitosan on leaf elongation is dependent on nutrient availability. Interestingly, all treatments with 200 kg/ha NPK yielded mean leaf lengths exceeding 50 cm, regardless of chitosan concentration, implying the presence of a nutrient threshold that supports maximum elongation.

The elongation observed may be due to enhanced nutrient uptake and hormone signaling triggered by chitosan, especially in pathways involving auxins and gibberellins (Ingle et al. 2022). Meanwhile, nitrogen supplied through NPK plays a fundamental role in promoting cell elongation and division, thereby facilitating leaf blade development (Sun et al. 2022). These results highlight that under optimal fertilization, the presence of chitosan can further amplify vegetative parameters such as leaf length, although further studies are needed to verify synergism.

Table 1. Number of leaves (mean ± SD) of *Eleutherine palmifolia* after treatment with chitosan and NPK fertilizer

Chitosan (%)	NPK 0 kg/ha	NPK 100 kg/ha	NPK 200 kg/ha
0.0	14.20 ± 6.22^{b}	15.40 ± 6.95^{a}	18.60 ± 5.90^{a}
0.3	7.80 ± 2.28^{a}	11.00 ± 5.00^{a}	12.80 ± 3.35^{a}
0.6	11.80 ± 3.70^{ab}	13.00 ± 4.80^{a}	16.40 ± 5.88^{a}

Note: Different superscript letters in the same column indicate significant differences at $p<0.05$ (DMRT)

Table 2. Leaf length (mean ± SD, in cm) of *Eleutherine palmifolia* after chitosan and NPK fertilizer treatments

Chitosan (%)	NPK 0 kg/ha	NPK 100 kg/ha	NPK 200 kg/ha
0.0	38.40 ± 8.39^{a}	33.50 ± 8.12^{a}	50.60 ± 4.38^{a}
0.3	49.58 ± 2.58^{b}	47.04 ± 4.45^{b}	51.04 ± 2.05^{a}
0.6	44.16 ± 7.15^{a}	45.74 ± 3.86^{b}	50.24 ± 4.88^{a}

Note: Different superscript letters in the same column indicate significant differences at $p<0.05$ (DMRT)

Variation in leaf width under chitosan and NPK application

Leaf width in *E. palmifolia* was also influenced by the interaction between chitosan and NPK fertilizer. As shown in Table 3, the widest leaves were observed in the treatment combination of 0.3% chitosan and 200 kg/ha NPK (K1N2), with a mean width of 2.94 ± 0.42 cm, followed closely by the 0.6% chitosan and 200 kg/ha NPK (K2N2) treatment (2.78 ± 0.32 cm). The narrowest leaves were recorded in the group receiving 0% chitosan and 100 kg/ha NPK (K0N1), which averaged only 1.82 ± 0.30 cm.

Statistical analysis confirmed a significant interaction between chitosan and NPK fertilizer ($p<0.05$), indicating that leaf width expansion was influenced by their combined application. The application of chitosan at both 0.3% and 0.6% concentrations enhanced leaf width more effectively when accompanied by higher NPK doses.

The increased width may be due to chitosan-induced expression of genes associated with photosynthesis and hormonal regulation (Landi et al. 2017). At the same time, the presence of essential macronutrients particularly potassium and phosphorus likely supported turgor maintenance and enhanced cell expansion, contributing to broader leaf blades (Yamika et al. 2021).

Flower emergence and flowering speed in response to treatment

The transition of *E. palmifolia* from the vegetative to the generative phase was assessed through the observation of flower emergence and flower count per plant. As shown in Figure 1, flowering occurred in only four out of the nine treatment combinations during the 11-week cultivation period. The treatment K2N2 (0.6% chitosan and 200 kg/ha NPK) recorded the highest average number of flowers (2.6 per plant), followed by K2N0, K1N2, and K0N2. In contrast, the other five treatments showed no flowering response by the end of the study.

The onset of flowering ranged from day 74 to 77 after sowing. Although these findings suggest that higher chitosan and NPK levels might promote earlier or more frequent flowering, statistical analysis revealed no significant differences among treatments ($p>0.05$). Therefore, the flowering pattern should be interpreted with caution and considered a supplementary outcome rather than a primary indicator of treatment effectiveness.

Since the tuber is the main organ of economic interest in *E. palmifolia*, floral traits such as flower number and timing hold limited agronomic relevance. Furthermore, floral emergence did not exhibit strong correlations with vegetative traits (e.g., leaf number) or final tuber yield. Thus, while biologically notable, further studies under extended cultivation periods would be needed to confirm any consistent flowering response.

Fresh leaf biomass accumulation across treatments

The accumulation of fresh leaf biomass in *E. palmifolia* was influenced by the combined application of chitosan and NPK fertilizer. As presented in Table 4, the highest fresh leaf weight was recorded in the K2N2 treatment (0.6% chitosan and 200 kg/ha NPK), averaging 9.07 ± 2.73 g per plant. In contrast, the lowest value was observed in the K1N0 treatment (0.3% chitosan without NPK), which averaged only 3.95 ± 2.37 g.

Table 3. Leaf width (mean ± SD, in cm) of *E. palmifolia* following chitosan and NPK fertilizer treatments

Chitosan (%)	NPK 0 kg/ha	NPK 100 kg/ha	NPK 200 kg/ha
0.0	2.20 ± 0.65[a]	1.82 ± 0.30[a]	2.31 ± 0.51[a]
0.3	2.52 ± 0.13[a]	2.68 ± 0.26[b]	2.94 ± 0.42[b]
0.6	2.28 ± 0.45[a]	2.60 ± 0.29[b]	2.78 ± 0.32[ab]

Note: Different superscript letters in the same column indicate significant differences at $p<0.05$ (DMRT)

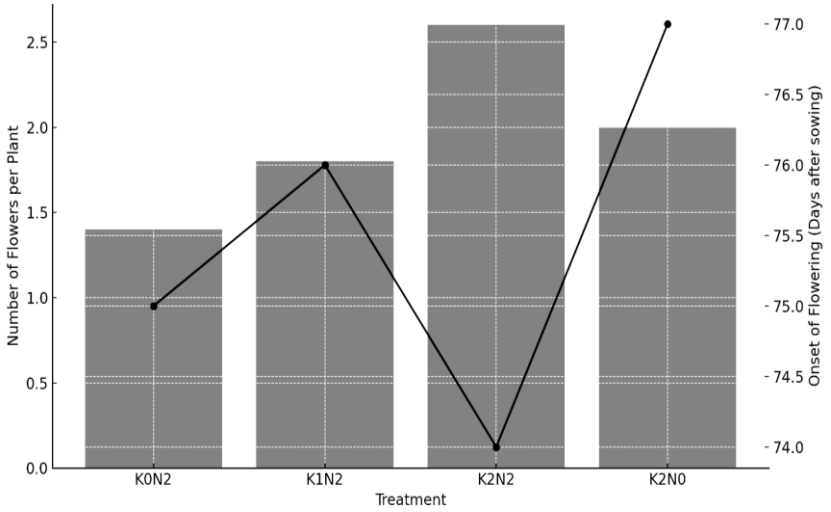

Figure 1. Number of flowers per plant and onset of flowering in *E. palmifolia* under various chitosan and NPK fertilizer treatments

Although statistical analysis did not reveal a significant interaction effect between chitosan and NPK fertilizer ($p>0.05$), a general trend was observed wherein higher doses of both inputs were associated with increased fresh leaf biomass. This pattern aligns with the established role of NPK macronutrients in supporting vegetative growth particularly nitrogen, which is crucial for chlorophyll synthesis, protein production, and cell expansion (Haryadi et al. 2015; Huang et al. 2019).

Chitosan may also contribute by enhancing nutrient absorption and water retention through improved membrane permeability and root function (Perez-de-Luque 2017). Although the differences were not statistically significant, the observed trends highlight the potential benefits of integrating biostimulants with conventional fertilizers. Additional studies with longer cultivation durations or increased replication may help clarify the extent of these effects.

Dry leaf biomass response to chitosan and NPK levels

Dry leaf weight is a key parameter indicating the accumulation of structural biomass and net photosynthate allocation in *E. palmifolia*. Based on the results in Table 5, the highest dry leaf weight was recorded in the K2N2 treatment (0.6% chitosan and 200 kg/ha NPK), with a mean of 2.04 ± 0.95 g per plant, while the lowest value was found in K1N0 (0.3% chitosan and 0 kg/ha NPK), averaging 1.02 ± 0.27 g.

Despite these differences, the statistical analysis did not show a significant interaction effect between chitosan and NPK fertilizer ($p>0.05$). The variation in dry biomass might be influenced by inconsistent rates of moisture loss during oven drying or by the diversion of photosynthates toward tuber development during later growth stages.

Nevertheless, a general increasing trend was observed with higher chitosan and NPK levels, particularly at 0.6% chitosan. Chitosan has been associated with enhanced photosynthetic enzyme activity and chloroplast integrity, which may contribute to greater dry matter accumulation (El-Miniawy et al. 2014; Acemi et al. 2021). Meanwhile, NPK fertilization supports cell wall thickening, structural protein synthesis, and other metabolic processes linked to dry biomass formation (Nuryani et al. 2019).

Fresh tuber weight as affected by treatment combinations

Fresh tuber weight is an important indicator of economic yield in *E. palmifolia*. As shown in Table 6, the highest average fresh tuber weight was obtained from the K2N2 treatment (0.6% chitosan and 200 kg/ha NPK), reaching 2.46 ± 0.95 g per plant. In contrast, the lowest value was recorded in the K1N0 treatment (0.3% chitosan and no NPK fertilizer), with a mean of 0.84 ± 0.37 g.

Statistical analysis revealed that only chitosan had a significant effect on fresh tuber weight ($p<0.05$), while the effects of NPK and the interaction between the two factors were not significant. This indicates that the observed increase in fresh tuber yield was mainly influenced by chitosan application. Notably, even in the absence of NPK, the 0.6% chitosan treatment (K2N0) still showed better results than several combinations that included fertilizer.

The stimulatory effect of chitosan on fresh tuber weight may be related to its role in improving root membrane permeability, enhancing nutrient absorption, and facilitating water retention, which collectively promote assimilate translocation to underground storage tissues (Duhan et al. 2017; Nuraini et al. 2019). Although NPK application alone did not produce significant effects, a general upward trend in fresh tuber weight with increasing fertilizer dose suggests potential additive benefits in longer-term or field-scale studies.

Dry tuber biomass and its variability among treatments

Dry tuber weight is considered a stable metric for evaluating storage biomass in *E. palmifolia*, as it reflects net assimilate accumulation after moisture removal. As shown in Table 7, the highest dry tuber weight was recorded in the K2N2 treatment (0.6% chitosan and 200 kg/ha NPK), averaging 2.46 ± 0.87 g per plant, followed by K2N1 and K0N1. The lowest value was found in the K0N0 group, with a mean of 2.04 ± 0.54 g.

Despite numerical variation, statistical analysis indicated no significant differences ($p>0.05$) among treatment combinations. This suggests that neither chitosan nor NPK fertilizer significantly influenced dry tuber weight under the current experimental conditions. Nonetheless, a consistent trend of increasing dry weight with higher chitosan concentrations especially when combined with moderate to high NPK doses was apparent.

Table 4. Fresh leaf weight (mean ± SD, in grams) of *E. palmifolia* after chitosan and NPK fertilizer treatments

Chitosan (%)	NPK 0 kg/ha	NPK 100 kg/ha	NPK 200 kg/ha
0.0	5.27 ± 1.30	6.57 ± 2.94	8.28 ± 2.37
0.3	3.95 ± 2.37	6.72 ± 3.04	7.26 ± 2.48
0.6	7.18 ± 1.26	5.95 ± 1.84	9.07 ± 2.73

Table 5. Dry leaf weight (mean ± SD, in grams) of *E. palmifolia* after chitosan and NPK fertilizer treatments

Chitosan (%)	NPK 0 kg/ha	NPK 100 kg/ha	NPK 200 kg/ha
0.0	1.15 ± 0.57	1.34 ± 0.47	1.60 ± 0.60
0.3	1.02 ± 0.27	1.23 ± 0.41	1.52 ± 0.64
0.6	1.71 ± 0.83	1.22 ± 0.48	2.04 ± 0.95

Table 6. Fresh tuber weight (mean ± SD, in grams) of *E. palmifolia* after chitosan and NPK fertilizer treatments

Chitosan (%)	NPK 0 kg/ha	NPK 100 kg/ha	NPK 200 kg/ha
00.00	1.21 ± 0.53^{ab}	1.47 ± 0.72^{a}	2.01 ± 0.84^{a}
00.03	0.84 ± 0.37^{a}	1.08 ± 0.39^{a}	1.15 ± 0.99^{a}
00.06	1.72 ± 0.54^{b}	2.16 ± 1.58^{a}	2.46 ± 0.95^{a}

Note: Different superscript letters indicate significant differences at $p<0.05$ (DMRT)

The absence of statistical significance may be attributed to several factors, including variability in drying rates, limited experimental duration, or diversion of assimilates to reproductive or foliar tissues. While the fresh weight showed clearer distinctions, the dry weight data suggest that chitosan primarily enhanced water retention and physiological activity rather than biomass structure alone.

Total chlorophyll content in leaves under chitosan and NPK treatment

Total chlorophyll content in the leaves of *E. palmifolia* exhibited notable variation in response to chitosan and NPK fertilizer treatments. As shown in Table 8, the highest chlorophyll level was observed in the K2N2 treatment (0.6% chitosan and 200 kg/ha NPK), reaching 1.79 ± 0.98 mg/g, while the lowest was recorded in K0N1 (0% chitosan and 100 kg/ha NPK), with a mean of 0.64 ± 0.06 mg/g.

Statistical analysis confirmed a significant interaction effect ($p<0.05$) between chitosan and NPK fertilizer, indicating that chlorophyll content was influenced by the combined action of biostimulant and macronutrient inputs. Treatments with 0.3% and 0.6% chitosan generally showed elevated chlorophyll levels, particularly when combined with 100-200 kg/ha NPK.

This enhancement can be attributed to the positive effect of chitosan on chloroplast development and nutrient absorption, including nitrogen and magnesium, which are critical for chlorophyll biosynthesis (Landi et al. 2017). Additionally, NPK fertilizer contributes essential building blocks for pigment formation and metabolic activity (Nur and Thohari 2007; Ebadi et al. 2024). These findings support the conclusion that combining chitosan and NPK enhances photosynthetic potential and overall plant vigor.

Carotenoid levels in leaves under different treatment combinations

Carotenoids are essential pigments involved in light harvesting and photoprotection in plant leaves. In *E. palmifolia*, carotenoid levels showed significant variation across the treatment groups. As presented in Table 9, the highest carotenoid content was observed in the K2N2 treatment (0.6% chitosan and 200 kg/ha NPK), reaching 21.04 ± 3.13 µmol/g, while the lowest was recorded in K0N1 (0% chitosan and 100 kg/ha NPK) with a mean of 4.47 ± 0.65 µmol/g.

A two-way ANOVA confirmed a significant interaction ($p<0.05$) between chitosan and NPK fertilizer, indicating that carotenoid accumulation was influenced by both factors. Across all NPK levels, carotenoid content increased consistently with rising chitosan concentration, demonstrating a clear dose-dependent trend. This trend was most pronounced at the highest fertilizer level (200 kg/ha NPK), where chitosan application resulted in sharp increases in carotenoid production.

The enhanced carotenoid synthesis can be attributed to the elicitor properties of chitosan, which are known to activate the isoprenoid and phenylpropanoid pathways, including the upregulation of key biosynthetic enzymes such as phytoene synthase (Fanciullino et al. 2014; Rahman et al. 2018). Meanwhile, NPK fertilizer provides essential precursors for energy metabolism and pigment synthesis, such as nitrogen and phosphorus. These findings emphasize the synergistic potential of combining biostimulants and macronutrients to enhance secondary metabolite accumulation in medicinal plants.

Total flavonoid content of tuber extracts

Flavonoids are important bioactive compounds with antioxidant, anti-inflammatory, and therapeutic properties, making their quantification a key component in medicinal plant research. In *E. palmifolia*, total flavonoid content in tuber ethanol extracts varied significantly across treatment combinations, as illustrated in Figure 2.

The highest flavonoid level was recorded in the K2N2 treatment (0.6% chitosan and 200 kg/ha NPK), reaching 6.30 mg quercetin equivalent (QE)/g dry tuber, followed by K2N1 (5.90 mg QE/g) and K2N0 (5.34 mg QE/g). The lowest flavonoid content was found in the control treatment (K0N0), with 3.45 mg QE/g.

Table 7. Dry tuber weight (mean ± SD, in grams) of *E. palmifolia* after chitosan and NPK fertilizer treatments

Chitosan (%)	NPK 0 kg/ha	NPK 100 kg/ha	NPK 200 kg/ha
0.0	2.04 ± 0.54	2.56 ± 0.26	2.07 ± 0.44
0.3	2.13 ± 0.55	2.15 ± 0.16	2.16 ± 0.53
0.6	2.09 ± 0.27	2.36 ± 0.48	2.46 ± 0.87

Note: No significant differences were detected among treatments (DMRT, $p>0.05$

Table 8. Total chlorophyll content (mean ± SD, in mg/g) of *E. palmifolia* leaves after chitosan and NPK fertilizer treatments

Chitosan (%)	NPK 0 kg/ha	NPK 100 kg/ha	NPK 200 kg/ha
0.0	0.74 ± 0.07^{a}	0.64 ± 0.06^{a}	0.64 ± 0.07^{a}
0.3	0.75 ± 0.14^{a}	1.52 ± 0.37^{b}	0.76 ± 0.27^{a}
0.6	0.89 ± 0.27^{a}	0.96 ± 0.35^{a}	1.79 ± 0.98^{b}

Note: Different superscript letters in the same column indicate significant differences at $p<0.05$ (DMRT)

Table 9. Carotenoid content (mean ± SD, in µmol/g) of *E. palmifolia* leaves after chitosan and NPK fertilizer treatments

Chitosan (%)	NPK 0 kg/ha	NPK 100 kg/ha	NPK 200 kg/ha
0.0	7.48 ± 1.00^{a}	4.47 ± 0.65^{a}	10.54 ± 0.85^{a}
0.3	10.60 ± 2.16^{ab}	12.54 ± 0.72^{b}	8.34 ± 2.61^{a}
0.6	13.56 ± 3.75^{b}	14.48 ± 5.81^{b}	21.04 ± 3.13^{b}

Note: Different superscript letters in the same column indicate significant differences at $p<0.05$ (DMRT)

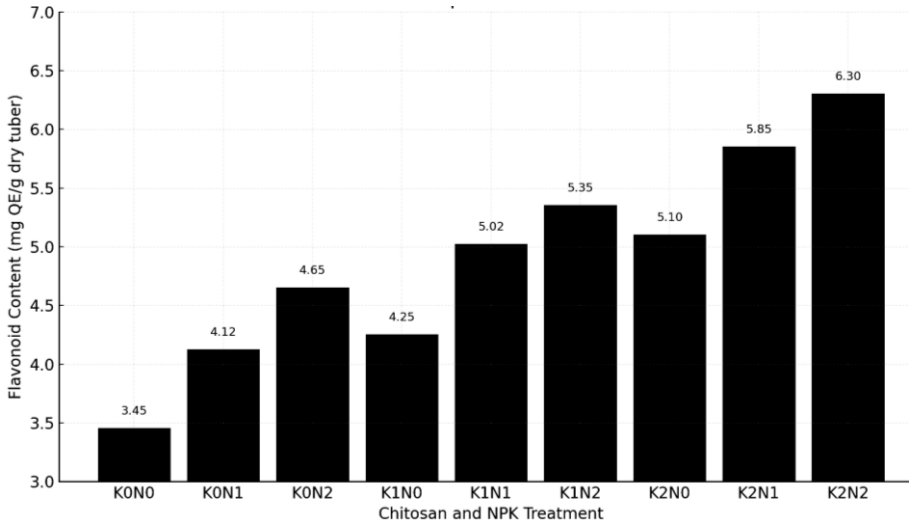

Figure 2. Total flavonoid content (mg quercetin equivalent/g dry tuber) of *E. palmifolia* under different combinations of chitosan and NPK fertilizer treatments

Statistical analysis revealed that chitosan concentration had a significant effect ($p<0.05$), while the effect of NPK and the interaction term were not statistically significant ($p>0.05$). Nevertheless, a consistent upward trend in flavonoid accumulation was observed with increasing levels of both chitosan and NPK, suggesting a possible additive response.

The increase in flavonoid content is likely linked to the elicitor activity of chitosan, which activates the phenylpropanoid pathway and stimulates the expression of biosynthetic enzymes such as Phenylalanine Ammonia-Lyase (PAL), Chalcone Synthase (CHS), and Flavonol Synthase (FLS) (Xing et al. 2015; Sathiyabama and Indhumathi 2022). The presence of sufficient NPK may further facilitate these biosynthetic processes by ensuring nutrient availability required for energy production and enzymatic activity. These findings suggest that chitosan-based biostimulant strategies, particularly when complemented by adequate fertilization, may enhance the accumulation of valuable secondary metabolites in underground organs.

Discussion

Morphological response to chitosan and NPK treatments

This study demonstrated that the morphological performance of *E. palmifolia* was moderately influenced by the interaction between chitosan and NPK fertilizer. Significant treatment effects were observed on key traits such as leaf number, length, and width ($p<0.05$). In particular, the K2N2 combination (0.6% chitosan with 200 kg/ha NPK) produced the highest average number of leaves (18.60 ± 5.90), indicating a possible additive effect of both treatments. However, the statistical differentiation among some treatment combinations remained limited, as reflected by overlapping superscript letters in Table 1. This suggests that although trends were visible, the effects were not uniformly strong across all levels.

Leaf length and width were also significantly affected, with the longest (51.04 ± 2.05 cm) and widest leaves (2.94 ± 0.42 cm) recorded under the K1N2 treatment (0.3% chitosan and 200 kg/ha NPK). These results support previous findings that chitosan can enhance vegetative traits by influencing hormonal activity such as auxin and gibberellin-mediated elongation (Ingle et al. 2022), while nitrogen and potassium contribute to cell expansion and division (Yamika et al. 2021; Sun et al. 2022). The significant interaction between chitosan and NPK for these traits suggests that their combined application may enhance morphological outcomes, especially under sufficient nutrient supply. Nonetheless, the magnitude of improvement was moderate and context-dependent, highlighting the need for further validation under field conditions.

Flowering and biomass accumulation

Although flowering frequency and timing did not show statistically significant differences ($p>0.05$), a trend was observed in which plants treated with both chitosan and higher doses of NPK tended to flower earlier and more frequently. The K2N2 treatment initiated flowering at day 74 and produced the highest flower count (2.6 per plant), followed by K2N0 and K1N2. While biologically suggestive, this trend should be interpreted cautiously due to the limited number of flowering individuals and the short duration of the experiment. A possible influence of chitosan on reproductive transition may involve enhanced sugar translocation and hormonal modulation, such as abscisic acid and carbohydrate signaling (Sharif et al. 2018; Alsanam et al. 2021), but further investigation under controlled flowering studies is needed.

For biomass parameters, both fresh and dry weights of leaves and tubers showed positive trends across increasing chitosan and NPK levels, with the highest values generally observed in the K2N2 group. Statistical significance was confirmed only for certain traits (e.g., fresh tuber weight and total chlorophyll content), while others displayed non-significant trends. These improvements may reflect enhanced nutrient absorption and water retention associated with

chitosan application (Gornik et al. 2008), along with improved leaf morphometry and photosynthetic capacity contributing to increased assimilate production. Although NPK fertilization alone contributed to growth, its combination with chitosan appeared more effective in optimizing biomass accumulation in several parameters. Nitrogen and potassium likely supported protein synthesis and osmotic adjustment, respectively, contributing to the observed physiological responses.

Pigment content and photosynthetic capacity

Chlorophyll and carotenoid contents responded significantly to the chitosan and NPK treatments ($p<0.05$), with the highest values observed in the K2N2 group. The increase in total chlorophyll, particularly chlorophyll a, was also accompanied by visibly greener foliage, suggesting improved photosynthetic efficiency. These results are consistent with previous findings that link biostimulant use with enhanced physiological traits. Chitosan may enhance nitrogen assimilation by stimulating nitrate reductase activity, thus promoting chlorophyll biosynthesis (Limpanavech et al. 2008), while nitrogen and magnesium from NPK fertilizer contribute structurally to the chlorophyll molecule.

Carotenoid accumulation also increased under combined treatments, potentially improving photoprotection and oxidative stress tolerance. The observed pigment responses help explain the improved vegetative growth under these treatments, as they indicate more robust photosynthetic machinery. These findings underline that the interaction between chitosan and NPK not only influences structural traits but also improves physiological function, particularly in photosynthetic pigment accumulation.

Flavonoid accumulation and chitosan as a metabolic elicitor

Total flavonoid content in *E. palmifolia* tubers was significantly enhanced by chitosan-NPK combinations ($p<0.05$), with the highest level (6.30 mg QE/g) recorded under K2N2. This represents a substantial increase compared to the control, suggesting that the treatments acted synergistically to stimulate secondary metabolism. This effect may be explained by the elicitor role of chitosan in activating the phenylpropanoid pathway, including key enzymes such as Phenylalanine Ammonia-Lyase (PAL) and Chalcone Synthase (CHS), which are central to flavonoid biosynthesis (Sharif et al. 2018). Chitosan likely initiates signaling pathways, such as MAPK cascades, which lead to transcriptional activation of secondary metabolite biosynthetic genes.

Meanwhile, the contribution of NPK especially phosphorus may support flavonoid synthesis by enhancing carbohydrate availability and energy metabolism (Foyer and Noctor 2011), both of which are necessary for the biosynthesis of carbon-based secondary metabolites. These results suggest that chitosan not only functions as a growth promoter but also as a modulator of secondary metabolism, with potential applications in enhancing the phytochemical value of medicinal plants such as *E. palmifolia*.

Reproductive traits and their relation to secondary metabolism

Although the number of flowers and timing of floral initiation did not show statistically significant differences ($p>0.05$), the observed patterns suggest a potential influence of chitosan and NPK on the reproductive behavior of *E. palmifolia*. Flowering occurred in only four of the nine treatment groups, with the earliest onset and highest flower count recorded in the K2N2 treatment (2.6 flowers/plant, day 74), followed by K2N0, K1N2, and K0N2. This trend may reflect enhanced photosynthetic performance and assimilate availability in treatments with greater vegetative growth and pigment content.

Nonetheless, the low reproductive output and absence of flowering in more than half of the treatments—despite favorable vegetative development indicate that flowering in this species may require longer cultivation periods or specific environmental cues beyond nutrient and biostimulant inputs. Chitosan has been reported to influence flowering through hormonal and sugar-related signaling pathways (Alsanam et al. 2021), while phosphorus, as part of NPK, regulates meristem transition to reproductive development (Campbell et al. 2008). However, the present study's timeframe (11 weeks) might have limited the full expression of these responses.

It is also important to note that *E. palmifolia* is cultivated primarily for its tubers, not its flowers. The lack of correlation between flower number and tuber flavonoid content, as observed in K2N2 versus K2N0 treatments, supports the hypothesis that reproductive output does not directly determine secondary metabolite accumulation in storage organs. In fact, the highest flavonoid concentration was recorded under K2N2, not K2N0, despite K2N0 yielding the highest tuber biomass suggesting that flavonoid biosynthesis may be more tightly linked to biostimulant-induced elicitation than to reproductive development per se.

Future studies should consider extending the observation period beyond 11 weeks and employing a phenology-focused design to better characterize the generative potential of this species and its relation to phytochemical accumulation.

Integrative interpretation and practical implications

The integration of chitosan and NPK fertilizer yielded synergistic improvements across multiple parameters, notably in leaf development, chlorophyll content, and tuber flavonoid accumulation. The most consistent gains were observed in the K2N2 treatment, suggesting that chitosan functions optimally when nutrient availability is sufficient, likely through enhanced nutrient uptake and metabolic activation. This combination supports both vegetative growth and phytochemical enhancement, positioning it as a practical strategy for improving both yield and functional quality of *E. palmifolia* in greenhouse settings. While some effects were not statistically significant, observable trends suggest potential for optimized biostimulant-fertilizer regimes. These findings offer a baseline for the sustainable cultivation of medicinal plants, especially in systems targeting biomass and bioactive compound productivity.

Future studies should explore longer growth periods and molecular mechanisms to validate and expand these results.

In conclusion, the combined application of 0.6% chitosan and 200 kg/ha NPK fertilizer significantly enhanced vegetative growth, pigment accumulation, and flavonoid content in *E. palmifolia* under greenhouse conditions. Notably, improvements in leaf number, size, chlorophyll content, and tuber flavonoids suggest a synergistic interaction between biostimulant and nutrient inputs. Although flowering induction was limited within the cultivation period, observed trends point to chitosan's potential role in supporting reproductive transition when adequate macronutrients are present. These findings provide practical insights for optimizing agronomic yield and phytochemical quality in *E. palmifolia*, supporting its sustainable cultivation as a medicinal crop. Further research is needed to explore long-term effects and underlying molecular mechanisms.

REFERENCES

Abdel-Aziz HM, Hasaneen MN, Omer AM. 2016. Nano chitosan-NPK fertilizer enhances the growth and productivity of wheat plants grown in sandy soil. Spanish J Agric Res 14 (1): e0902-e0902. DOI: 10.5424/sjar/2016141-8205

Acemi A, Polat EG, Cakir M, Demiryürek E, Yavuz B, Özen F. 2021. Molecular weight and concentration of chitosan affect plant development and phenolic substance pattern in arugula. Notulae Botanicae Horti Agrobotanici Cluj-Napoca 49 (2): 12296-12296. DOI: 10.15835/nbha49212296.

Alsanam R, Alsahli A, Ibrahim M, Ahmad P. 2021. Chitosan-mediated plant growth and salt stress tolerance in *Vigna radiata*: Modulation of ABA signaling and antioxidant defense. Plant Physiol Biochem 159: 336-345. DOI: 10.1016/j.plaphy.2020.11.037

Atikah TA, Wardiyati T, Nihayati E, Saputera S, Nendissa DR. 2021. Inovasi teknologi budidaya bawang dayak (*Eleutherine palmifolia* Merr) untuk meningkatkan produktivitas dan analisis kelayakan ekonomi. AGROMIX 12 (1): 39-46. DOI: 10.35891/agx.v12i1.2331. [Indonesian]

Campbell CS, Watanabe N, Yamamoto M, Hakomori S, Kariyone S. 2008. Phosphorus regulation of flowering and floral organ development: Insights from gene expression studies. Plant Cell Environ 31 (10): 1416-1426.

Chadchawan S. Chamnanmanoontham N, Pongprayoon W, Pichayangkura R, Roytrakul S. 2015. Chitosan enhances rice seedling growth via gene expression network between nucleus and chloroplast Plant Growth Regul 75: 101-114. DOI: 10.1007/s10725-014-9935-7.

Cocozza C, Brilli F, Pignattelli S et al. 2020. The excess of phosphorus in soil reduces physiological performances over time but enhances prompt recovery of salt-stressed *Arundo donax* plants. Plant Physiol Biochem 151: 556-565. DOI: 10.1016/j.plaphy.2020.04.011.

Duhan JS, Kumar R, Kumar N, Kaur P, Nehra K, Duhan S. 2017. Nanotechnology: The new perspective in precision agriculture. Biotechnol Rep 15: 11-23. DOI: 10.1016/j.btre.2017.03.002

Ebaid M, El-Hady MA, El-Temsah ME et al. 2024. Combined vinasse and mineral NPK fertilizer affect physio-biochemical, root, and yield characters of faba bean (*Vicia faba* L.) genotypes grown on saline soil. J Soil Sci Plant Nutr 24 (2): 3178-3194. DOI: 10.1007/s42729-024-01743-8.

El-Miniawy SM, Ragab ME, Youssef SM, Metwally AA. 2014. Influence of foliar spraying of seaweed extract on growth, yield and quality of strawberry plants. J Appl Sci Res 10: 88-94.

Fanciullino R, Mollard S, Correard F, Giacometti S, Serdjebi C, Iliadis A, Ciccolini J. 2014. Biodistribution, tumor uptake and efficacy of 5-FU-loaded liposomes: Why size matters. Pharm Res 31: 2677-2684. DOI: 10.1007/s11095-014-1364-9.

Ferreyra SNE, Inzaugarat ME, Baz P, et al. 2012. The role of innate cells is coupled to a Th1-polarized immune response in pediatric nonalcoholic steatohepatitis. J Clin Immunol 32: 611-621. DOI: 10.1007/s10875-011-9635-2.

Foyer CH, Noctor G. 2011. Ascorbate and glutathione: The heart of the redox hub. Plant Physiol 155 (1): 2-18. DOI: 10.1104/pp.110.167569.

Gornik K, Grzesik M, Duda BR. 2008. The effect of chitosan on rooting of grapevine cuttings and on subsequent plant growth under drought and pathogen stress. Sci Hortic 117 (3): 274-280.

Haryadi D, Siregar FA, Sasmita P. 2015. Effect of NPK fertilizer on the growth and yield of shallots in dry climates. J Agric Sci 20 (1): 45-51.

Hendry GAF, Grime JP. 1993. Methods in Comparative Plant Ecology: A Laboratory Manual. Chapman & Hall, London. DOI: 10.1007/978-94-011-1494-3.

Huang M, Jiang L, Zou Y, Xu S, Deng Y. 2019. Effects of different potassium fertilizer levels on physiological traits and growth of medicinal plants. J Plant Nutr 42 (2): 201-214.

Ibrahim M. 2012. Design, synthesis, molecular docking and biological evaluation of some novel quinazolin-4 (3h)-one derivatives as anti-inflammatory agents. Al-Azhar J Pharm Sci 46 (2): 185-203. DOI: 10.21608/ajps.2012.7145.

Ingle N, Giri P, Joshi K. 2022. Role of chitosan in regulation of phytohormones and secondary metabolites in horticultural crops. Front Plant Sci 13: 927643. DOI: 10.3389/fpls.2022.927643

Kuntorini EM, Nugroho LH. 2010. Structural development and bioactive content of red bulb plant (*Eleutherine americana*); a traditional medicines for local Kalimantan people. Biodiversitas 11 (2): 102-106. DOI: 10.13057/biodiv/d110210.

Lalla MSP. 2022. Biostimulan Untuk Tanah Dan Tanaman. Penerbit Qiara Media, Pasuruan. [Indonesian]

Landi M, Esposito S, Nali C, Giordano C. 2017. Chitosan promotes antioxidative and photoprotective mechanisms under moderate UV-B radiation in lettuce plants. Sci Hortic 225: 295-302.

Limpanavech P, Chieochai S, Phornvillay S, Kumla S, Cha-um S. 2008. Chitosan effects on growth and postharvest quality of *Dendrobium* orchid. Sci Hortic 116: 65-72. DOI: 10.1016/j.scienta.2007.10.034.

Manurung B, Zahrah S. 2018. Pemberian Hormax dan NPK Mutiara 16: 16: 16 pada tanaman ubi jalar (*Ipomoea batatas* L.). Dinamika Pertanian 34 (2): 139-150. DOI: 10.25299/dp.2018.vol34(2).5423. [Indonesian]

Modi S, Kumar S, Dubey PK. 2021. Dynamics of chitosan based NPK-nanofertilizers in greenhouse cucumber production system. J Environ Biol 42 (1): 162-168. DOI: 10.22438/jeb/42/1/MRN-1251.

Moza A, Thomas T, Prasad ST. 2024. Local drug delivery using chitosan microspheres–A review of literature. Intl J Recenr Adv Multidiciplin Res 11 (04): 9714-9724.

Mutua CM, Ogweno JO, Gesimba RM. 2021. Effect of NPK fertilizer rates on growth and yield of field and greenhouse grown Pepino melon (*Solanum muricatum* Aiton). J Horticult Plant Res 13 (11): 10-23. DOI: 10.18052/www.scipress.com/JHPR.13.10.

Nur S, Thohari. 2007. Tanggap dosis nitrogen dan pemberian berbagai macam bentuk bolus terhadap pertumbuhan dan hasil tanaman bawang merah (*Allium ascalonicum* L). Jurnal Ilmiah Ilmu-Ilmu Pertanian 4 (1): 30-33. [Indonesian]

Nuraini A, Hamdani JS, Suminar E, Ardiansyah D. 2017. Aplikasi chitosan untuk meningkatkan hasil benih kentang G0 (*Solanum tuberosum* L.) kultivar granola pada berbagai jenis media tanam. Kultivasi 16 (3): 466-473. DOI: 10.24198/kultivasi.v16i3.14374. [Indonesian]

Nuryani E, Haryono G, Historiawati. 2019. Pengaruh dosis dan saat pemberian pupuk P terhadap hasil tanaman buncis (*Phaseolus vulgaris* L.) tipe tegak. Jurnal Ilmu Pertanian Tropika dan Subtropika 4 (1): 14-17. [Indonesian]

Paramita S, Nuryanto MK. 2018. Anti-inflammatory activity of bawang Dayak (*Eleutherine bulbosa* (Mill. Urb.)) ethanol bulb extracts. J Vocational Health Stud 2: 51-55. DOI: 10.20473/jvhs.V2.I2.2018.51-55.

Parvin K, Rahman MA, Islam MR, Jahan MS, Uddin MN, et al. 2019. Exogenous calcium alleviates salinity-induced oxidative stress in mustard (*Brassica juncea* L.). Plants 8: 151. DOI: 10.3390/plants8060151.

Patoni. 2000. Pengaruh Cekaman Kekeringan terhadap Pertumbuhan, Hasil, dan Kandungan Vitamin C Buah Tanaman Tomat (*Lycopersicum esculentum* Mill.). [Hon. Thesis]. Fakultas Biologi, Universitas Gadjah Mada, Yogyakarta. [Indonesian]

Perez-de-Luque A. 2017. Interaction of nanomaterials with plants: What do we need for real applications in agriculture? Front Environ Sci 5: 12. DOI: 10.3389/fenvs.2017.00012.

Rahman M, Mukta JA, Sabir AA et al. 2018. Chitosan biopolymer promotes yield and stimulates accumulation of antioxidants in strawberry fruit. PLoS One 13 (9): e0203769. DOI: 10.1371/journal.pone.0203769.

Rosmawaty T, Jumin HB, Mardaleni M, Sinaga C. 2019. Produksi dan kandungan flavonoid umbi tanaman bawang Dayak (*Eleutherine palmifolia*) dengan pemberian NPK 16: 16: 16 pada berbagai umur panen. Dinamika Pertanian 35 (3): 111-118. DOI: 10.25299/dp.2019.vol35(3).4574. [Indonesian]

Saharan V, Pal A. 2016. Properties and Types of Chitosan-Based Nanomaterials. SpringerBriefs in Plant Science. Springer, New Delhi. DOI: 10.1007/978-81-322-3601-6_3.

Sari VI, Saleh I, Ekawati R. 2020. Respons pertumbuhan, produksi, dan kandungan flavonoid bawang dayak (*Eleutherine palmifolia*) terhadap pengendalian gulma dan jarak tanam. Agrotechnol Res J 4 (2): 92-98. DOI: 10.20961/agrotechresj.v4i2.41725. [Indonesian]

Sathiyabama M, Indhumathi M. 2022. Chitosan thiamine nanoparticles intervene innate immunomodulation during Chickpea-*Fusarium* interaction. Intl J Biol Macromol 198: 11-17. DOI: 10.1016/j.ijbiomac.2021.12.105.

Sharif R, Mujtaba M, Rahman MU, Shalmani A, Ahmad H, Anwar T, Tianchan D, Xiping Wang X. 2018. The multifunctional role of chitosan in horticultural crops: A review. Molecules 23 (4): 872. DOI: 10.3390/molecules23040872.

Singh AK, Singla P. 2020. Root phenolics profile modulates microbial ecology of rhizosphere. Plant Phenol Sustain Agric 1: 555-578. DOI: 10.1007/978-981-15-4890-1_24.

Stankovic MS. 2011. Total flavonoid content in plant extracts using aluminum chloride colorimetric assay. J Med Plant Res 5 (25): 5555-5559. DOI: 10.5504/BBEQ.2011.0020.

Suci DAW. 2020. Pengaruh Kitosan Terhadap Kandungan Flavonoid pada Kalus Kesambi (*Schleichera oleosa* (Lour.) Merr) Secara in vitro. [Dissertation] Universitas Islam Negeri Maulana Malik Ibrahim, Malang. [Indonesian]

Sumarni N, Sopha GA, Gaswanto R. 2012. Respons tanaman bawang merah asal biji true shallot seeds terhadap kerapatan tanaman pada musim hujan. Indones Agency Agric Res Dev 22 (1): 23-28. DOI: 10.21082/jhort.v22n1.2012.p23-28.

Sun Q, Yang F, Liu M, Han Y, Dong M. 2022. Nitrogen metabolism and its relationship with plant growth under nitrogen supply. Front Plant Sci 13: 847650. DOI: 10.3389/fpls.2022.847650

Tamal MA, Aryanto D. 2020. Efektivitas air rebusan bawang dayak (*Eleutherine palmifolia* (L.) Merr) dalam menghambat pertumbuhan bakteri *Escherichia coli* pada daging sapi. Teknologi Pangan: Media Informasi Dan Komunikasi Ilmiah Teknologi Pertanian 11 (1): 16-26. DOI: 10.35891/tp.v11i1.1880. [Indonesian]

Xing HY, Cai YQ, Wang XF, Wang LL, Li P, Wang GY, Chen JH. 2015. The cytoprotective effect of hyperoside against oxidative stress is mediated by the Nrf2-ARE signaling pathway through GSK-3β inactivation. PLoS One 10 (12): e0145183. DOI: 10.1371/journal.pone.0145183.

Yamika W, Gunawan R, Riyadi P, Hasyim S. 2021. Response of growth and yield of shallot to potassium fertilization on entisol soil. IOP Conf Ser Earth Environ Sci 648: 012008. DOI: 10.1088/1755-1315/648/1/012008.

Yuswi NCR. 2017. Ekstraksi antioksidan bawang Dayak (*Eleutherine palmifolia*) dengan metode ultrasonic bath (kajian jenis pelarut dan lama ekstraksi). Jurnal Pangan dan Agroindustri 5 (1): 71-79. [Indonesian]

CELL BIOLOGY & DEVELOPMENT
Volume 9, Number 1, June 2025
Pages: 37-53

E-ISSN: 2580-4499
DOI: 10.13057/cellbioldev/v090104

Structural traits and carbon storage potential of tree and pole vegetation in three land-use types in Ngargoyoso, Central Java, Indonesia

ULFI HANUM[1], WINDA SAGITA ARMADHAN[1], ZAHRA HANUN[1], ZHALZABILLA SHAFA[1], SESILIA RETNO AYU NINGTYAS[1], ALYA AFRA INAS NUR[1], MUHAMMAD INDRAWAN[1], SUNARTO[1], SUGIYARTO[2], AHMAD DWI SETYAWAN[1,3,♥]

[1]Department of Environmental Science, Faculty of Mathematics and Natural Sciences, Universitas Sebelas Maret. Jl. Ir. Sutami 36A, Surakarta 57126, Central Java, Indonesia. Tel./fax.: +62-271-663375, ♥email: volatileoils@gmail.com
[2]Department of Biology, Faculty of Mathematics and Natural Sciences, Universitas Sebelas Maret. Jl. Ir. Sutami 36A, Surakarta 57126, Central Java, Indonesia
[3]Biodiversity Research Group, Universitas Sebelas Maret. Jl. Ir. Sutami 36A, Surakarta 57126, Central Java, Indonesia

Manuscript received: 20 January 2024. Revision accepted: 17 May 2025.

Abstract. *Hanum U, Armadhan WS, Hanun Z, Shafa Z, Ningtyas SRA, Nur AAI, Indrawan M, Sunarto, Sugiyarto, Setyawan AD. 2025. Structural traits and carbon storage potential of tree and pole vegetation in three land-use types in Ngargoyoso, Central Java, Indonesia. Cell Biol Dev 9: 37-53.* Understanding the relationship between plant structural characteristics and carbon storage is not just essential for ecological management and climate mitigation, but also highly relevant and applicable. This study investigates how Aboveground Biomass (AGB) and carbon stock correlate with the structural traits of tree and pole vegetation across three land-use types: pine forest, agroforestry, and rubber plantation in Ngargoyoso Sub-district, Central Java, Indonesia. Field sampling was conducted using 90 plots divided equally across the sites, with vegetation categorized into trees (DBH>20 cm) and poles (DBH 10-20 cm). Non-destructive measurements of diameter at breast height (DBH) and tree height were used to estimate biomass through species-specific allometric equations. Carbon stock was then calculated using a standardized conversion factor (0.47×AGB). The results show that agroforestry systems exhibit the highest total carbon stock (82.46 MgC/ha), followed by rubber forest (81.41 MgC/ha) and pine forest (66.29 MgC/ha). Variations in carbon accumulation are strongly influenced by vegetation composition, structural diversity, and DBH distribution. The predominance of fast-growing, nitrogen-fixing species such as *Leucaena leucocephala* in agroforestry contributed to higher biomass accumulation. These findings emphasize the practical implications of this study, highlighting the importance of structural traits such as DBH and height, which reflect physiological growth status and are key determinants in carbon storage capacity across different vegetation types.

Keywords: Aboveground biomass, agroforestry, carbon stock, DBH, structural traits, tropical forest physiology

INTRODUCTION

The continuous increase of greenhouse gas concentrations in the atmosphere, particularly carbon dioxide (CO_2), is the primary driver of global climate change and warming (Dewa and Sejati 2019). Forest ecosystems play a critical role in mitigating these changes through carbon sequestration, a process where atmospheric carbon is absorbed and stored in plant biomass via photosynthesis. In this context, trees function not only as carbon sinks but also as living indicators of how structural and physiological traits affect carbon accumulation across different vegetation systems (Ferrini et al. 2020; Qiu et al. 2020).

Photosynthesis is the primary physiological mechanism by which plants convert atmospheric CO_2 into organic compounds. The products of this process are stored as biomass, predominantly in the stem, branches, and leaves. Among these, the stem particularly in tree-level vegetation accounts for the largest portion of Aboveground Biomass (AGB), which is directly proportional to carbon stock (SNI 2011). The size and volume of the stem are strongly influenced by morphological traits, such as stem diameter and height, which are outcomes of both genetic growth potential and environmental adaptation. This implies that diameter at breast height (DBH) and total plant height are not merely biometric data but physiological proxies of cumulative growth and carbon assimilation capacity (Diana et al. 2022).

The anatomical and physiological traits of plant species, such as the density and distribution of stomata, vascular cambium activity, wood density, and growth form, also influence their capacity to accumulate biomass. Plants with a high stomatal density exhibit greater carbon fixation potential (Praseti et al. 2018). Similarly, species that develop large-diameter stems and higher wood density generally possess greater biomass and carbon stock per unit area. As a result, species composition and structural diversity significantly affect the overall carbon sequestration potential of a given vegetation system (Ambarwati et al. 2019).

In the Indonesian context, forest degradation and land-use change have dramatically altered the country's carbon budget. Indonesia ranks among the top global emitters of carbon, primarily due to forest clearing, fires, and unsustainable land conversion (Syah 2017; Han et al. 2019). Despite this, the country also holds great potential for climate mitigation through the rehabilitation and sustainable management of forests. Approaches such as agroforestry—integrating trees with crops and/or livestock have been

promoted as nature-based solutions that combine ecological restoration with socio-economic benefits (Alinus et al. 2017).

Ngargoyoso Sub-district, located on the diverse slopes of Mount Lawu in Central Java, presents a rich and varied landscape of vegetation systems. These include pine forests, rubber plantations, and agroforestry areas, each with its own uniqueness (BPS 2021; Sanjaya and Kurniawan 2021). Each land-use type demonstrates different levels of structural complexity and species richness. The largely homogenous pine (*Pinus merkusii*) and rubber (*Hevea brasiliensis*) stand in contrast with the diverse agroforestry systems that incorporate a mix of plantation crops with indigenous forest species such as *Leucaena leucocephala*, *Tectona grandis*, and *Swietenia mahagoni* (Bachtiar and Resti 2017; Minarno 2022).

Previous studies in Ngargoyoso, Karanganyar, Indonesia have highlighted that carbon stock varies greatly between these systems due to differences in species composition, DBH range, stand density, and vertical stratification (Utami et al. 2020; Wijayanto and Prasetyo 2021). Minarno (2022) reported that the carbon stock in Ngargoyoso ranged from 0.80 to 9,018.41 tons/ha, depending on vegetation type and sampling location. This indicates a strong need for a more structured evaluation focusing on the physiological and structural underpinnings of carbon storage.

Moreover, despite general knowledge of forest carbon dynamics, limited studies have explicitly quantified how structural plant traits contribute to AGB and carbon accumulation in mixed systems like agroforestry compared to monocultures. The use of species-specific allometric equations that consider DBH and height provides a more accurate and biologically grounded method to estimate biomass and carbon stock (Banaticla 2003; Chave et al. 2005; Siregar 2007).

This study aims to estimate the aboveground biomass and carbon stock of tree and pole vegetation in three different land-use types in Ngargoyoso Sub-district pine forest, agroforestry, and rubber plantation. It emphasizes the role of structural plant traits such as DBH, plant height, and species composition in carbon accumulation. These findings will not only contribute to a better understanding of carbon dynamics across land-use gradients but also offer practical insights into how plant structural characteristics can inform forest management and carbon monitoring strategies from a physiological perspective.

MATERIALS AND METHODS

Study area

This study was conducted in Ngargoyoso Sub-district, Karanganyar District, Central Java, Indonesia, located on the western slope of Mount Lawu (elevation: 673-1,079 m asl). The area is characterized by a tropical montane climate with moderate to high rainfall and supports diverse vegetation systems, including pine forest, agroforestry, and rubber plantation (Figure 1).

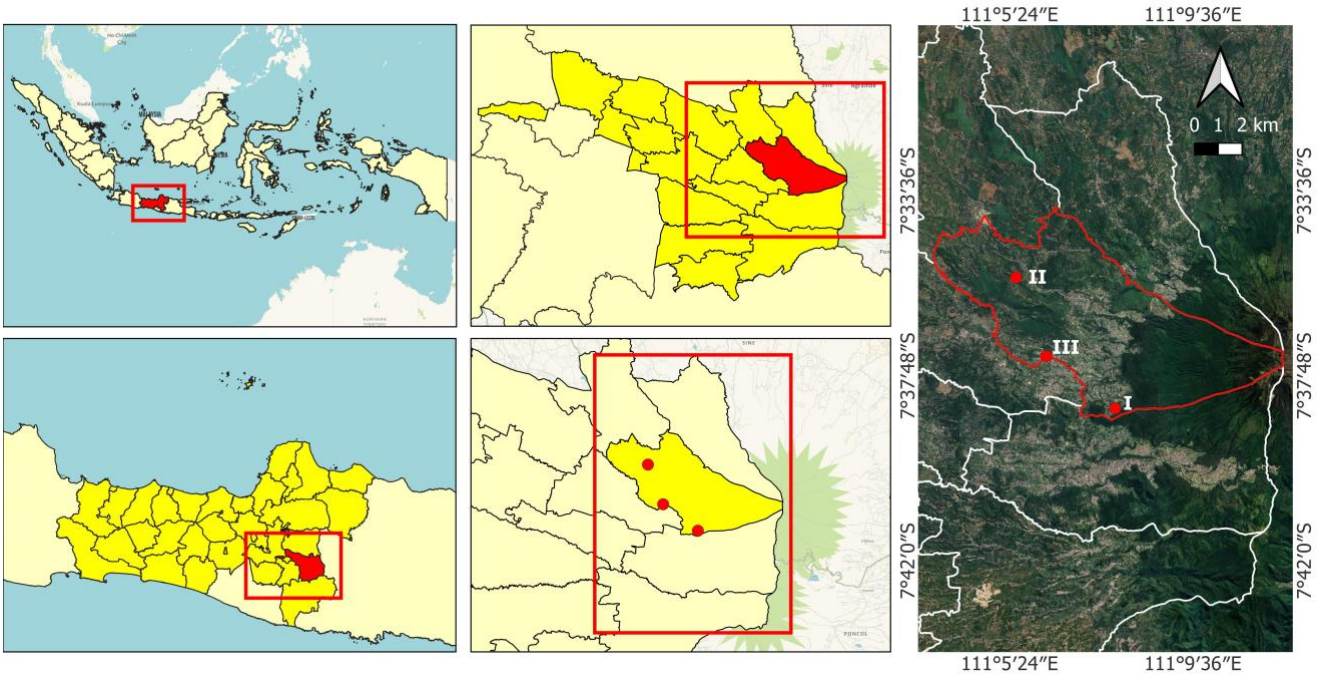

Figure 1. Map of research location in Ngargoyoso Sub-district, Karanganyar District, Central Java, Indonesia. I: Pine forest, II: Agroforestry area; III: Rubber plantation

Three land-use types were selected to represent different vegetation structures and management intensities. Three distinct land-use types were selected to represent different vegetation compositions and structural complexities namely (i) Pine forest (Site I): Located in Berjo Village (1,079 m asl; -7.6418137, 111.1301613), dominated by *Pinus merkusii*, with a uniform canopy structure, used primarily for timber and resin production; (ii) Agroforestry area (Site II): Situated in Surodadi Village (676 m asl; -7.5930470, 111.0922240), characterized by high species richness and vertical stratification, combining timber (*Tectona grandis*, *S. mahagoni*), legumes (*L. leucocephala*), and fruit trees (*Mangifera indica*, *Durio zibethinus*); (iii) Rubber plantation (Site III): Located in Puntukrejo (673 m asl; -7.6223074, 111.1038714), dominated by *Hevea brasiliensis* in monoculture stands with limited inclusion of other species. These sites represent a structural and functional gradient from homogeneous monocultures to diverse, mixed-use systems, offering an ideal framework to examine the influence of vegetation traits on aboveground biomass and carbon storage.

Sampling design

Vegetation sampling employed a stratified design across three land-use types: pine forest, agroforestry, and rubber plantation. Each site was subdivided into two vegetation strata based on stem diameter: (i) Tree stratum: Individuals with DBH>20 cm, (ii) Pole stratum: Individuals with DBH 10-20 cm. For each stratum, 15 plots were established per site, resulting in a total of 90 sampling plots (3 sites×2 strata×15 plots). Plot sizes were: (i) 20×20 m (400 m²) for the tree stratum, (ii) 10×10 m (100 m²) for the pole stratum

Plot locations were selected randomly within representative areas of each land-use type and georeferenced using GPS. Within each plot, all woody individuals meeting the DBH criteria were inventoried. For each individual, the following were recorded: species identity, DBH (via stem circumference), and estimated total height.

Species identification was conducted using local names and verified through botanical references or expert consultation. This stratification allowed the analysis of biomass contribution across developmental stages and structural layers, facilitating comparison within and between land-use types in terms of regeneration, productivity, and carbon storage potential.

Measurement of structural parameters

The assessment of vegetation structure was based on two key biometric indicators: diameter at breast height (DBH) and total plant height, both of which are widely recognized as reliable proxies for plant growth and aboveground biomass accumulation. DBH was measured at 1.3 meters above ground level using a diameter tape. For individuals with irregular stem forms such as buttresses or basal swellings the measurement was taken above the deformity where the stem resumed a cylindrical shape. DBH values were obtained by dividing the measured stem circumference by π (3.14), following the standard forestry formula. Total plant height was estimated for representative individuals in each plot using a hypsometer or visual estimation, particularly for tall species such as *P. merkusii*, *T. grandis*, and *S. mahagoni*. These height measurements complemented DBH data and were used in allometric equations that required both parameters. Species identification was conducted in the field using vernacular names provided by local informants and confirmed through taxonomic references. Each individual was subsequently categorized into one of two structural strata pole (DBH 10-20 cm) or tree (DBH>20 cm) to reflect different stages of ontogenetic development. This stratification facilitated the evaluation of growth patterns, carbon input from younger vegetation, and the contribution of mature individuals to the total biomass pool. Together, DBH and height data provided a comprehensive picture of stand structure, enabling accurate estimation of biomass and carbon stock across different land-use types.

Table 1. Estimation of aboveground biomass (AGB) using species-specific allometric equations

Species	Allometric equation (AGB in kg)	Reference
Pinus merkusii Jungh. & de Vriese	AGB = 0.0936 × D^2.4323	Siregar 2007
Leucaena leucocephala (Lam.) de Wit	AGB = 0.206 × D^2.305	Banaticla 2003
Acacia auriculiformis A.Cunn. ex Benth	AGB = 0.077 × D^0.90	Arupa 2014
Swietenia mahagoni (L.) Jacq.	AGB = 0.290091 × D^2.3	Hendri 2001
Albizia chinensis (Osbeck) Merr.	AGB = 0.0272 × D^2.831	Ketterings et al. 2001
Cocos nucifera L.	AGB = 4.5 + 7.7 + H[1]	Hairiah et al. 2001
Artocarpus heterophyllus Lam.	AGB = 0.1792 × D^2.25112	Samsu 2019
Gmelina arborea Roxb.	AGB = 0.153 × D^2.217	Banaticla 2003
Hevea brasiliensis Muell Arg.	AGB = 0.11 × 0.63 × D^2.62	Ketterings et al. 2001
Mangifera indica L.	AGB = -2.43 + 0.154 × D + 0.193 × H[2]	Chavan et al. 2012
Averrhoa bilimbi L.	AGB = 0.3699 × D^1.9374	Ilyas 2013
Hibiscus tiliaceus L.	AGB = 0.168 × 0.47 × D^2.47	Chave et al. 2005
Other species (branched trees)	AGB = 0.11 × ρ × D² + 0.62	Ketterings et al. 2001

Note: D: diameter at breast height (cm); H: total tree height (m); ρ: wood density (g/cm³); AGB: aboveground biomass (kg); [1]For *Cocos nucifera*, the equation represents composite biomass: 4.5 (trunk) + 7.7 (fronds) + H (crown), as per Hairiah et al. 2001; [2]Equation for *Mangifera indica* is valid only for trees with D≥10 cm and H≥5 m to avoid negative estimates, based on calibration range in Chavan et al. 2012

Biomass estimation

Aboveground biomass (AGB) was estimated non-destructively using species-specific allometric equations that relate measurable structural traits primarily DBH and height to biomass accumulation. These equations typically follow the form AGB = $a \times D^b$ or $a \times D^b \times H^c$, where D is diameter at breast height (cm), H is total height (m), and a, b, and c are species-specific constants derived empirically. A set of allometric models was selected based on species identity and growth form, as summarized in Table 1, drawing from previously validated equations for tropical species (e.g., Banaticla 2003; Chave et al. 2005; Siregar 2007). For species lacking specific models, generalized equations based on wood density or branching type were applied. The calculated biomass of each individual was aggregated at the plot level and extrapolated to a per-hectare basis (MgB/ha), enabling comparison across sites and structural strata. This approach ensures ecological accuracy while capturing functional differences in biomass allocation driven by vegetation structure and composition.

Carbon stock calculation

The aboveground carbon stock was derived from the estimated biomass values using a standardized conversion factor of 0.47, which reflects the average proportion of carbon in dry plant biomass. This coefficient, endorsed by the Indonesian National Standard (SNI 7724:2011) and consistent with IPCC guidelines, assumes that 47% of dry biomass consists of organic carbon bound in structural compounds such as cellulose and lignin. For each sampled individual, the calculated biomass (in mg/ha) was multiplied by 0.47 to obtain its carbon equivalent. Carbon values were computed separately for each stratum tree and pole and then aggregated to generate the total aboveground carbon stock per land-use type. This approach allows for the integration of species- and size-specific biomass variation into landscape-level carbon accounting. The use of a fixed conversion factor ensures comparability across sites, while still capturing structural differences in carbon accumulation that result from variations in DBH, height, wood density, and vegetation composition. By linking structural traits to functional outcomes, this method provides ecologically meaningful insights into the role of vegetation systems in carbon sequestration.

Data analysis

Data analysis focused on quantifying and comparing Aboveground Biomass (AGB) and carbon stock across different land-use types and structural strata. For each plot, individual AGB values derived from allometric equations were summed and converted to a per-hectare basis. Carbon stock was then calculated using the standard factor (0.47×AGB). These values were averaged for the tree and pole strata separately, allowing for stratified comparisons that reflect differences in structural development and regenerative status. Site-level totals were obtained by aggregating values from both strata. Visual representations were employed to illustrate variation across land uses, including stacked bar charts that displayed the relative contribution of trees and poles to total biomass and carbon stock. Additionally, DBH class distributions were plotted to assess population structure and regeneration dynamics. Rather than applying inferential statistics, the analysis emphasized descriptive comparisons, highlighting how variations in species composition, stem diameter, and canopy layering shape the carbon storage potential of each system. This approach aligns with the study's objective to link structural traits with ecological function and provides a framework for interpreting the role of vegetation architecture in long-term carbon dynamics.

RESULTS AND DISCUSSION

Species composition and site characteristics

Vegetation composition and structure differed markedly among the three land-use types in Ngargoyoso pine forest, agroforestry system, and rubber plantation. A total of 32 occurrences of species were recorded across both tree (DBH>20 cm) and pole (DBH 10-20 cm) strata, representing 25 unique species after accounting for overlaps between strata. Several species, such as *L. leucocephala* and *S. mahagoni*, were present in both strata, indicating active regeneration and demographic continuity across growth stages. These variations reflect differences in land management practices and species selection, which in turn shape the ecological functions related to aboveground biomass accumulation. Structural traits such as stem diameter and plant height played a significant role in determining the carbon stock potential at each site, underscoring the importance of both floristic diversity and vertical stratification in vegetation-based carbon storage.

The pine forest, although dominated by *P. merkusii*, did not exhibit the lowest species richness among the three land-use types. In fact, the rubber plantation recorded the lowest species richness, with only four species identified, despite having a higher total number of individuals. In the pine forest, the tree stratum was densely populated with mature *P. merkusii* individuals, whereas the pole stratum was sparsely populated, with limited regeneration. This lack of vertical stratification and reduced undergrowth diversity is characteristic of monoculture systems, where dense canopies and allelopathic litter inhibit seedling establishment. Consequently, the pine forest presents a static biomass structure, limited ecological resilience, and constrained potential for long-term carbon accumulation.

In contrast, the agroforestry system supported the highest species richness and structural complexity. It combined timber species such as *T. grandis* and *S. mahagoni* with nitrogen-fixing legumes like *L. leucocephala* and fruit-bearing trees such as *D. zibethinus* and *M. indica*. The pole stratum was well-populated, indicating active regeneration and layered canopy development. This multi-strata configuration allows for efficient resource use, improved soil fertility, and continuous carbon input across different growth stages.

The rubber plantation presented an intermediate pattern, with *H. brasiliensis* as the dominant species, accompanied by scattered individuals of *S. mahagoni*. While this system

was more structurally diverse than the pine forest, it still lacked the species richness and vertical complexity observed in agroforestry. The vegetation profile reflects a production-oriented system, where species selection is driven primarily by economic value particularly latex production rather than ecological function.

These distinctions are reflected in Table 2, which shows higher total biomass and carbon stock in the agroforestry site, particularly within the pole stratum. The results affirm that vegetation composition and structural diversity are central to optimizing carbon storage and should be integral to sustainable land use and climate mitigation strategies.

Dominance of vegetation in each land-use type

Vegetation dominance across the three land-use systems pine forest, agroforestry area, and rubber plantation was shaped by plantation design, species composition, and specific management objectives. As shown in Table 2, the tree stratum consistently contributed the majority of aboveground biomass (AGB) and carbon stock at all sites, reflecting the structural maturity of dominant canopy species. Figure 2 illustrates this trend, where the three layers visually dominate the stacked bars while the contribution of the pole stratum varies. This variation reveals differences in regeneration dynamics and vertical complexity, with profound implications for long-term carbon sequestration and ecosystem resilience, underscoring the importance of this research.

In the pine forest, *Pinus merkusii* was the predominant species, forming a nearly homogeneous stand with large-diameter trees and a dense canopy. These characteristics restricted light availability in the understory, resulting in minimal regeneration and poor pole development. The pole stratum contributed only 3.99 MgB/ha of biomass and 1.87 MgC/ha of carbon—less than 4% of the tree layer's total indicating a sharply skewed structure. Such imbalance is typical of monoculture pine systems, where shade-intolerant secondary species are unable to establish. While these stands can accumulate substantial biomass in mature individuals, they lack vertical diversity and regenerative capacity, reducing their ecological resilience and long-term adaptability.

In contrast, the agroforestry system exhibited a more balanced vertical profile, with significant contributions from both tree and pole strata. Tree biomass reached 125.13 MgB/ha, while pole biomass was the highest among all sites at 50.29 MgB/ha. This structure reflects active regeneration, age diversity, and multi-layered canopy development. Species like *L. leucocephala*, *G. gnemon*, and *T. grandis* were present across strata, supporting ongoing biomass input and ecological succession. The resulting vertical integration enhances resilience, nutrient cycling, and carbon assimilation, establishing agroforestry as a functionally superior system.

The rubber plantation, dominated by *H. brasiliensis*, recorded the highest tree biomass (131.41 mgB/ha) and a moderate contribution from the pole layer (41.80 mgB/ha). The presence of *S. mahagoni* in both strata contributed to limited structural diversity within an otherwise monocultural system. Though less heterogeneous than agroforestry, this configuration still supports modest vertical layering and under-canopy productivity.

Overall, vegetation dominance patterns across land uses reveal that systems with species diversity and well-developed strata, such as agroforestry, achieve superior carbon storage and ecological function. These findings highlight the value of structural complexity in shaping long-term carbon dynamics and land-use sustainability.

Ecological implications of vegetation composition

Variations in species composition among the three land-use types pine forest, agroforestry, and rubber plantation have notable ecological consequences, particularly in terms of biodiversity, structural complexity, and carbon storage potential. This study demonstrates that agroforestry systems, which host a more diverse assemblage of species and a balanced distribution between tree and pole strata, deliver more dynamic and resilient ecological functions than monoculture systems. The resilience of agroforestry systems, even in the face of environmental challenges, should reassure us of their potential to sustain our ecosystems. These compositional differences are reflected not only in the diversity of species but also in the ability of each system to support multi-layered canopies and sustain long-term carbon accumulation.

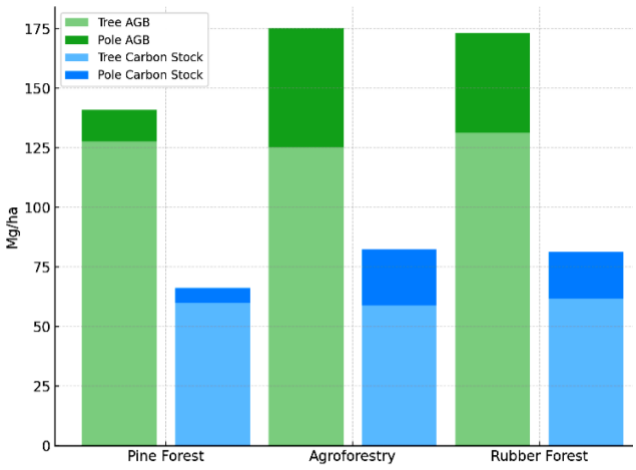

Figure 2. Stacked aboveground biomass and carbon stock by forest

Table 2. Aboveground biomass and carbon stock - tree and pole category (all sites)

Site	Stratum	AGB (MgB/ha)	Carbon stock (MgC/ha)
Pine forest	Tree	127.61	59.95
Pine forest	Pole	13.44	6.32
Agroforestry	Tree	125.13	58.83
Agroforestry	Pole	50.29	23.63
Rubber forest	Tree	131.41	61.76
Rubber forest	Pole	41.80	19.65

As indicated in Table 2, the agroforestry area exhibited the highest combined aboveground biomass and carbon stock, largely due to the strong contribution from the tree stratum (183.96 mgB/ha), with the pole stratum (73.92 mgB/ha) also contributing significantly. This structure reflects a productive overstory coexisting with an actively regenerating understory, resulting in a vertically integrated and ecologically functional system. The coexistence of timber, fruit, and leguminous species promotes niche differentiation, optimizes light capture across canopy layers, and enhances microclimatic buffering factors that collectively improve ecosystem productivity and carbon sequestration (Chave et al. 2005; Ferrini et al. 2020). The presence of nitrogen-fixing plants such as *L. leucocephala* further supports soil fertility and understory development, reinforcing the long-term sustainability of the agroforestry system.

In contrast, the pine forest, although dominated by large trees, lacked species diversity and vertical stratification. Its understory was sparse, resulting in minimal ecological layering and reduced habitat heterogeneity. This system's homogeneity limits its capacity to support broader ecosystem services and increases its vulnerability to pests, climatic stress, and ecological disruption (Han et al. 2019). The rubber plantation, while exhibiting slightly higher diversity than the pine forest with four recorded species and a pole stratum biomass of 40.63 MgB/ha still fell short of agroforestry in both structural richness and regenerative layering. In comparison, the agroforestry site contained 29 species across both strata, with the pole layer alone contributing 73.92 MgB/ha of biomass, indicating a more robust regenerative profile. These differences underscore the superior vertical integration and compositional heterogeneity of agroforestry systems.

Vegetation composition also affects litter quality, soil nutrient cycling, and faunal interactions. In agroforestry systems, the mix of leguminous shrubs, hardwoods, and fruit trees not only sustains high carbon inputs but also supports biodiversity through pollination and seed dispersal networks. The balanced biomass contributions from tree and pole strata enhance structural stability, which may buffer carbon storage under environmental fluctuations (Figure 2).

Ultimately, the ecological integrity and carbon performance of a land-use system are closely linked to its vegetative composition. Diverse, multi-functional systems like agroforestry provide greater long-term benefits by integrating productive and ecological functions within a single landscape framework (Ambarwati et al. 2019; Ferrini et al. 2020).

Aboveground biomass and carbon stock by land-use type

Pine forest

The pine forest site, characterized by a monocultural stand of *P. merkusii*, demonstrated a relatively high accumulation of aboveground biomass primarily concentrated in the tree stratum. As presented in Table 2, tree biomass in this site reached 127.61 MgB/ha, corresponding to a carbon stock of 59.95 MgC/ha. In contrast, the pole stratum contributed only 13.44 MgB/ha (or 6.32 MgC/ha), accounting for less than 10% of the total biomass (Figure 2).

The dominance of the tree stratum is consistent with the plantation's structure, where uniform canopy height, wide spacing, and absence of understory cultivation limit regeneration and pole development. This pattern reflects typical characteristics of conifer-based monocultures in tropical uplands, which tend to produce high per-individual biomass due to rapid trunk expansion but support relatively low structural heterogeneity (Han et al. 2019).

While the total AGB of 141.05 MgB/ha and carbon stock of 66.27 MgC/ha are moderately high, they are lower than those observed in agroforestry and rubber plantation systems (Table 3, Figure 3). This suggests that despite the high biomass per tree, the uniform structure and low undergrowth density limit total site productivity. Similar observations were reported by Ambarwati et al. (2019), where monoculture pine plantations had lower total carbon stock than mixed-species stands of similar age due to their reduced vertical complexity and canopy layering.

Moreover, the limited pole contribution indicates weak regeneration or shade intolerance of young individuals under dense pine canopies. Pine litter, known for its high lignin and resin content, may also inhibit seedling growth and soil microbial activity, thereby reducing below-canopy productivity (Ferrini et al. 2020). This ecological limitation not only affects biomass dynamics but also poses long-term sustainability concerns under climate variability.

Table 3. Comparison of total aboveground biomass and carbon stock per site

Site	Total AGB (MgB/ha)	Total carbon stock (MgC/ha)
Pine forest	141.05	66.29
Agroforestry	175.42	82.46
Rubber forest	173.21	81.41

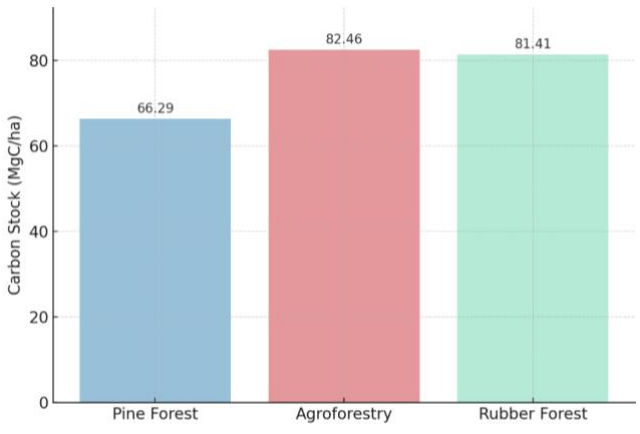

Figure 3. Total carbon stock in each land use type

In terms of carbon sequestration, *P. merkusii* is recognized for its rapid early-stage growth and wood density, contributing effectively to short- to medium-term carbon storage (Siregar 2007). However, the lack of species diversity and multi-age structure in pine forests is a significant constraint, reducing their long-term stability and adaptive capacity. This emphasizes the need for more diverse systems like agroforestry, which can offer more sustained carbon storage. Therefore, while pine forests contribute to immediate biomass accumulation, their ecological and physiological contributions to sustained carbon storage are relatively constrained when compared to more heterogeneous systems like agroforestry.

Agroforestry area

Among the three land-use types examined, the agroforestry site exhibited the highest structural complexity and species richness, which was clearly reflected in its aboveground biomass and carbon storage capacity. As reported in Table 2, the tree stratum contributed 125.13 MgB/ha of biomass and 58.83 MgC/ha of carbon. Notably, the pole stratum yielded 50.29 MgB/ha and 23.63 MgC/ha, making it the most productive understory layer among all studied sites. These values indicate active regeneration and continuous biomass input, highlighting the site's dynamic growth profile and ecological functionality.

The total aboveground biomass and carbon stock at the agroforestry site reached 175.42 MgB/ha and 82.46 MgC/ha, respectively, outperforming both the pine and rubber plantations (Table 3). This elevated accumulation is attributed to the vertically layered structure and diverse species composition specific to the agroforestry system. Within this site, timber species such as *T. grandis*, fast-growing nitrogen-fixing trees like *L. leucocephala*, and fruit trees including *D. zibethinus* and *M. indica* coexisted, creating a mosaic of ecological niches. This botanical diversity supports various growth forms and promotes vertical resource partitioning, thereby enhancing overall system productivity.

The significant biomass contribution of the pole stratum in agroforestry, as shown in Figure 2, indicates active regeneration and ongoing structural renewal. This vertical stratification enhances light interception and spatial resource efficiency, thereby supporting higher net primary productivity (Chave et al. 2005; Ferrini et al. 2020). Moreover, the presence of nitrogen-fixing species such as *L. leucocephala* contributes indirectly to biomass accumulation by enriching soil nutrient levels and promoting the growth of adjacent vegetation (Qiu et al. 2020; Diana et al. 2022).

The distribution of individuals across DBH classes (Figure 3) confirms the presence of a balanced age structure and steady regeneration. Individuals were recorded across all diameter ranges, supporting sustained growth and ecological resilience. This distribution enhances the system's capacity to withstand environmental disturbances such as drought, pests, or selective harvesting (Ambarwati et al. 2019).

In summary, agroforestry effectively integrates productive land use with ecosystem services such as carbon sequestration and biodiversity support. Its high carbon stock, spread across both juvenile and mature strata, demonstrates its potential as a sustainable landscape model and a key strategy for climate change mitigation.

Rubber plantation

The rubber plantation, dominated by *H. brasiliensis*, exhibited the highest total tree biomass among the three land-use systems analyzed. According to Table 2, the tree stratum accounted for 131.41 MgB/ha of aboveground biomass and 61.76 MgC/ha of carbon stock, indicating the strong contribution of mature individuals. The pole stratum also played a meaningful role, contributing 41.80 MgB/ha and 19.65 MgC/ha, which reflects moderate levels of regeneration and a degree of vertical stratification. These figures suggest that while the system remains largely monocultural, it exhibits more structural layering than typically observed in production-focused plantations.

Overall, the site's total aboveground biomass and carbon stock amounted to 173.21 MgB/ha and 81.41 MgC/ha, respectively (Table 3), placing it between the more diverse agroforestry system and the structurally simplified pine forest in terms of carbon storage potential. The high tree biomass corresponds with the mature age of the stand, where most individuals surpass 30 cm in DBH and exhibit uniform stem development. This structural consistency aligns with standard monoculture management for latex harvesting, where stand age and planting density are tightly controlled (Siregar 2007). Nevertheless, the existence of pole-sized individuals implies opportunities for natural regeneration or underplanting.

Visualized in Figure 2, the pole stratum's contribution was greater than in the pine forest, suggesting limited but notable vertical complexity. This may be attributed to the presence of shade or intercrop species such as *S. mahagoni* and *M. indica*, which introduce additional layers and modest ecological benefits. Despite the relatively low species richness, this structural enhancement improves the system's ecological functionality compared to a pure monoculture.

Figure 4 shows a bimodal DBH distribution, with peaks in the 21-30 cm and 31-40 cm classes. This likely results from interplanting or canopy openings that enable light penetration and understory growth. However, the benefits of such a structure are limited by the plantation's simplified species composition and management intensity, which constrain resilience and multifunctionality (Ambarwati et al. 2019; Ferrini et al. 2020). While *H. brasiliensis* provides effective medium-term carbon storage, long-term sustainability may depend on strategies like enrichment planting and the integration of multi-strata vegetation to enhance biodiversity and ecosystem services.

Summary of biomass and carbon stock by stratum

Biomass distribution across tree and pole strata

Stratifying aboveground biomass and carbon stock into tree and pole layers provides valuable insights into the structural maturity and regenerative potential of various land-use types. As shown in Table 2, the tree stratum consistently held the majority of AGB across all sites, indicating the critical role of mature canopy trees in carbon

accumulation. However, the varying contribution of the pole stratum across land uses reveals important differences in age structure, vegetation dynamics, and succession stages. This stratified perspective not only reflects the current biomass profile but also signals each system's capacity to sustain long-term carbon storage.

In the pine forest, biomass distribution was heavily skewed toward the tree layer, which contributed 127.61 mgB/ha, around 90.5% of the site's total AGB. The pole stratum added just 13.44 MgB/ha, highlighting poor regeneration and limited vertical complexity. This pattern, visible in Figure 2, is typical of even-aged monocultures like *P. merkusii*, where dense canopies and allelopathic litter inhibit light penetration and understory establishment (Han et al. 2019). The lack of a robust pole layer indicates reduced ecological succession and poses challenges for future carbon continuity without active management intervention.

In comparison, the agroforestry system displayed a more balanced vertical structure, with 125.13 MgB/ha in the tree layer and 50.29 MgB/ha in the pole stratum, or 28.7% of total AGB. This distribution suggests active recruitment, diverse age classes, and multi-species participation. The presence of fast-growing, nitrogen-fixing species like *L. leucocephala* in the pole layer supports rapid canopy renewal and consistent carbon input from younger cohorts (Qiu et al. 2020; Diana et al. 2022). Such complexity enhances the system's ecological resilience and long-term carbon sequestration potential.

The rubber plantation presented an intermediate scenario. While dominated by *H. brasiliensis*, the inclusion of secondary species like *S. mahagoni* resulted in moderate pole development. Tree biomass reached 131.41 mgB/ha, with 41.80 MgB/ha from the pole stratum, indicating some regeneration and layering, albeit less dynamic than agroforestry. This structure reflects a system with modest potential for enrichment and structural improvement (Ambarwati et al. 2019).

Overall, vertical biomass partitioning serves as a functional indicator of ecological health and carbon sustainability. Agroforestry, with its balanced stratification, exemplifies effective carbon management, whereas systems with limited pole development may face declining resilience and productivity over time (Ferrini et al. 2020).

Contribution of pole stratum to carbon continuity

Although mature trees contribute the majority of current aboveground biomass (AGB), the pole stratum—comprising individuals with diameters at breast height (DBH) between 10-20 cm—plays a crucial role in sustaining carbon stocks over time. As illustrated in Tables 4-6, the pole stratum's biomass contribution varies considerably across land-use types. However, its ecological significance surpasses its numeric share, as it reflects regeneration dynamics, successional progression, and long-term productivity. A well-established pole layer functions as a continuous input source for future canopy biomass, ensuring carbon accumulation persists even as mature trees decline.

In the agroforestry system, the pole stratum contributed 50.29 mgB/ha, or roughly 29% of the site's total AGB, indicating robust regeneration and age diversity. This substantial figure is supported by the presence of fast-growing and multipurpose species such as *L. leucocephala* and *G. gnemon*, which promote rapid biomass accumulation during early growth stages. These species not only enrich the structural diversity but also enhance system resilience by buffering biomass loss from tree harvest or mortality. Such a turnover mechanism supports sustained carbon flux and aligns with ecological models emphasizing functional redundancy and continuity (Chave et al. 2005).

As depicted in Figure 2, the pole layer in agroforestry makes a visually evident and meaningful contribution to total biomass. Trees with varying growth rates and wood densities coexist, supporting complementary roles in carbon dynamics (Diana et al. 2022). In stark contrast, the pine forest exhibited a poorly developed pole stratum, contributing only 13.44 MgB/ha, less than 10% of the total AGB. This structural gap reflects low recruitment and minimal understory activity, increasing the forest's vulnerability to stagnation and long-term decline (Ferrini et al. 2020).

Table 4. Aboveground biomass and carbon stock of pine forest in the tree and pole category

Categories	Family	Local name	Scientific name	Σ individuals	AGB (MgB/ha)	Carbon stock (MgC/ha)
Tree	Pinaceae	Pinus	*Pinus merkusii* Jungh. & de Vriese	106	124.73	58.62
	Fabaceae	Lamtoro	*Leucaena leucocephala* (Lam.) de Wit	1	2.20	1.03
	Meliaceae	Mahoni	*Swietenia mahagoni (L.) Jacq.*	4	0.68	0.32
Pole	Fabaceae	Akasia	*Acacia auriculiformis A.Cunn. ex Benth.*	1	0.01	0.004
	Pinaceae	Pinus	*Pinus merkusii* Jungh. & de Vriese	5	3.99	1.87
	Theaceae	Puspa	*Schima wallichii* (DC.) Korth.	3	2.67	1.25
	Fabaceae	Lamtoro	*Leucaena leucocephala* (Lam.) de Wit	2	1.14	0.54
	Moraceae	Ara	*Ficus carica* L	4	1.35	0.64
	Myrtaceae	Pucuk Merah	*Syzygium paniculatum* Gaertn.	1	0.57	0.27
	Sapindaceae	Rambutan	*Nephelium lappaceum* L.	2	1.42	0.67
	Meliaceae	Mahoni	*Swietenia mahagoni* (L.) Jacq.	9	2.29	1.07

Table 5. Aboveground biomass and carbon stocks of agroforestry areas: tree and pole category

Categories	Family	Local name	Scientific name	Σ individuals	AGB (MgB/ha)	Carbon Stock (MgC/ha)
Tree	Fabaceae	Lamtoro	*Leucaena leucocephala* (Lam.) de Wit	21	28.80	13.54
	Theaceae	Puspa	*Schima wallichii* (DC.) Korth.	1	0.63	0.30
	Meliaceae	Suren	*Toona sinensis* (A.Juss.) M.Roem	2	3.21	1.51
	Malvaceae	Durian	*Durio zibethinus* Murray	10	8.63	4.06
	Gnetaceae	Melinjo	*Gnetum gnemon* Linn.	3	5.17	2.43
	Fabaceae	Petai	*Parkia speciosa* Hassk	2	4.06	1.91
	Lamiaceae	Jati	*Tectona grandis* Linn. F	8	23.83	11.20
	Meliaceae	Mahoni	*Swietenia mahagoni (L.*) Jacq.	5	3.12	1.47
	Fabaceae	Sengon	*Albizia chinensis* (Osbeck) Merr.	4	22.52	10.58
	Myrtaceae	Cengkeh	*Syzygium aromaticum* L.	1	4.16	1.96
	Arecaeae	Kelapa	*Cocos nucifera* L.	5	0.27	0.13
	Lauraceae	Alpukat	*Persea americana* P. Mill	2	9.33	4.39
	Malvaceae	Waru	*Hibiscus tiliaceus* L.	1	0.48	0.23
	Moraceae	Ara	*Ficus carica* L	2	4.79	2.25
	Lamiaceae	Jati Putih	*Gmelina arborea* Roxb. ex Sm.	1	0.43	0.20
	Sapindaceae	Rambutan	*Nephelium lappaceum* L.	3	5.69	2.67
	Fabaceae	Akasia	*Acacia auriculiformis* A. Cunn. ex Benth.	2	0.01	0.00
Pole	Fabaceae	Lamtoro	*Leucaena leucocephala* (Lam.) de Wit	17	25.65	12.05
	Malvaceae	Durian	*Durio zibethinus* Murray	6	6.77	3.18
	Meliaceae	Suren	*Toona sinensis* (A.Juss.) M.Roem	1	0.96	0.45
	Myrtaceae	Cengkeh	*Syzygium aromaticum* L.	4	3.95	1.86
	Gnetaceae	Melinjo	*Gnetum gnemon* Linn.	2	2.22	1.05
	Meliaceae	Mahoni	*Swietenia mahagoni* (L.) Jacq.	2	0.58	0.27
	Malvaceae	Waru	*Hibiscus tiliaceus L.*	1	0.51	0.24
	Fabaceae	Sengon	*Albizia chinensis* (Osbeck) Merr.	5	2.48	1.16
	Euphorbiaceae	Macaranga	*Macaranga* Thouars	5	3.58	1.68
	Moraceae	Nangka	*Artocarpus heterophyllus* Lam.	1	0.36	0.17
	Oxalidaceae	Belimbing wuluh	*Averrhoa bilimbi L.*	2	1.80	0.85
	Lamiaceae	Jati	*Tectona grandis* L.f.	1	0.79	0.37
	Myrtaceae	Jambu Bol	*Syzygium malaccense* (L.) Merr. & L.M.Perry	1	0.34	0.16
	Anacardiaceae	Mangga	*Mangifera indica* L.	1	0.30	0.14

Table 6. Aboveground biomass and carbon stocks of rubber plantations: tree and pole category

Categories	Family	Local name	Scientific name	Σ individuals	AGB (MgB/ha)	Carbon Stock (MgC/ha)
Tree	Euphorbiaceae	Karet	*Hevea brasiliensis* (Willd. ex A.Juss.) Müll.Arg.	159	122.07	57.37
	Meliaceae	Mahoni	*Swietenia mahagoni* (L.) Jacq.	6	9.34	4.39
Pole	Euphorbiaceae	Karet	*Hevea brasiliensis* (Willd. ex A.Juss.) Müll.Arg.	137	40.63	19.10
	Meliaceae	Mahoni	*Swietenia mahagoni* (L.) Jacq.	4	1.17	0.55

The rubber plantation presented an intermediate pattern, with the pole layer contributing 41.80 MgB/ha or 24% of total AGB. Although dominated by *H. brasiliensis*, the inclusion of shade-tolerant or intercrop species lends moderate vertical layering. However, without sustained recruitment of diverse species, the system risks plateauing in its regenerative capacity (Ambarwati et al. 2019). Ecologically, the pole stratum acts both as a buffer that maintains carbon levels during canopy turnover and as a bridge to future tree biomass. Systems with healthy pole populations are better equipped to recover from disturbance and sustain long-term carbon sequestration. Integrating pole strata into monitoring and management strategies is thus essential for accurately forecasting future carbon dynamics (Poorter et al. 2017; Diana et al. 2022).

Structural efficiency in biomass allocation

Structural efficiency in vegetation systems refers to the ability to convert space and light into aboveground biomass through optimized organization of tree diameters, vertical stratification, and canopy height variability. Efficient systems feature well-developed tree and pole strata, enabling active biomass accumulation across multiple age cohorts. This configuration minimizes competition within stands and supports continuous growth, a dynamic process that enhances both carbon capture and long-term ecological productivity. These structural traits are crucial indicators of how well a system can sustain carbon dynamics over time.

Among the land-use types studied, agroforestry demonstrated the highest level of structural efficiency. As

shown in Table 2, biomass was distributed between the tree (125.13 mgB/ha) and pole (50.29 mgB/ha) strata, indicating effective vertical space utilization. Figure 2 illustrates this balance, with stacked bars revealing a well-stratified canopy composed of overstory, sub-canopy, and regenerating individuals. This multi-tiered structure allows for the efficient light interception, reduced self-shading, and continued regeneration, contributing to long-term carbon accumulation (Poorter et al. 2017; Ferrini et al. 2020).

Diameter distribution in agroforestry (Figure 4) further confirms structural density and demographic diversity. High variability in DBH classes supports stand complexity and correlates with greater crown complementarity and spatial efficiency. The coexistence of fast-growing legumes like *L. leucocephala* and dense-wood species such as *T. grandis* and *S. mahagoni* enables both rapid and sustained carbon storage (Chave et al. 2005; Qiu et al. 2020). These synergies reduce the risk of self-thinning and improve resilience to environmental changes.

In comparison, the pine forest exhibited structural stagnation, with 90.5% of its total AGB (127.61 mgB/ha) concentrated in the tree stratum and only 13.44 MgB/ha contributed by the pole layer, despite the presence of 40 individuals in that category (Table 4). The dominance of *P. merkusii* and the narrow DBH distribution indicate limited functional regeneration and inefficient vertical space utilization (Han et al. 2019). Although poles were present, their low biomass contribution suggests poor structural layering, which compromises redundancy and reduces the forest's carbon buffering capacity.

The rubber plantation showed intermediate efficiency. While tree biomass was dominant (131.41 MgB/ha), the pole layer contributed 41.80 MgB/ha, supported by underplanted species like *S. mahagoni*. Despite moderate vertical layering, limited diameter diversity reduced its ecological adaptability (Ambarwati et al. 2019). Overall, agroforestry systems exemplify structural efficiency by combining species diversity, vertical layering, and regenerative dynamics, making them a model for both carbon productivity and sustainability (Diana et al. 2022).

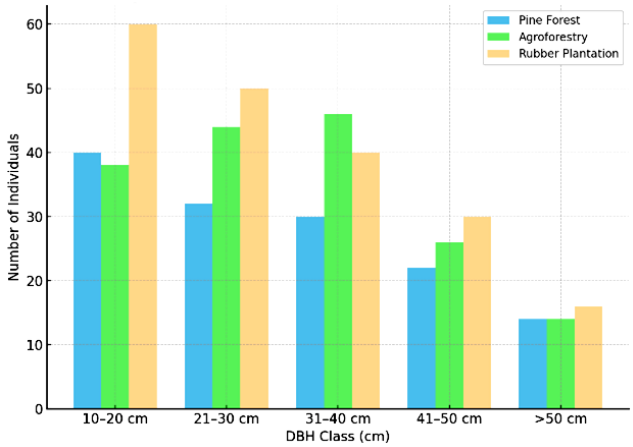

Figure 4. Distribution of DBH class across sites

Management implications of vertical stratification

The vertical stratification of vegetation into tree and pole layers provides essential ecological insights and practical guidance for sustainable land use and forest management. By understanding how aboveground biomass (AGB) and carbon are distributed vertically, land managers can develop more effective strategies to enhance productivity and secure long-term carbon retention. As shown in Table 2, the proportion of biomass within the pole stratum varied notably across land-use types, from just 9.5% in the pine forest to 28.7% in agroforestry. Figure 2 further illustrates these contrasts, underscoring the greater vertical complexity of multi-strata systems. This stratified perspective is crucial for informing carbon monitoring, regeneration planning, and the design of ecosystem service-based incentive schemes.

Incorporating layer-specific data into carbon inventories is essential for capturing the full dynamics of biomass accumulation, particularly in diverse systems like agroforestry. Standard approaches often emphasize mature trees, underrepresenting the pole stratum's contribution to both current biomass and future carbon potential. This study demonstrates that poles can account for up to one-third of AGB, underscoring their ecological and functional significance (Ferrini et al. 2020; Diana et al. 2022). Therefore, carbon assessment protocols especially within frameworks such as REDD+ should adopt stratified reporting to avoid underestimation and better support mitigation strategies (Chave et al. 2005).

The pole stratum also serves as a regenerative buffer that facilitates biomass turnover as older trees senescence or are harvested. In systems where this layer is underdeveloped, such as the pine forest, restoration should prioritize reestablishing pole-sized individuals using practices like enrichment planting, understory release, or gap creation. Selecting fast-growing, mid-canopy and shade-tolerant species can help rebuild vertical complexity and improve future carbon input (Poorter et al. 2017; Ambarwati et al. 2019). These strategies are particularly relevant in degraded sites or aging plantations with limited natural regeneration.

Moreover, vertical stratification provides a foundation for integrating forest management with Payment for Ecosystem Services (PES) and carbon credit initiatives. Agroforestry systems with well-developed strata not only offer high carbon storage but also deliver co-benefits like soil stabilization, habitat provision, and climate regulation. Recognizing the role of the pole layer enhances policy frameworks such as REDD+ benefit-sharing and community forest agreements (Qiu et al. 2020). Lastly, integrating stratification knowledge into training programs can promote more holistic, system-based management approaches, shifting focus from overstory trees to the broader regenerative potential of diverse forest layers.

Comparison of total biomass and carbon stock across sites

Total aboveground biomass by land-use type

The comparison of total aboveground biomass (AGB) among the three land-use types—agroforestry, rubber

plantation, and pine forest reveals notable differences in structural composition and ecological function. As reported in Table 5, agroforestry recorded the highest total AGB at 175.42 MgB/ha, followed closely by the rubber plantation at 173.21 MgB/ha, while the pine forest trailed behind with 141.05 MgB/ha. These variations are not solely a reflection of the land-use category but rather stem from differences in species diversity, stand structure, and vertical stratification.

The agroforestry system's superior biomass accumulation is closely tied to its heterogeneous composition, which includes a mix of fast-growing legumes and long-lived hardwood species. The presence of *L. leucocephala*, *T. grandis*, and *S. mahagoni* creates a layered canopy structure that maximizes vertical light capture and allows for simultaneous growth across multiple strata. This structural complexity supports higher light-use efficiency and stand productivity (Poorter et al. 2017; Qiu et al. 2020). As shown in Table 2 and Figure 2, the relatively balanced contribution of both tree and pole strata illustrates the efficient spatial organization of biomass in agroforestry.

In the rubber plantation, the total AGB was only slightly lower than that of agroforestry, largely due to the mature age and uniform spacing of *H. brasiliensis*. Interplanted hardwoods like Swietenia mahagoni introduced some structural variation, but the biomass remained concentrated in the tree stratum. The system's vertical stratification was less developed, limiting regeneration and understory productivity. Although productive, the plantation exhibits reduced resilience due to limited age diversity and ecological layering (Ambarwati et al. 2019).

The pine forest, dominated by *P. merkusii*, showed the lowest AGB, reflecting its simple, even-aged structure and low wood density. The dense, uniform canopy suppresses understory growth and regeneration, leading to minimal pole development and underutilized vertical space (Han et al. 2019). With biomass concentrated in mature individuals, the system shows signs of stagnation and limited long-term productivity. Overall, these findings suggest that vegetation diversity, structural layering, and species composition are stronger determinants of total biomass than land-use type alone. Agroforestry's combination of regenerative layering and functional diversity makes it a more resilient and sustainable model for carbon accumulation (Chave et al. 2005; Ferrini et al. 2020).

Total carbon stock and sequestration potential

Aboveground carbon stock, derived from biomass (AGB), provides a crucial measure of an ecosystem's capacity to mitigate climate change through carbon sequestration. As presented in Table 6 and illustrated in Figure 3, the agroforestry system recorded the highest carbon stock at 82.46 MgC/ha, followed closely by the rubber plantation with 81.41 MgC/ha. The pine forest exhibited the lowest value at 66.29 MgC/ha. These differences are largely driven by variations in vegetation structure, species diversity, and regeneration dynamics across the three land-use types.

The strong carbon performance of the agroforestry system is closely tied to its rich species composition and vertically stratified structure. The inclusion of fast-growing nitrogen-fixing species such as *L. leucocephala*, high-density hardwoods like *T. grandis* and *S. mahagoni*, as well as *A. chinensis* the third highest contributor to AGB enhances both short-term accumulation and long-term carbon storage (Chave et al. 2005; Diana et al. 2022). Notably, the pole stratum contributes 28.7% of the total biomass, indicating active recruitment and a strong foundation for future carbon input (Table 5). This dynamic structural profile enables agroforestry systems to sustain consistent carbon levels across developmental stages.

Beyond current stock levels, agroforestry demonstrates high potential for long-term carbon sequestration due to its continuous biomass turnover. The coexistence of various growth stages ensures that as mature trees are harvested or decline, younger individuals continue to contribute to the carbon pool. This contrasts with the pine forest, where most carbon is stored in mature *P. merkusii* trees, and little regeneration occurs, resulting in limited future sequestration capacity (Figure 2). The rigidity of such even-aged monocultures restricts adaptability and reduces resilience to environmental change.

The rubber plantation showed carbon stock levels comparable to agroforestry but lacked equivalent structural diversity; the dominance of *H. brasiliensis*, with minimal support from underplanted hardwoods, limits regeneration, and vertical complexity. While productive in the short term, the system's static structure may not sustain carbon levels in the long run without management interventions (Ambarwati et al. 2019; Ferrini et al. 2020).

Overall, these findings highlight the critical role of structural diversity and regenerative layering in sustaining carbon stocks. Agroforestry's combination of high biomass, dynamic structure, and species functionality makes it a strong candidate for inclusion in REDD+ programs and ecosystem-based carbon strategies (Qiu et al. 2020).

Structural and functional basis of biomass differences

Variations in total aboveground biomass (AGB) and carbon stock across land-use types are shaped more by structural traits than by plantation area or age. Key parameters such as diameter at breast height (DBH), tree height, stand density, and species functional diversity play a central role in biomass accumulation. These structural characteristics interact with physiological functions like photosynthesis and nutrient uptake, influencing how efficiently vegetation captures and stores carbon. Therefore, analyzing these traits provides a meaningful framework for assessing the carbon storage capacity of different land-use systems.

The agroforestry system demonstrated the highest total AGB and carbon stock (Table 3), strongly associated with its diverse DBH distribution and vertically layered canopy structure (Figure 2, Figure 4). Trees were represented across a wide range of diameter classes, indicating ongoing recruitment and demographic diversity. This structural layering allows for efficient vertical light use and spatial partitioning, supporting multiple photosynthetic levels (Poorter et al. 2017). Furthermore, the presence of high wood-density species such as *T. grandis* and *S. mahagoni* enhances the amount of carbon stored per unit volume (Chave et al. 2005).

Functionally, the agroforestry system incorporates a mix of fast-growing pioneers like *L. leucocephala*, fruit trees such as *M. indica*, and durable hardwoods. This mixture promotes complementarity in resource use, growth rate, and development stages, contributing to both rapid biomass gain and long-term storage (Qiu et al. 2020; Diana et al. 2022). As a result, agroforestry exhibits high productivity and resilience.

In contrast, the pine forest, dominated by *P. merkusii*, exhibited narrow DBH distribution and limited understory development (Table 2, Figure 4). Biomass was concentrated in a single canopy layer, indicating structural stagnation and low regenerative capacity. The low wood density of *P. merkusii* further limits carbon storage efficiency, explaining the site's lowest AGB and carbon stock values (Han et al. 2019).

The rubber plantation presented an intermediate scenario with broader DBH classes and modest pole contributions. However, dominated by *H. brasiliensis*, the inclusion of intercropped hardwoods added limited structural variation. However, the system's uniform design and mid-range wood density constrain its overall biomass potential (Ambarwati et al. 2019). Land-use systems with greater structural complexity such as agroforestry demonstrate superior carbon storage capacity. These traits support more efficient ecological processes and highlight the value of diversity and layering in sustainable biomass management (Ferrini et al. 2020).

Implications for land-use strategy and carbon policy

The observed variation in aboveground biomass (AGB) and carbon stock across pine forest, agroforestry, and rubber plantation systems has significant implications for land-use planning, forest rehabilitation, and climate policy development. The structural and functional differences between these systems reveal distinct ecosystem services and strategic values, allowing them to be aligned with specific landscape objectives such as carbon sequestration, biodiversity support, and socio-economic resilience. The findings underscore the urgent need for differentiated approaches based on vegetation structure and ecological performance.

Agroforestry emerged as the most effective carbon sink, with the highest AGB (175.42 MgB/ha) and carbon stock (82.46 MgC/ha), alongside rich species diversity and well-developed vertical stratification (Tables 2-3; Figures 2-3). This system supports simultaneous ecological and livelihood goals, making it ideal for buffer zones, community-managed areas, and transition zones at agricultural frontiers. Its layered structure promotes continuous regeneration and stable carbon accumulation while also delivering timber, fruit, and fuelwood. Such multifunctionality aligns with national climate-smart land-use strategies and international initiatives like REDD+ and Payment for Ecosystem Services (PES) (Diana et al. 2022; Ferrini et al. 2020).

The rubber plantation, although largely monocultural, recorded a high carbon stock (81.41 MgC/ha) due to mature tree stands and moderate contributions from the pole layer. The integration of intercrop species such as *S. mahagoni* has added some structural diversity. As a transitional land-use model, rubber plantations hold the potential for enrichment through underplanting and species diversification. When supported by reforestation frameworks such as the Bonn Challenge or Forest Landscape Restoration (FLR), they can evolve into more functionally complex systems with enhanced carbon and biodiversity benefits (Ambarwati et al. 2019).

In contrast, the pine forest, dominated by *P. merkusii*, showed the lowest carbon stock (66.29 MgC/ha) and weak regenerative capacity. Its biomass was concentrated in mature trees with limited understory development and pole presence, resulting in structural stagnation. Rehabilitation strategies such as gap enrichment, selective thinning, and underplanting of broadleaf species could improve its resilience and carbon dynamics (Han et al. 2019; Ferrini et al. 2020). These interventions are suitable for REDD+ readiness efforts, particularly in forest enhancement or restoration contexts.

Policy recommendations based on this analysis include prioritizing agroforestry in multi-functional land-use programs, enhancing rubber plantations for carbon and ecological gains, and investing in structural rehabilitation for pine systems. Integrating vertical stratification data into national monitoring protocols would support more accurate assessments of forest carbon and help optimize climate-related land-use strategies.

Distribution of DBH class across vegetation types

Distribution of DBH classes between sites

Diameter at breast height (DBH) class distribution is a key structural indicator that reveals the age structure, regeneration dynamics, and management effects within different land-use systems. As illustrated in Figure 4, DBH patterns varied markedly across the three sites, indicating differences in stand composition and growth-stage representation. These patterns offer insight into each system's capacity for long-term biomass turnover and carbon storage, as well as its ecological resilience and management needs.

In the pine forest, individuals were heavily concentrated in larger DBH classes (≥31 cm), with minimal representation in the lower diameter ranges (10-20 cm). This pattern reflects the even-aged, mature character of the *Pinus merkusii* monoculture, which is managed primarily for resin and timber extraction. The lack of young stems and a poorly developed understory indicate minimal natural recruitment, likely due to dense canopy closure and allelopathic effects from pine litter (Han et al. 2019). Without interventions such as underplanting or gap creation, this static structure may limit long-term carbon accumulation and reduce the forest's adaptive capacity.

In contrast, the agroforestry system showed a more evenly distributed DBH profile, with a strong presence of individuals in the 10-30 cm range. This distribution reflects ongoing regeneration and the coexistence of multiple growth forms, from juvenile shrubs to mature canopy trees. The presence of fast-growing and nitrogen-fixing species such as *L. leucocephala* enhances the occupation of lower DBH classes, promoting rapid canopy renewal and vertical complexity (Qiu et al. 2020). Such diversity contributes to

biomass turnover and improves resilience to disturbances, supporting long-term ecosystem stability and productivity (Chave et al. 2005; Ambarwati et al. 2019).

The rubber plantation exhibited a moderate DBH distribution, with peaks in the 21-40 cm classes. While *H. brasiliensis* dominated, the inclusion of species like *S. mahagoni* and *M. indica* introduced some variation. Regeneration was more apparent than in the pine forest but remained less dynamic than in agroforestry. The relatively narrow spread of DBH classes suggests limited structural plasticity, which could constrain the system's long-term ecological flexibility (Ferrini et al. 2020).

Overall, DBH class distribution offers a useful lens for assessing forest succession and regenerative capacity. Agroforestry's continuous diameter representation supports its role as a resilient, carbon-rich system, while monocultures like pine forests may benefit from targeted silvicultural interventions to enhance sustainability (Diana et al. 2022).

Correlation of number of individuals and diameter class

The distribution of individuals across diameter at breast height (DBH) classes provides important insights into forest population structure, regeneration status, and long-term sustainability. As shown in Figure 3, each land-use type displayed a distinct DBH pattern, reflecting differences in species composition, management intensity, and stand development. These structural differences influence how biomass is turned over and how carbon is stored or replenished over time. Therefore, DBH class analysis serves as a valuable indicator of ecosystem function, resilience, and future productivity.

In the pine forest, most individuals were concentrated in intermediate DBH classes, peaking at 31-40 cm, with few trees in the smallest class (10-20 cm). This indicates an even-aged structure likely established through a single planting cycle of *P. merkusii*, which dominates the canopy. The scarcity of younger individuals reflects weak regeneration, likely caused by dense canopy cover that restricts light and by allelopathic litter suppressing seedling growth (Han et al. 2019; Ferrini et al. 2020). Such a skewed structure is common in monocultures and signals low capacity for natural succession and long-term carbon continuity.

Conversely, the agroforestry system exhibited a classic inverse-J distribution, with a high number of individuals in the smallest DBH class, gradually declining across larger classes. This structure reflects continuous recruitment and a healthy, multi-aged population. The presence of fast-growing and nitrogen-fixing species like *L. leucocephala* ensures rapid early-stage biomass input while supporting long-term canopy renewal (Qiu et al. 2020; Diana et al. 2022). These conditions contribute to high resilience and sustained ecosystem productivity, positioning agroforestry as a structurally and functionally superior system.

The rubber plantation showed a relatively uniform DBH distribution, with a concentration in the 21-40 cm range, suggesting a synchronized planting history with limited regeneration. While some pole-sized individuals were present, mainly from interplanted species like Swietenia mahagoni, the overall structure lacked the recruitment dynamics seen in agroforestry. This intermediate profile may support stable short-term carbon storage, but without enhanced diversity or undergrowth development, long-term sustainability could be compromised (Ambarwati et al. 2019).

DBH class patterns reveal key aspects of forest dynamics. Systems with continuous diameter distribution, like agroforestry, offer greater ecological stability and long-term carbon potential. At the same time, monocultures with limited size classes may require active intervention to support regeneration and carbon resilience (Poorter et al. 2017).

Structural contributions to biomass and carbon accumulation

Role of tree vs pole

Stratifying vegetation into tree (DBH>20 cm) and pole (DBH 10-20 cm) categories provides a valuable framework for assessing biomass accumulation across developmental stages. As shown in Table 5, the tree stratum consistently accounted for the majority of aboveground biomass and carbon stock across all land-use types. However, the relative contribution of the pole stratum varied widely among the sites, highlighting differences in structural complexity, regeneration potential, and vegetation dynamics. These stratification patterns offer important insights into the long-term sustainability of biomass and carbon storage in different systems.

In the pine forest, the pole stratum contributed only 13.44 MgB/ha, less than 10% of the total AGB, compared to 127.61 MgB/ha from the tree stratum. This imbalance reflects a structurally stagnant monoculture dominated by *P. merkusii*, where dense canopies, thick needle litter, and limited understory light prevent natural regeneration (Han et al. 2019). The near-absence of young individuals in lower strata indicates a discontinuity in biomass input, raising concerns about long-term carbon decline. Without interventions such as underplanting or thinning, the system is at risk of reduced productivity as mature trees age.

In contrast, the agroforestry system showed a much more balanced structure, with the pole stratum contributing 50.29 MgB/ha, approximately 29% of the total AGB. This robust lower layer reflects active recruitment and species turnover, supported by a diverse mix of fast-growing and nitrogen-fixing species like *L. leucocephala*, *G. gnemon*, and *P. speciosa* (Qiu et al. 2020; Diana et al. 2022). The structural layering enhances resilience and enables carbon continuity, ensuring that future canopy layers are already in development. Such dynamic systems maintain long-term biomass productivity and ecological stability.

The rubber plantation exhibited an intermediate pattern, with 41.80 MgB/ha (24% of total AGB) in the pole layer. While *H. brasiliensis* dominates the canopy, the presence of understorey species like *S. mahagoni* and *M. indica* adds structural depth and modest regeneration. Although more flexible than pine systems, its stratification is still less dynamic than agroforestry (Ambarwati et al. 2019).

Figure 2 visually confirms these differences, emphasizing the pole layer's ecological significance. Serving as both buffer and bridge, the pole stratum stabilizes current carbon

stocks while supporting future canopy development. Its presence is crucial for sustaining biomass continuity and resilience in multi-layered forest landscapes.

Impact of species composition and wood density

Species composition and wood density (ρ) are fundamental factors influencing aboveground biomass and carbon storage potential. Variations in these attributes across different land-use types significantly shape biomass structure and accumulation efficiency, as reflected in Table 5 and Figure 4. Wood density, in particular, is directly correlated with carbon content per unit volume, meaning that ecosystems dominated by high-density species tend to store more carbon over time (Chave et al. 2005). Therefore, both the diversity and functional traits of species present in a system play pivotal roles in determining its carbon sequestration capacity.

The agroforestry system demonstrated the highest AGB (175.42 MgB/ha) and carbon stock (82.46 MgC/ha), supported by its diverse species assemblage. It included fast-growing nitrogen-fixing legumes (*L. leucocephala*), fruit-bearing trees (*D. zibethinus*, *M. indica*), and high-density hardwoods like *T. grandis* and *S. mahagoni*. This combination allows for rapid biomass accumulation in early growth stages while ensuring long-term carbon stability due to the presence of dense, slow-growing species. The functional complementarity between species with differing growth rates and wood densities enhances both temporal and vertical occupation of space, leading to greater ecosystem productivity and resilience (Poorter et al. 2017; Diana et al. 2022).

By contrast, the pine forest, dominated by Pinus merkusii, exhibited a lower total AGB (141.05 MgB/ha) and carbon stock (66.29 MgC/ha). Despite some individuals reaching large sizes, the relatively low wood density of this softwood species limits its carbon storage efficiency. Furthermore, the system's structural uniformity and lack of understorey diversity reduce the potential for complementary resource use, regeneration, and long-term carbon gain (Siregar 2007; Ferrini et al. 2020).

The rubber plantation presented an intermediate scenario. While *H. brasiliensis* contributes most of the biomass with its moderate wood density, the inclusion of species like *S. mahagoni* in the pole layer enhances density variation and structural heterogeneity. This results in a respectable AGB (173.21 MgB/ha) and carbon stock (81.41 MgC/ha), though still less dynamic than agroforestry in terms of ecological function.

Ultimately, systems with diverse species composition and a range of wood densities, such as agroforestry, offer greater carbon sequestration potential through both rapid initial accumulation and sustained long-term storage. In contrast, low-diversity monocultures lack these synergies, reducing their ecological efficiency under changing environmental conditions.

Stacked AGB and carbon stock per stratum

Figure 2 effectively visualizes the relative contributions of tree and pole strata to total aboveground biomass and carbon stock through stacked bar charts for each land-use type. These graphics complement the numerical data in Table 2, offering a clear comparison of vertical biomass distribution. By distinguishing the contributions of each stratum, the figure highlights differences in structural complexity, regeneration dynamics, and carbon storage efficiency among systems. This visual approach is particularly helpful in conveying ecological patterns that may not be immediately evident from tabular data alone.

In the pine forest, the chart clearly shows the overwhelming dominance of the tree stratum, with the pole layer forming only a minor component. This top-heavy structure reflects the homogeneity of the *P. merkusii* monoculture, where dense canopy cover and low understory light limit the development of lower vegetation layers. While such stands can accumulate significant biomass early in their growth cycle, the lack of regeneration diminishes long-term carbon sustainability (Han et al. 2019; Ferrini et al. 2020). Over time, this structural limitation reduces resilience as the forest becomes increasingly dependent on aging canopy trees.

The agroforestry system, in contrast, presents a more balanced vertical structure, as seen in the near-proportional stacking of tree and pole biomass in Figure 2. With 125.13 MgB/ha in trees and 50.29 MgB/ha in poles (Table 2), the system supports continuous recruitment and multi-aged stand development. This configuration promotes long-term carbon storage through sustained turnover and supports ecosystem functions such as nutrient cycling and biodiversity conservation (Chave et al. 2005; Qiu et al. 2020). The visual harmony between strata underscores the structural efficiency and ecological value of agroforestry systems.

The rubber plantation falls between the two extremes. Although dominated by *H. brasiliensis* with 131.41 MgB/ha in the tree stratum, the pole layer contributes a notable 41.80 MgB/ha, forming a visible secondary tier in the chart. The presence of shade species like *S. mahagoni* enhances vertical complexity and suggests moderate regenerative activity (Ambarwati et al. 2019). Overall, Figure 2 visually affirms that systems with more evenly stratified biomass, such as agroforestry, tend to be more productive, adaptive, and carbon-efficient.

Physiological interpretation and ecological implications

Relationship between DBH, tree age, plant type, and carbon stock

Diameter at breast height (DBH) is a widely used structural indicator in forest ecology, closely linked to aboveground biomass and carbon stock accumulation. As shown in Table 2 and calculated using the species-specific allometric models in Table 1, DBH is a key variable in estimating tree biomass due to its strong correlation with stem volume and woody tissue density. This non-linear relationship means that larger DBH values often translate into disproportionately higher carbon content, though wood density also plays a significant role (Chave et al. 2005). Evaluating DBH distribution across land-use types thus offers insight into stand development, regeneration dynamics, and carbon sequestration potential.

In the pine forest, large DBH values were primarily associated with *P. merkusii*, a fast-growing species with tall, slender stems. Although these trees contribute significantly to total biomass due to their size, their softwood characteristics result in lower carbon density per unit volume (Siregar 2007). The narrow DBH distribution and limited presence of smaller stems suggest minimal recruitment, highlighting a structurally stagnant stand dominated by a single cohort. This uniformity reduces both structural resilience and long-term carbon continuity.

By contrast, the agroforestry system exhibited a wide distribution of DBH classes, indicating active regeneration and species turnover. Lower DBH classes included fast-growing pioneers such as *L. leucocephala* and *G. gnemon*, while high-density hardwoods like *T. grandis* and *S. mahagoni* occupied the upper classes. This diversity reflects functional complementarity among species, allowing the system to capture carbon quickly in the early stages while maintaining long-term carbon reserves in slower-growing, dense-wood trees (Poorter et al. 2017; Diana et al. 2022). Such multi-stage development supports greater ecosystem productivity and stability.

In the rubber plantation, *H. brasiliensis* was dominant in the middle DBH classes, offering steady biomass contribution but limited structural variation. While interplanted species such as *S. mahagoni* provide some enrichment, the overall functional diversity is lower than in agroforestry (Ambarwati et al. 2019). As a result, the system performs well in current carbon storage but lacks the regenerative layering needed for long-term sequestration.

These findings emphasize the combined importance of DBH, species identity, and wood density in determining carbon storage. Agroforestry's integration of diverse DBH classes and wood densities explains its superior carbon accumulation, as reflected in Table 3 and Figure 3.

Physiological influences: Stomata, canopy density, and productivity

Structural parameters such as DBH, height, and biomass are physical manifestations of underlying physiological traits, particularly those associated with canopy architecture, stomatal regulation, and photosynthetic capacity. These physiological mechanisms influence how vegetation captures light, regulates water loss, and absorbs nutrients, ultimately shaping aboveground biomass accumulation and carbon storage across different land-use systems. Differences in carbon sequestration performance among the sites studied can be attributed to how effectively each system converts environmental resources into plant biomass through these physiological pathways. Consequently, evaluating structure offers a window into the functional performance of each vegetation type.

Among the three land-use systems, the agroforestry site exhibited the highest total AGB and carbon stock, as supported by Table 3 and Figure 3. This result reflects the system's multi-layered canopy and species diversity, which enhance vertical light distribution and minimize shading redundancy. Trees with varying heights and crown shapes such as *L. leucocephala*, *S. mahagoni*, and *M. indica* optimize the use of solar radiation across the vertical profile. Such vertical stratification allows for more sustained photosynthesis and biomass accumulation throughout different canopy layers (Poorter et al. 2017; Ferrini et al. 2020).

Physiologically active species in agroforestry, including *L. leucocephala*, *P. speciosa*, and *G. gnemon*, are known for high stomatal density and transpiration rates. These characteristics promote efficient carbon assimilation and nutrient cycling, especially under favorable moisture conditions. Their presence in the pole stratum supports rapid turnover and regeneration, allowing the system to maintain productivity and carbon input across successional stages (Qiu et al. 2020; Diana et al. 2022). This physiological dynamism is key to the resilience of agroforestry under fluctuating environmental conditions.

In contrast, the pine forest dominated by *P. merkusii* is characterized by a closed, coniferous canopy with low stomatal conductance. Although efficient under water-limited conditions, this conservative strategy limits long-term carbon gain and regeneration. The dense needle-leaf canopy also blocks light from reaching lower strata, suppressing understory growth and physiological activity (Han et al. 2019). This explains the low pole biomass and stagnant productivity observed in Table 2 and Figure 2.

The rubber plantation represents an intermediate case, where *H. brasiliensis* shows moderate stomatal behavior and an open crown. While this supports steady carbon assimilation, the plantation lacks the physiological and structural diversity needed for high ecological resilience (Ambarwati et al. 2019). Overall, the synergy of structural complexity and physiological variation in agroforestry provides superior conditions for efficient and sustained carbon sequestration.

Land-use management and carbon sequestration potential

Agroforestry as the highest carbon absorption system

The findings of this study highlight the superior carbon sequestration performance of agroforestry systems, reinforcing their relevance for sustainable land-use planning and climate change mitigation. As indicated in Table 3, the agroforestry area recorded the highest total aboveground biomass (175.42 MgB/ha) and carbon stock (82.46 MgC/ha) among the three land-use types. These values surpass those of the rubber plantation (81.41 MgC/ha) and pine forest (66.29 MgC/ha), with Figure 3 clearly showing agroforestry's dominant position in carbon accumulation. Such outcomes underscore the ecological and functional advantages of structurally diverse vegetation systems.

These results can be directly attributed to the structural and compositional characteristics of agroforestry. The presence of multiple canopy layers, species diversity, and nitrogen-fixing plants such as *L. leucocephala* enhances nutrient cycling, improves soil fertility, and supports continuous biomass input from various growth stages (Qiu et al. 2020; Diana et al. 2022). This diversity of form and function contributes to stable and efficient carbon assimilation, making agroforestry systems more resilient to disturbances such as drought, pests, or harvesting events.

The system's regenerative potential is particularly important for maintaining long-term carbon stocks.

Unlike monocultures, which are typically uniform in age and canopy structure, agroforestry integrates trees, poles, shrubs, and herbaceous species in complementary arrangements. This spatial and functional integration increases light interception, root overlap, and water-use efficiency, resulting in higher total productivity and carbon gain (Chave et al. 2005; Poorter et al. 2017; Ferrini et al. 2020). Agroforestry's heterogeneity also supports biodiversity and enhances ecological resilience, contributing to its multi-functional value.

Beyond carbon storage, agroforestry systems offer co-benefits, including biodiversity conservation, livelihood diversification, and improved soil health. These characteristics make agroforestry a strategic land-use model for community-based forest management and national carbon offset initiatives. As Ambarwati et al. (2019) suggest, well-managed agroforestry systems can rival natural forests in ecological productivity and sustainability.

However, the widespread adoption of agroforestry as a carbon mitigation strategy requires supportive institutions, targeted training, and incentive-based policy frameworks. Integrating agroforestry into climate-smart initiatives such as REDD+ and Payment for Ecosystem Services (PES) could enhance its value within carbon markets and rural development agendas (Diana et al. 2022). From a management perspective, prioritizing agroforestry in landscape restoration programs could yield dual benefits: restoring degraded lands and stabilizing carbon stocks through structurally and functionally complex vegetation systems.

Recommendations for heterogeneous vegetation management

The findings of this study reaffirm the critical role of vegetation heterogeneity, most clearly exemplified in the agroforestry system, as a primary driver of aboveground biomass accumulation and long-term carbon storage. Systems characterized by diverse species compositions, layered vertical structures, and functional complementarity consistently outperform homogeneous plantations in carbon sequestration capacity. The stratified biomass and carbon data presented in Table 2, alongside total site comparisons in Table 3, demonstrate that structurally complex vegetation supports more effective carbon capture. Visual evidence from Figure 2 reinforces this, showing balanced contributions from both tree and pole strata in agroforestry, while monoculture systems like pine forests rely heavily on a single dominant layer. This highlights the importance of designing and managing landscapes with vertical complexity and species interactions in mind.

To maintain and enhance such beneficial heterogeneity, several strategic recommendations can be proposed. First, the integration of mixed-species planting schemes should be encouraged, combining fast-growing pioneers, nitrogen-fixing legumes, and high-density timber species such as *L. leucocephala*, *S. mahagoni*, and *T. grandis*. This combination balances rapid early-stage biomass accumulation with long-term carbon stability. Second, functional layering must be maintained, ensuring that tree, pole, and understory strata remain active. Over-pruning or canopy homogenization should be avoided, as diverse vertical layers enhance light use efficiency and support natural regeneration processes. Third, the role of the pole stratum must be recognized and protected. As shown in this study, poles contribute significantly to biomass and act as a buffer for future carbon input, yet they are often underrepresented in forest inventories and management practices.

Furthermore, successful system design should be guided by ecological succession, allowing for a gradual transition from early-successional species to structurally and functionally dominant late-successional trees. Management should also be adapted to site-specific landscape contexts, taking into account variables such as slope, soil fertility, and local biodiversity. These factors influence both structural development and carbon dynamics. From a policy perspective, incorporating carbon stock and vegetation structure into land-use regulations can support more informed and targeted investment, especially within REDD+ and climate-smart agriculture initiatives. Finally, agroforestry should be promoted as a leading model for carbon-smart landscapes. Its demonstrated performance in carbon stock, vertical integration, and resilience makes it ideal for rehabilitation efforts, particularly in upland tropical regions. Through these measures, land managers and policymakers can foster multi-functional systems that deliver both ecological restoration and climate mitigation benefits.

In conclusion, this study demonstrated that land-use systems with greater structural and species heterogeneity, particularly agroforestry, are more effective in accumulating aboveground biomass and sequestering carbon than monoculture plantations. Among the three evaluated land-use types in Ngargoyoso Sub-district, agroforestry recorded the highest total biomass (175.42 MgB/ha) and carbon stock (82.46 MgC/ha), followed by rubber plantation and pine forest. This superior performance is attributed to its multi-strata structure, functional species diversity, and balanced contributions from both tree and pole strata. Vegetation characteristics such as DBH, wood density, and vertical stratification were found to be closely associated with physiological processes, including photosynthesis, canopy efficiency, and regeneration potential. Systems dominated by single-aged or softwood species, like Pinus merkusii, accumulated less carbon and showed lower regenerative capacity, whereas systems integrating fast-growing pioneers and dense hardwoods showed sustained carbon accumulation and structural renewal. Stacked biomass data and DBH class distributions revealed that pole strata play a critical role in maintaining carbon continuity, especially in heterogeneous systems. Furthermore, species composition influenced not only total biomass but also the ecological resilience and adaptability of the system to long-term environmental change. The findings highlight agroforestry as a promising land-use model for integrated carbon management and biodiversity conservation. Promoting structurally diverse vegetation through informed management strategies can enhance carbon sequestration, ecosystem services, and landscape resilience in tropical upland regions. These insights are essential for shaping effective

climate-smart land-use policies and sustainable forest development programs.

REFERENCES

Adinugroho WC. 2001. Model Pendugaan Biomassa Pohon Mahoni (*Swietenia macrophylla* King) di Atas Permukaan Tanah. Pusat Litbang Hutan Tanaman. Bogor. [Indonesian]

Alinus, Rafdinal, Riza L. 2017. Biomassa dan cadangan karbon di kawasan agroforestri karet tradisional di Desa Nanga Pemubuh Kecamatan Sekadau Hulu Kabupaten Sekadau. Jurnal Protobiont 6 (3): 249-254. [Indonesian]

Ambarwati A, Duryat D, Hidayat W. 2019. INP vegetasi dan karbon tersimpan pada HKM Bina Wana Kecamatan Kebun Tebu Kabupaten Lampung Barat. Jurnal Hutan Tropis 7 (2): 112-119. DOI: 10.29303/jbl.v2i2.127. [Indonesian]

Arupa. 2014. Proyeksi Cadangan Karbon Hutan Rakyat Desa Terong, Kecamatan Dlingo, Kabupaten Bantul. Biro Penerbit Arupa, Sleman. [Indonesian]

Bachtiar B, Resti U. 2017. Pengaruh tegakan lamtoro gung *Leucaena leucocephala* L. terhadap kesuburan tanah di Kawasan Hutan Ko'mara Kabupaten Takalar. Jurnal Ilmu Alam dan Lingkungan 8 (15): 1-6. [Indonesian]

BPS [Badan Pusat Statistika]. 2021. Kecamatan Ngargoyoso Dalam Angka 2021. Badan Pusat Statistika, Jakarta. [Indonesian]

Banaticla. 2023. Carbon Storage of Land Cover Types in The Western Margin of Mt. Makiling, Laguna, Philippines.

Chave J, Andalo C, Brown S, Cairns MA, Chambers JQ, Eamus D, Fölster H, Fromard F, Higuchi N, Kira T, Lescure J-P, Nelson BW, Ogawa H, Puig H, Riéra B, Yamakura T . 2005. Tree allometry and improved estimation of carbon stocks and balance in tropical forests. Oecologia 145: 87-99. DOI: 10.1007/s00442-005-0100-x.

Dewa DD, Sejati AW. 2019. Pengaruh perubahan tutupan lahan terhadap emisi GRK pada wilayah cepat tumbuh di Kota Semarang. Jurnal Penginderaan Jauh Indonesia 1: 24-31. DOI: 10.12962/jpji.v1i1.254. [Indonesian]

Diana R, Situmorang O, Hastaniah, Sutedjo, Boer C. 2022. Estimasi karbon stok pada pepohonan di Arboretum Laboratorium Sumberdaya Hayati Kalimantan (LSHK), Universitas Mulawarman Samarinda. Jurnal Tengkawang 12 (1): 105-115. [Indonesian]

Ferrini F, Fini A, Mori J, Gori A. 2020. Role of vegetation as a mitigating factor in the urban context. Sustainability 12 (10): 4247. DOI: 10.3390/su12104247.

Hairiah K, Sitompul SM, Noordwijk MV, Palm C. 2001. Methods for Sampling Carbon Stocks Above and Below Ground. ASB Lecture Note ICRAF, Bogor.

Han ES, Goleman D, Boyatzis R, Mckee A. 2019. Lahan dan Hutan Dalam Skala Besar. J Chem Inform Model 53 (9): 1689-1699.

Hendri. 2001. Analisis Emisi dan Penyerapan Gas Rumah Kaca (Baseline) dan Evaluasi Teknologi Mitigasi Karbon Di Wilayah Perum Perhutani. [Master Thesis]. Program Pasca Sarjana Institut Pertanian Bogor, Bogor. [Indonesian]

Ilyas S. 2013. Carbon sequestration and growth of stands of *Cassia siamea* Lamk. in Coal mining reforestation area. Indian J Sci Technol 6: 5405-5410. DOI: 10.17485/ijst/2013/v6i11.1.

Ketterings QM, Coe R, Noordwijk MV, Ambagau Y, Palm CA. 2001. Reducing uncertainty in the use of allometric biomass equations for predicting above-ground tree biomass in mixed secondary forest. For Ecol Manag 146: 199-209. DOI: 10.1016/S0378-1127(00)00460-6.

Minarno PE. 2022. Upaya Pengelolaan Lahan Untuk Pengendalian Erosi dan Peningkatan Cadangan Karbon di Kecamatan Ngargoyoso Kabupaten Karanganyar. [Dissertation]. Universitas Sebelas Maret, Surakarta. [Indonesian].

Poorter L, van der Sande MT, Arets EJ et al. 2017. Biodiversity and climate determine the functioning of Neotropical forests. Glob Ecol Biogeogr 26 (12): 1423-1434. DOI: 10.1111/geb.12668.

Praseti H, Riduan R, Annisa N. 2018. Variasi kemampuan beberapa jenis pohon dalam menyerap CO_2 pada taman Kota Banjarbaru. Jurnal Teknik Lingkungan 4 (2): 72-76. DOI: 10.20527/jukung.v4i2.6586. [Indonesian]

Qiu Z, Feng Z, Song Y, Li M, Zhang P. 2020. Carbon sequestration potential of forest vegetation in China from 2003 to 2050: Predicting forest vegetation growth based on climate and the environment. J Clean Product 252: 119715. DOI: 10.1016/j.jclepro.2019.119715.

Samsu AKA. 2019. Pendugaan potensi simpanan karbon permukaan pada ruang terbuka hijau di Hutan Kota Jompie Kecamatan Soreang Kota Parepare. Jurnal Envisoil 1: 34-43. DOI: 10.26618/jlinears.v1i1.1321. [Indonesian]

Sanjaya ZT, Kurniawan E. 2021. Analisis perubahan perkebunan dan hutan menjadi tempat wisata di Kecamatan Ngargoyoso Kabupaten Karaganyar. Geo Image (Spatial-Ecological-Regional) 10: 149-157.

Siregar CA. 2007. Pendugaan biomasa pada hutan tanaman pinus (*Pinus merkusii* Jungh et de Vriese) dan konservasi karbon tanah di Cianten, Jawa Barat. Jurnal Penelitian Sosial dan Ekonomi Kehutanan 4 (3): 251-266. DOI: 10.20886/jphka.2007.4.3.251-266. [Indonesian]

Syah RF. 2017. Analisa kebijakan sektor lingkungan: Permasalahan implementasi kebijakan pengelolaan Kawasan Hutan di Indonesia. J Govern 2 (1): 2-17. DOI: 10.31506/jog.v2i1.2117. [Indonesian]

Utami N, Himawati S, Handayani DP, Surachman M, Tanjung A, Royani JI. 2020. Keberhasilan stek tanaman lamtoro varietas tarramba (*Leucaena leucocephala* cv. Tarramba) karena pengaruh umur fisiologis dan zat pengatur tubuh. Pastura 10 (1): 42-45. DOI: 10.24843/Pastura.2020.v10.i01.p10. [Indonesian]

Wijayanto N, Prasetyo A. 2021. Struktur vegetasi, komposisi, dan serapan karbon pekarangan di Desa Duyung, Kecamatan Trawas, Kabupaten Mojokerto. Jurnal Silvikultur Tropika 12 (3): 144-150. DOI: 10.29244/j-siltrop.12.3.144-150. [Indonesian]

CELL BIOLOGY & DEVELOPMENT
Volume 9, Number 1, June 2025
Pages: 54-63

E-ISSN: 2580-4499
DOI: 10.13057/cellbioldev/v090105

Integrated application of granular and liquid bioorganic fertilizers improves corn productivity and soil fertility in light chestnut soils

KUANYSH KARABAYEV[1,♥], BEIBUT SULEIMENOV[2], YERSULTAN SONGULOV[2], ULAN AKHMURZIN[1], ASHIRALI SMANOV[3]

[1]LLP- Kazakh Research Institute of Agriculture and Plant Growing. Almaty Region, Kazakhstan. Tel.: +7-72771-53130, ♥email: kuanish_kz_92@mail.ru
[2]U. Uspanov Kazakh Research Institute of Soil Sciences and Agrochemistry. Almaty, Kazakhstan
[3]Kazakh National Agrarian University. Almaty, Kazakhstan

Manuscript received: 16 December 2024. Revision accepted: 7 June 2025.

Abstract. *Karabayev K, Suleimenov B, Songulov Y, Akhmurzin U, Smanov A. 2025. Integrated application of granular and liquid bioorganic fertilizers improves corn productivity and soil fertility in light chestnut soils. Cell Biol Dev 9: 54-63.* This study evaluated the effectiveness of integrated granular and liquid bioorganic fertilizers in enhancing soil fertility and corn (*Zea mays*) productivity on light chestnut soils in the Agopark Ontusik region. Field experiments were conducted using three rates of granular organic fertilizer (0, 1000, and 2000 kg ha^{-1}) combined with four concentrations of a humic-based foliar biostimulant (0, 2, 4, and 6 mL L^{-1}). Agronomic performance was assessed through vegetative traits, biomass accumulation, yield components, and grain productivity. Soil fertility parameters and economic profitability were also evaluated. The results showed that both fertilizer types significantly improved plant height, leaf area, and biomass, with the highest values recorded under the combined treatment of 2000 kg ha^{-1} + 6 mL L^{-1}. Grain yield increased from 7.4 t/ha in the control to 13.5 t/ha in the best treatment. Available phosphorus (P_2O_5) in the topsoil rose from 14.0 to 26.0 mg/kg, while exchangeable potassium (K_2O) declined due to high plant uptake. Economic analysis revealed that the most intensive treatment produced the highest net income (339,520 tenge/ha) and lowest cost per 100 kg of grain (2,519 tenge). Correlation analysis confirmed strong associations between biomass and yield, highlighting the importance of balanced nutrient supply. These findings demonstrate that bioorganic fertilization strategies are effective in restoring fertility and improving productivity on marginal soils, offering a sustainable alternative to conventional inputs in dryland cropping systems.

Keywords: Bioorganic fertilizer, corn, dryland, humic substances, soil fertility, sustainable agriculture

INTRODUCTION

Sustainable intensification of agricultural production remains a central challenge in semi-arid and dryland regions worldwide, where land degradation, declining soil fertility, and climatic variability threaten crop productivity and food security (Tefera et al. 2024). In such environments, soils are often characterized by poor physical structure, low organic matter, and limited nutrient retention capacity, making them marginal for intensive farming. These constraints are particularly pronounced in Central Asia, where vast areas are dominated by light chestnut soils with inherently low humus content, poor buffering capacity, and rapid nutrient leaching. Managing crop production in these soils requires targeted interventions that enhance both soil fertility and plant resilience to abiotic stress (Pankova and Chernousenko 2018).

Corn (*Zea mays* L.) is a globally important cereal crop with wide ecological adaptability and high economic value (Edmeades et al. 2017). Its cultivation has expanded into marginal zones, including light chestnut soil areas of Kazakhstan, Uzbekistan, and other Central Asian countries (Samenova 2024). However, the success of maize production in such fragile environments depends on improving nutrient availability, rooting conditions, and soil biological activity. Traditional approaches relying on high rates of mineral fertilizers have shown diminishing returns in these systems, with growing evidence of long-term soil degradation and ecological disruption. Therefore, there is a growing interest in bioorganic fertilization approaches that combine the benefits of organic matter input and biologically active compounds to restore soil functionality and support crop productivity (Wu et al. 2024).

Bioorganic fertilizers, particularly those containing humic substances, have been widely recognized for their ability to improve soil fertility and plant growth through multiple mechanisms (Gao et al. 2020). Humic acids, fulvic acids, and associated organic compounds function as natural biostimulants that enhance nutrient uptake, promote root elongation, improve cell permeability, and regulate hormone-like activity in plants. These substances also stimulate microbial activity and soil enzymatic functions, creating favorable conditions for nutrient cycling and organic matter stabilization. Several studies have reported that humic-based amendments increase photosynthetic efficiency, improve drought tolerance, and accelerate reproductive development in cereals and other field crops (Rigobelo 2024).

In addition to soil application, foliar delivery of humic-based liquid bioorganic formulations has shown promise in enhancing nutrient absorption and plant vigor, particularly under limiting soil conditions. Foliar-applied humic substances can bypass root zone constraints and directly influence metabolic processes in leaves, leading to improved chlorophyll

synthesis, stomatal conductance, and assimilate partitioning (Tambhekar 2013). When applied in combination with soil-applied organic fertilizers, such strategies may yield synergistic effects by concurrently enhancing soil structure and nutrient mobility while promoting efficient nutrient use aboveground (Srivastava and Ngullie 2009).

Despite the growing body of evidence supporting the use of humic-based biofertilizers, field-level studies evaluating their combined impact with granular organic inputs on maize productivity, soil nutrient dynamics, and economic returns remain limited especially in the context of light chestnut soils. These soils, common across the dry steppe zones of Central Asia, are known for their low Cation Exchange Capacity (CEC), weak structural stability, and rapid moisture loss. Their management requires inputs that not only supply nutrients but also improve organic matter retention and biological functioning. Previous findings suggest that organic fertilizers can gradually increase soil humus and microbial biomass, while humic-based foliar applications provide immediate physiological benefits to plants (Lumactud et al. 2022). However, studies quantifying the interaction of both approaches under field conditions, particularly on marginal soils, are scarce.

Furthermore, the long-term sustainability of any fertilization strategy must be assessed in relation to its economic feasibility. Smallholder and commercial farmers alike require solutions that improve yields without imposing excessive costs or labor burdens. Although organic inputs are often perceived as more expensive than conventional fertilizers, they may offer better cost-effectiveness over time by improving input-use efficiency and reducing environmental risks. Therefore, assessing profitability indicators such as net income, input-output ratios, and unit production cost is essential for informing adoption decisions (Tellarini and Caporali 2000).

In this study, we investigate the agronomic and economic effects of integrating granular organic fertilizer with a humic-based liquid biostimulant on corn growth, yield, soil fertility, and profitability in the Agropark Ontusik Region, which is representative of light chestnut soil agroecosystems. Specifically, this study aims to (i) assess the response of vegetative and reproductive traits of maize to different treatment combinations, (ii) evaluate changes in topsoil nutrient availability and organic matter following fertilization, (iii) determine correlations between biomass and yield performance, and (iv) analyze economic viability of each fertilization regime. The results are expected to inform best practices for maize cultivation in dryland areas with similar soil limitations and contribute to broader efforts in agroecological intensification.

MATERIALS AND METHODS

Study site description

The experiment was conducted at Agropark Ontustik, located in the Almaty region of Southeast Kazakhstan (coordinates: 43.2589° N, 76.9151° E). The area experiences a semi-arid continental climate characterized by distinct seasonal temperature variations and limited precipitation. The average annual temperature is approximately 7.8°C, with July as the warmest month averaging 22.1°C, and January as the coldest with an average of -7.9°C. Total annual rainfall averages 494 mm, with the majority falling during spring (April-May), while late summer and early autumn are relatively dry (Ualiyeva et al. 2022).

The soil in the experimental area is classified as light chestnut soil, a common soil type in Central Asian semi-arid steppes. These soils exhibit a loamy texture with low organic matter content, typically ranging from 1.8% to 1.9% humus in the topsoil. The soil pH is alkaline, between 8.8 and 8.9, reflecting high base saturation but also indicating limited nutrient availability in certain forms. Light chestnut soils generally have low Cation Exchange Capacity (CEC) and poor moisture retention, contributing to rapid nutrient leaching and posing challenges for sustainable crop production (Chatzistathis et al. 2021).

Such edaphic characteristics render these soils vulnerable to degradation under intensive cropping systems, necessitating tailored fertility management strategies to maintain soil health and productivity (Khan 2024). The experimental site's climatic and soil conditions make it representative of marginal dryland agroecosystems where innovative bioorganic fertilization methods may offer agronomic and environmental benefits.

Experimental design and treatment structure

The field experiment was arranged in a factorial Randomized Complete Block Design (RCBD) with three replications. Two factors were tested: Granular Organic Fertilizer (GOF) and Liquid Bioorganic Fertilizer (LBF). The GOF was applied at three rates: G0 (0 kg ha^{-1}, control), G1 (1000 kg ha^{-1}), and G2 (2000 kg ha^{-1}). The LBF factor consisted of four concentrations of BioEcoGum: P0 (0 mL L^{-1}, control), P1 (2 mL L^{-1}), P2 (4 mL L^{-1}), and P3 (6 mL L^{-1}).

BioEcoGum is a commercial liquid bioorganic fertilizer characterized by a humic substance content of 60 g L^{-1} humic acids, 20 g L^{-1} fulvic acids, and 40 g L^{-1} potassium oxide (K_2O), with total organic matter content ranging from 80 to 85%, a pH between 9.5 and 10.0, and a density of approximately 1.10 to 1.15 g cm^{-3}. This product was applied as a foliar spray at three critical growth stages of maize: V4 (four-leaf stage), tasseling, and early grain filling.

Each experimental plot measured 3 m by 4 m, with 1-m buffer zones separating plots to minimize nutrient and moisture interference. Granular organic fertilizer was uniformly incorporated into the soil prior to planting, while the foliar applications of BioEcoGum were performed using a backpack sprayer in the early morning to maximize absorption.

This factorial design allowed the evaluation of both main effects and interaction effects between soil-applied granular fertilizer and foliar bioorganic fertilization on corn growth, yield, soil fertility, and economic performance.

Crop management practices

Maize hybrid Porumbene 458, known for its adaptability to semi-arid environments (Andriucă et al. 2016), was used in the experiment. Seeds were sown manually at a spacing

of 70 cm between rows and 25 cm between plants, with one seed per hill, resulting in a planting density of approximately 57,000 plants per hectare. Planting occurred in early May, corresponding to the beginning of the growing season in the region.

Irrigation was applied daily during the first four weeks after sowing to ensure uniform germination and early establishment, followed by biweekly irrigation until physiological maturity. Weed control was conducted twice using mechanical weeding and manual hoeing. Pest and disease management followed Integrated Pest Management (IPM) principles, with applications of environmentally safe insecticides only when pest populations exceeded economic thresholds.

Fertilization followed the treatment regimen described in Experimental design and treatment structure section, with granular organic fertilizer incorporated into the soil before sowing, and BioEcoGum applied as foliar sprays during key growth stages. Other agronomic practices, such as thinning and earthing up, were standardized across all plots to minimize variability.

Harvesting was carried out approximately 102 days after planting, at physiological maturity, by manually cutting the ears from five representative plants per plot for yield and biomass assessments.

Agronomic measurements

Growth parameters were recorded at critical growth stages to assess the effects of treatments on maize development. Plant Height (PH) was measured from the soil surface to the tip of the tallest leaf on five randomly selected plants per plot at the tasseling stage. The Number of Leaves (NL) was counted on the same plants. Leaf area (LA) was estimated using a portable leaf area meter (Model LI-3000C, LI-COR Biosciences) on fully expanded leaves sampled from five plants per plot.

Reproductive parameters included days to Male Flowering (MF) and Female Flowering (FF), recorded as the number of days from sowing until 50% of plants in a plot exhibited tassel emergence and silking, respectively. At physiological maturity, Ear Weight (EW) and Grain Weight per ear (GW) were determined by harvesting and weighing ears from five representative plants per plot. Aboveground biomass was sampled by cutting the five plants at ground level; fresh biomass was recorded immediately, and subsamples were oven-dried at 70°C until constant weight to determine dry biomass (Total Dry Biomass/TDB). All measurements were performed following standard agronomic protocols, ensuring accuracy and repeatability. Data were averaged per plot for subsequent statistical analysis.

Soil sampling and laboratory analysis

Soil samples were collected from the 0-20 cm depth before planting and immediately after harvest to assess changes in soil fertility parameters. For each plot, five subsamples were taken at random points and composited into a single representative sample. Soil pH was measured in a 1:2.5 soil-to-water suspension using a calibrated pH meter. Organic matter content (humus) was determined by the Walkley-Black dichromate oxidation method. Hydrolyzable nitrogen (N) was measured using alkaline hydrolysis diffusion techniques. Available phosphorus (P_2O_5) was analyzed using the Bray I extraction method, and exchangeable potassium (K_2O) was extracted with ammonium acetate and measured by flame photometry.

The liquid bioorganic fertilizer used in this study (BioEcoGum) is a humic-based formulation designed to enhance nutrient availability and plant vigor, as previously described (Lavanya 2022). All soil analyses were performed at the certified Soil Testing Laboratory of Kazakh Research Institute of Agriculture and Plant Growing, following standardized protocols to ensure data accuracy and reproducibility.

Economic evaluation

An economic analysis was conducted to evaluate the profitability and cost-effectiveness of the different fertilizer treatments. Input costs included expenses for seeds, labor, Granular Organic Fertilizer (GOF), liquid bioorganic fertilizer (LBF, BioEcoGum), irrigation, pest control, and other cultural practices. All costs were calculated based on local market prices prevailing during the 2021 growing season.

Gross revenue was estimated by multiplying grain yield per hectare by the average market price of maize at harvest time. Net income was determined by subtracting total production costs from gross revenue. Additional economic indicators calculated included the Benefit-Cost (B/C) ratio and the production cost per 100 kg of grain.

Economic data were analyzed to provide insights into the financial feasibility of applying integrated granular and liquid bioorganic fertilizers in maize cultivation on light chestnut soils.

Statistical analysis

All experimental data were subjected to two-way analysis of variance (ANOVA) to examine the effects of Granular Organic Fertilizer (GOF), Liquid Bioorganic Fertilizer (LBF), and their interaction on growth, yield, soil properties, and economic parameters. Mean comparisons were conducted using the Least Significant Difference (LSD) test at significance levels of 5% ($p<0.05$) and 1% ($p<0.01$).

Pearson correlation coefficients were calculated to assess relationships among agronomic traits, biomass accumulation, and grain yield (Ayoubi et al. 2009). Statistical analyses were performed using SPSS version 25 (IBM Corp., Armonk, NY, USA). Data visualization was done using Microsoft Excel 2019 and GraphPad Prism 8 software. Assumptions of normality and homogeneity of variance were verified prior to analysis, and data transformations were applied when necessary.

RESULTS AND DISCUSSION

Growth response of corn to bioorganic fertilizer treatments

The application of bioorganic fertilizers significantly influenced several vegetative growth parameters of corn, including plant height, number of leaves, stem diameter,

and leaf area. As shown in the ANOVA results, granular organic fertilizer had a significant effect on plant height ($p<0.05$), with the highest values recorded under G2 treatment (2000 kg ha^{-1}). Similarly, BioEcoGum liquid fertilizer showed a significant impact on the number of leaves and leaf area ($p<0.05$), particularly at concentrations of 4 and 6 mL L^{-1} (Table 1).

Leaf area was especially responsive to the interaction between granular and liquid fertilizer treatments. As visualized in Figure 1, the control treatment (G0-P0) produced the smallest leaf area (419.4 cm²), while the highest value (648.9 cm²) was recorded under the G0-P3 treatment (6 mL L^{-1} BioEcoGum without granular fertilizer). In contrast, the G1 and G2 groups exhibited a more stable leaf area response across BioEcoGum concentrations, suggesting a buffering effect of the organic matter on foliar nutrient uptake. Although granular fertilizer alone contributed positively to overall leaf expansion, the enhancement due to BioEcoGum foliar application was more prominent in plots with limited soil nutrient amendment.

Stem diameter showed no statistically significant differences across treatments ($p>0.05$), indicating that this trait may be less responsive to external nutrient inputs under the given environmental conditions. However, the combined use of both fertilizer types tended to promote uniform vegetative development, supporting a more robust canopy structure and potential improvement in early-stage light interception. These findings demonstrate the capacity of BioEcoGum to enhance early vegetative growth even under limited soil fertility input, especially through increased photosynthetically active surface area. This suggests its potential as a strategic foliar supplement in low-input or degraded soil systems.

Flowering time and reproductive traits

The timing of male and female flowering in corn was moderately affected by fertilizer treatments. Although granular and liquid bioorganic fertilizers did not significantly alter the flowering time at the 5% significance level (Table 1), slight trends in developmental acceleration were observed under higher BioEcoGum concentrations. Specifically, male flowering occurred earlier by approximately 1-2 days in treatments with 4-6 mL L^{-1} BioEcoGum, particularly when combined with the 2000 kg ha^{-1} granular dose (G2-P2 and G2-P3). These shifts, although not statistically significant, may reflect enhanced nutrient assimilation and hormonal balance during the pre-reproductive phase.

Female flowering followed a similar trend but exhibited slightly lower sensitivity to the treatments. The average reduction in flowering time across BioEcoGum-treated plots was about one day compared to the control (G0-P0), indicating improved synchrony between vegetative and reproductive development. This effect is ecologically advantageous, as more uniform flowering can lead to better pollination efficiency and kernel set (Uribelarrea et al. 2008).

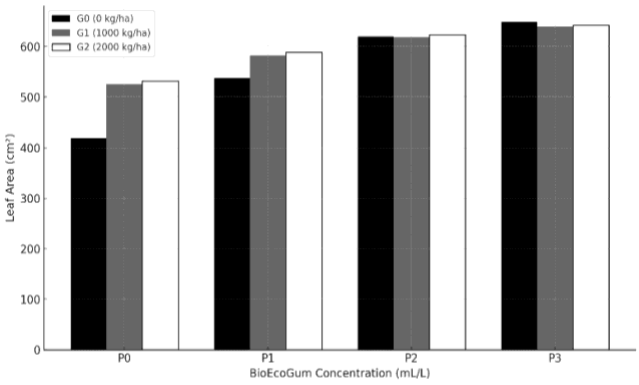

Figure 1. Effect of BioEcoGum and granular organic fertilizer on corn leaf area

Table 1. Results of analysis of variance (ANOVA) for the effects of granular and liquid bioorganic fertilizers on corn growth, yield components, and biomass traits

Variable	GOF (F)	LBF (F)	GOF × LBF (F)	CVA (%)	CVB (%)
Plant height (cm)	127.71	74.39	30.95	4.05	2.45
Number of leaves (no.)	0.23	1.09	0.57	2.19	4.40
Stem diameter (cm)	ns	ns	ns	5.28	2.26
Leaf area (cm²)	10,256.44	21,083.13 **	9,008.70 *	15.59	9.59
Male flowering age (days)	0.86	1.30	0.71	2.69	1.67
Female flowering age (days)	0.58	0.25	1.36	1.07	2.04
Ear weight (g)	58.54 *	6.61 *	1.08	18.96	14.18
Grain weight per cob (g)	7.06	2.80 *	0.63	12.94	9.56
Grain yield (t/ha)	**61.82 ***	**9.73 **	**4.39 * **	8.44	6.27
Harvest index (ratio)	ns	ns	ns	12.33	8.14
Fresh stem biomass (g plant^{-1})	37,632.69 *	730.91	1,250.30	11.87	9.26
Dry stem biomass (g plant^{-1})	4,979.19 **	84.60 *	25.65	18.37	11.16
Fresh leaf biomass (g plant^{-1})	8,153.81 *	1,673.10	608.34	16.54	15.41
Dry leaf biomass (g plant^{-1})	449.20 **	226.45 **	13.68	6.81	5.01
Total fresh biomass (g plant^{-1})	196,749.11 **	14,169.93	7,005.33	14.15	13.31
Total dry biomass (g plant^{-1})	5,274.38 **	237.08 **	60.01	12.13	6.41

Notes: GOF: Granular Organic Fertilizer; LBF: Liquid Bioorganic Fertilizer (BioEcoGum); CVA: Coefficient of variation for GOF treatment; CVB: for LBF treatment; *p<0.05, **p<0.01, ***p<0.001 indicate significant differences based on the Least Significant Difference (LSD) test; ns: not significant (p>0.05)

Reproductive structure development, particularly ear weight, showed a statistically significant response to both granular ($p<0.05$) and liquid ($p<0.05$) fertilizer treatments (Table 1). The highest ear weight values were recorded under combined G2-P3 treatment, suggesting a synergistic effect between soil and foliar nutrient sources in promoting reproductive biomass accumulation. This aligns with prior findings that reproductive traits in maize are highly responsive to nutrient availability, especially under conditions that support sustained photosynthate allocation to developing ears (Maiti and Singh 2017). These findings imply that, while flowering time may not be significantly shifted under current treatment levels, reproductive output in terms of ear development can be effectively enhanced through integrated fertilization approaches.

Biomass accumulation and yield performance

The combined application of granular and liquid bioorganic fertilizers had a pronounced effect on biomass accumulation and grain yield in corn (Alfarisy et al. 2021). As indicated in Table 1, both fertilizer types significantly influenced several biomass components, including fresh and dry biomass of stems and leaves, as well as total plant biomass ($p<0.05$ or $p<0.01$).

Dry stem biomass showed the strongest response to granular organic fertilizer (GOF), with G2 (2000 kg ha^{-1}) producing significantly greater values than G0 and G1. Similarly, dry leaf biomass increased with both GOF and BioEcoGum concentrations, reaching maximum values under the G2-P3 combination. These responses suggest improved nitrogen and potassium availability for structural growth when both soil amendment and foliar supplementation were applied.

Total dry biomass exhibited a significant increase under all treatment combinations involving BioEcoGum, with the G2-P3 treatment outperforming others (Table 1). This highlights the additive or possibly synergistic effects of humic substances and organic matter in supporting whole-plant productivity. Fresh biomass patterns followed similar trends, reinforcing the consistency of treatment effects across multiple parameters.

Grain yield, as estimated from grain weight per ear (GW), responded strongly to both fertilizer sources, with the highest grain weights observed in P2 and P3 treatments. Although not all combinations produced statistically distinct yield differences, grain weight was positively correlated with both dry stem biomass (r = 0.34) and total dry biomass (r = 0.60), as visualized in Figure 2. This suggests that improved biomass accumulation translates into higher sink strength and better assimilate partitioning into grains.

The consistent increase in dry matter accumulation, particularly in the reproductive organs, reflects improved photosynthetic capacity, possibly due to enhanced root vigor, foliar nutrient uptake, and hormonal modulation stimulated by BioEcoGum (Bhattachary 2021). These findings demonstrate that integrated bioorganic fertilization can substantially enhance biomass productivity and yield potential in light chestnut soils, which are typically low in fertility.

Correlation among agronomic traits

To better understand the relationships among growth, biomass, and reproductive traits, a Pearson correlation analysis was conducted across all treatment combinations. The results are presented in Table 2. Grain weight per ear exhibited the strongest positive correlation with ear weight (r = 0.81), confirming the direct association between cob size and grain productivity. Moreover, grain weight was significantly correlated with total dry biomass (r = 0.60), dry stem biomass (r = 0.34), and dry leaf biomass (r = 0.41), indicating that vegetative vigor and assimilate storage are key determinants of reproductive success.

These patterns are further illustrated in Figure 2, where grain weight demonstrates a positive linear relationship with all three biomass components. The trend lines show that increases in biomass particularly total dry matter are associated with higher grain yields, although with differing slopes. This supports the notion that total biomass serves as a reliable proxy for sink strength and assimilate availability in grain-filling stages.

Interestingly, vegetative parameters such as plant height and number of leaves were only moderately or weakly correlated with grain yield (r = 0.57 and r = 0.04, respectively), suggesting that morphological size alone may not predict yield performance under these treatments. In contrast, physiological indicators like leaf area showed a negative or inconsistent correlation with yield, potentially due to trade-offs between vegetative expansion and reproductive resource allocation.

These correlations reinforce the role of dry biomass, particularly that of the stem and total plant, as a key intermediate variable linking nutrient availability with final grain yield. Therefore, treatments that promote efficient biomass production without excessive vegetative overhead are likely to be the most effective for improving productivity in light chestnut soils.

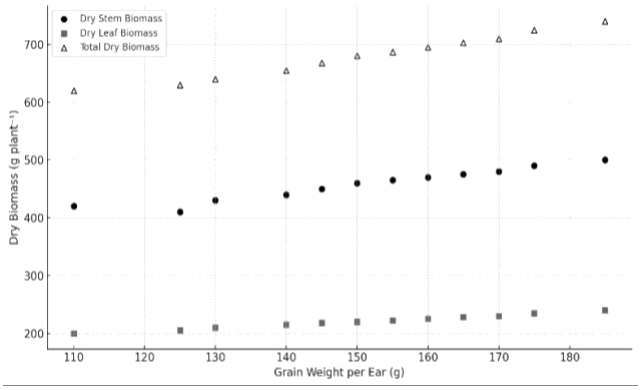

Figure 2. Relationship between grain weight and biomass components in corn

Soil fertility dynamics

The application of granular and liquid bioorganic fertilizers was found to moderately alter the chemical properties of light chestnut soils, particularly in the surface layer (0-20 cm). As presented in Table 3, soil organic matter (humus) content remained relatively stable across the two years of study, declining slightly from 1.93% to 1.83%. This modest change suggests that while organic amendments supported microbial activity and nutrient cycling, a longer application period may be needed to effect significant changes in soil organic carbon pools.

More pronounced shifts were observed in the availability of key macronutrients. Notably, available phosphorus (P_2O_5) increased substantially from 14.0 to 26.0 mg/kg in the surface soil layer, likely as a result of the combined input of soluble phosphates from the granular fertilizer and microbial mobilization enhanced by BioEcoGum. This improvement is particularly important given that phosphorus is often a limiting nutrient in alkaline soils like those of the study area.

In contrast, exchangeable potassium (K_2O) declined from 585 to 420 mg/kg, as shown in Figure 3. This reduction may reflect rapid uptake by vigorously growing plants, which outpaced the soil's replenishment capacity. While total potassium content remained relatively stable, the depletion of exchangeable forms indicates the need for balanced nutrient replenishment strategies to maintain long-term productivity. Hydrolyzable nitrogen (available N) levels decreased only slightly, from 35.0 to 33.6 mg/kg, indicating moderate biological nitrogen turnover during the growing season. This stability may be due to the buffering effect of microbial communities stimulated by humic substances, which improve nitrogen use efficiency.

Overall, the data suggest that bioorganic fertilization enhances soil fertility through improved phosphorus availability and nutrient cycling, although potassium management may require additional attention in subsequent planting seasons. These findings support the strategic use of humic-based biostimulants and composted organics in sustainable nutrient management programs.

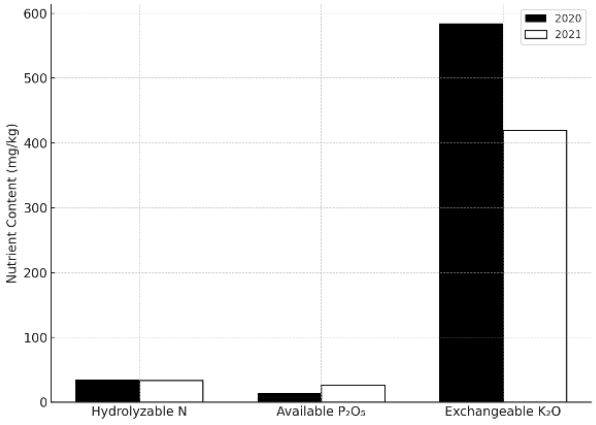

Figure 3. Changes in soil available nutrients (0-20 cm) before and after treatment

Table 2. Pearson correlation coefficients among selected agronomic traits of corn under different fertilizer treatments

Variable	PH	NL	LA	MF	FF	EW	GW	TDB	Yield
Plant height (PH)	1	0.48	-0.38	0.39	0.31	0.45	0.57	0.37	-0.05
Number of leaves (NL)		1	-0.31	0.33	0.11	0.38	0.57	0.39	0.04
Leaf area (LA)			1	-0.52	-0.40	-0.54	-0.54	-0.37	-0.07
Male flowering age (MF)				1	0.62	0.57	0.56	0.51	-0.02
Female flowering age (FF)					1	0.44	0.56	0.49	0.08
Ear weight (EW)						1	0.81	0.76	0.01
Grain weight per ear (GW)							1	0.60	-0.14
Total dry biomass (TDB)								1	0.10
Yield (final harvest weight)									1

Note: PH: Plant height; NL: Number of leaves; LA: Leaf area; MF: Male flowering age; FF: Female flowering age; EW: Ear weight; GW: Grain weight per ear; TDB: Total dry biomass; Yield: Final harvest weight per plant or plot. Values in bold (not shown here) indicate significant correlations at $p < 0.05$. Only the upper triangular matrix is shown, as the correlation matrix is symmetrical.

Table 3. Agrochemical characteristics of light chestnut soils before and after bioorganic fertilizer application

Year	Depth (cm)	Humus (%)	pH (H_2O)	Total N (%)	Total P_2O_5 (%)	Total K_2O (%)	Hydrolyzable N (mg/kg)	Available P_2O_5 (mg/kg)	Exchangeable K_2O (mg/kg)
2020	0-20	1.93	8.84	0.154	0.190	2.50	35.0	14.0	585
	20-40	1.46	8.90	0.112	0.216	2.44	30.8	9.0	340
2021	0-20	1.83	8.81	0.168	0.212	2.43	33.6	26.0	420
	20-40	1.46	8.87	0.112	0.212	2.37	28.0	10.0	260

Note: Soil samples were taken from the top 0-20 cm layer before treatment (early May) and after harvest (late August). P_2O_5 and K_2O are expressed in mg/kg, N as hydrolyzable N (mg/kg), and humus content in percentage (%). Values represent mean concentrations across treatment replicates.

Table 4. Economic performance of corn and broccoli production in 2021 under different treatments

Crop	Yield (t/ha)	Gross Revenue (tenge/ha)	Production Cost (tenge/ha)	Net Income (tenge/ha)	Cost per 100 kg (tenge)	Profitability (%)
Broccoli	24.9	883,000	454,496	428,504	18,253	94.3
Corn (control)	7.4	515,667	308,045	207,622	4,162	67.4
Corn (best yield)	**13.5**	**945,000**	605,480	339,520	2,519	56.1

Note: Total cost includes inputs, labor, and field operations. Net income was calculated as total revenue minus total cost. Cost per 100 kg refers to production cost per unit yield. All values are expressed in tenge per hectare (₸/ha) or per 100 kg of grain.

Economic performance and profitability

Economic analysis was conducted to assess the feasibility of integrating bioorganic fertilizers into corn production on light chestnut soils (Imran 2024). As shown in Table 4, the use of the highest-performing treatment combination (G2-P3) resulted in a corrected grain yield of 13.5 t/ha, producing a gross revenue of 945,000 tenge/ha. Although production costs under this treatment reached 605,480 tenge/ha due to the dual application of granular and foliar inputs, the resulting net income was 339,520 tenge/ha, with a profitability rate of 56.1%.

In comparison, the control treatment (no fertilizer input) yielded only 7.4 t/ha, with net income of 207,622 tenge/ha and a lower profitability rate of 67.4%. Interestingly, although the profit margin percentage appears higher in the control, the absolute profit was substantially lower than that of the best treatment. This reflects the classic trade-off between input investment and yield return, and highlights that high-efficiency treatments, despite greater initial cost, may be more advantageous in terms of total income generated.

Broccoli, included in the comparison as a high-value crop, produced a yield of 24.9 t/ha with a net income of 428,504 tenge/ha and the highest profitability rate (94.3%). While this demonstrates the economic potential of alternative crops, corn remains a staple with broader agronomic resilience and post-harvest market demand.

The cost of production per 100 kg of corn was lowest under the best treatment (2,519 tenge), compared to 4,162 tenge in the control. This reduction in unit production cost reinforces the economic efficiency of integrated fertilization and the contribution of BioEcoGum in improving both biological productivity and cost-effectiveness. Overall, these results demonstrate that the combined use of granular and liquid bioorganic fertilizers not only enhances agronomic performance but also provides tangible economic benefits, justifying their adoption under semi-arid soil conditions.

Discussion

Enhanced vegetative growth through bioorganic fertilization

The application of bioorganic fertilizers significantly enhanced vegetative growth parameters in corn, particularly plant height, leaf area, and number of leaves. These improvements are consistent with the observed statistical significance in the ANOVA results (Table 1) and reflect the capacity of humic-based liquid formulations, such as BioEcoGum, to stimulate early plant development through multiple physiological pathways. The pronounced expansion of leaf area under foliar BioEcoGum treatment (Figure 1) indicates improved chlorophyll content and photosynthetic surface, which are critical during the rapid vegetative phase of corn.

Humic substances, the active component of BioEcoGum, are known to influence membrane permeability, enhance nutrient uptake, and activate hormonal pathways such as auxin-like responses, leading to increased cell elongation and division (Suleimenov et al. 2019). In this study, even in the absence of granular organic inputs (G0), foliar BioEcoGum application at 6 mL L^{-1} (P3) resulted in a 54.7% increase in leaf area compared to the untreated control (P0), suggesting that foliar pathways are effective routes for nutrient and biostimulant assimilation under nutrient-limited soil conditions.

Granular organic fertilizer further supported vegetative growth by improving soil structure and microbial activity, contributing to sustained nutrient release (Tian et al. 2022). However, the response was more gradual compared to the liquid treatment, indicating complementary modes of action. Treatments combining both fertilizer types generally showed the most stable and consistent improvements, suggesting a synergistic effect. These findings underscore the potential of integrated bioorganic strategies in enhancing early plant vigor, especially in low-fertility or degraded soils such as light chestnut types. Improved vegetative growth lays the foundation for better reproductive development, which is discussed in the following sections.

Modulation of reproductive development and yield formation

Reproductive development in corn is sensitive to both nutrient availability and timing of assimilate allocation, and this study demonstrates that bioorganic fertilization contributes to improved yield formation through multiple mechanisms. Although flowering time did not differ significantly across treatments (Table 1), a consistent trend of earlier male and female flowering was observed under higher BioEcoGum concentrations, particularly in combination with granular fertilizer. Such shifts, though subtle, are agronomically relevant, as synchronized and timely flowering supports optimal pollination and kernel set.

The most notable reproductive improvement was observed in grain yield components, particularly grain weight per ear and ear weight. Both parameters showed statistically significant responses to fertilizer application (Table 1). Treatments involving higher BioEcoGum levels (P2 and P3) produced heavier ears, with the best performance under the G2-P3 combination. This suggests that nutrient uptake and hormonal stimulation through humic substances not

only enhance vegetative vigor but also improve reproductive sink strength.

Increased leaf area under BioEcoGum treatments (Figure 1) likely contributed to enhanced assimilate production during the critical grain-filling period. Improved photosynthetic efficiency, driven by broader leaf surfaces, may have supported a larger carbohydrate pool for grain development. This is further supported by the strong positive correlation between grain weight and total biomass components, discussed in the next section.

Importantly, the combined application of granular and foliar bioorganic fertilizers did not merely additively increase yield; rather, the interaction appeared synergistic, as the highest grain weights were not observed under single-source treatments. This implies that both soil and foliar nutrient pathways must be simultaneously optimized to fully unlock the reproductive potential of corn, particularly under conditions of moderate soil fertility.

Correlation between biomass and yield potential

Understanding the relationship between vegetative biomass and grain yield is critical for optimizing input strategies in maize cultivation. In this study, correlation analysis revealed that grain weight per ear had a strong and significant positive relationship with ear weight ($r = 0.81$), as well as moderate correlations with dry stem biomass ($r = 0.34$), dry leaf biomass ($r = 0.41$), and total dry biomass ($r = 0.60$) (Table 2). These findings confirm that robust vegetative growth contributes to grain yield not merely through structural size, but through effective source-sink dynamics.

The relationships are further visualized in Figure 2, where the linear trends suggest that as biomass accumulation increases, grain weight improves proportionally especially with total dry biomass. This underscores the importance of assimilate availability during the grain-filling period, which is driven by cumulative photosynthetic output and internal remobilization of stored carbohydrates.

Interestingly, plant height and number of leaves, while often considered basic indicators of vigor, showed weaker correlations with grain weight ($r = 0.57$ and $r = 0.04$, respectively). This suggests that sheer plant size or morphology alone may not be a reliable predictor of yield, especially in systems influenced by organic amendments where physiological efficiency matters more than physical dimensions.

These results emphasize that total dry matter particularly stem biomass, which functions as both a structural support and a reservoir for remobilized carbohydrates is a more reliable yield predictor than superficial growth traits. Consequently, fertilization strategies that promote biomass accumulation without excessive vegetative expansion can lead to improved yield efficiency, especially under resource-limited conditions.

Such insights align with the findings in other organic and semi-arid production systems, where biomass-to-grain conversion efficiency becomes a key trait under fluctuating environmental and nutrient conditions.

Soil fertility restoration in light chestnut soils

Soil fertility restoration is a major challenge in light chestnut soils due to their low organic matter content, limited cation exchange capacity, and often alkaline pH (Vittori Antisari et al. 2013). The application of bioorganic fertilizers in this study resulted in moderate but meaningful changes in soil chemical properties, particularly in the upper 0-20 cm layer, where root activity is concentrated. As shown in Table 3, the most substantial improvement was observed in the availability of phosphorus (P_2O_5), which increased from 14.0 to 26.0 mg/kg. This change is likely attributable to the combined effects of mineral inputs from the granular fertilizer and the solubilization of bound phosphorus by humic substances and microbial activity stimulated by BioEcoGum.

In contrast, a marked reduction in exchangeable potassium (K_2O) was recorded, decreasing from 585 to 420 mg/kg over the same period. This decline, visualized in Figure 3, may be explained by high plant uptake during vigorous biomass accumulation and possible leaching losses not fully compensated by the fertilizer treatment. Although potassium is generally abundant in many soils, its readily available form can be rapidly depleted without adequate replenishment highlighting the need for balanced nutrient management in organic systems.

Nitrogen levels, measured as hydrolyzable N, decreased only slightly from 35.0 to 33.6 mg/kg, indicating a relatively stable N pool likely supported by microbial mineralization of organic matter. Meanwhile, soil humus content declined marginally (from 1.93% to 1.83%), suggesting that one season of organic application is not sufficient to build up stable organic carbon in light-textured soils. Overall, these findings point to the partial restoration of soil fertility, with improved phosphorus availability as a key benefit, while highlighting potassium as a potentially limiting factor in repeated cropping cycles. Long-term studies and nutrient budgeting are needed to ensure sustainable soil health under intensive bioorganic fertilizer use.

Economic implications of integrated bioorganic fertilizer use

Economic viability is a critical determinant in the adoption of sustainable agricultural technologies (Ochieng et al. 2022). In this study, the combined application of granular and liquid bioorganic fertilizers not only improved agronomic performance but also enhanced profitability, as reflected in the cost-benefit analysis summarized in Table 4. The best-performing treatment (G2-P3) resulted in a grain yield of 13.5 t/ha and generated a net income of 339,520 tenge/ha, despite higher production costs compared to the control. This represents a 63.5% increase in net return over the non-fertilized treatment (G0-P0), which yielded only 7.4 t/ha.

Interestingly, while the profitability ratio of the control was higher (67.4%) due to minimal input costs, the absolute profit was significantly lower. This highlights a common economic trade-off: low-input systems may appear efficient per unit cost, but high-input systems often produce greater net returns due to yield maximization. Moreover, the cost per 100 kg of corn was lowest under the G2-P3 treatment

(2,519 tenge), indicating greater cost efficiency per output unit.

The inclusion of broccoli as a reference high-value crop illustrates that, while alternative crops may offer superior economic margins (94.3% profitability), corn remains a strategically important commodity for both food security and market stability in semi-arid regions. Thus, enhancing its productivity through bioorganic means is a viable strategy for resource-limited farmers. From a broader perspective, these findings validate the economic rationale for adopting integrated fertilization practices. Although initial costs are higher, returns in both yield and profitability justify the investment, especially when external inputs are derived from renewable or locally available organic sources. Long-term implementation may also reduce dependency on synthetic fertilizers, contributing to both economic resilience and environmental sustainability.

Comparison with previous studies and agroecological relevance

The results of this study are largely consistent with previous research demonstrating the agronomic and ecological benefits of integrating organic and bio-based fertilizers. Similar yield enhancements following humic substance application have been reported in maize by Song et al. (2022) and Verlinden et al. (2009) who attributed the improvements to increased nutrient uptake efficiency and enhanced photosynthetic activity. The observed increase in leaf area and biomass in the current study corroborates these findings, indicating that humic-rich foliar applications can play a significant role in boosting vegetative growth under nutrient-limited conditions.

In terms of yield formation, the synergistic effect of combined granular and liquid organic fertilizers aligns with studies conducted in dryland and degraded soils, such as those by Liu et al. (2021) and Tian et al. 2022, where integrated organic fertilization improved not only yield but also soil structure and microbial function. The modest changes in humus content and nitrogen levels in this study reflect the need for longer-term applications, a limitation frequently noted in organic soil fertility programs.

Soil phosphorus availability showed significant improvement, paralleling findings from Habib (2021) in semi-arid soils, where humic acids enhanced phosphate solubilization and plant uptake. However, the depletion of exchangeable potassium observed here highlights a divergence from studies in heavier soils, where organic matter often contributes to greater K retention. From an agroecological standpoint, the adoption of bioorganic fertilizers offers a sustainable intensification pathway for marginal lands such as the light chestnut soils of the Ontusik Region. These systems typically suffer from poor nutrient retention, low microbial biomass, and erratic rainfall. The use of biostimulants and organic amendments not only supports crop productivity but may also build resilience to climatic and edaphic stressors over time. Together, the findings validate the integration of organic and humic-based inputs as a promising approach for environmentally sound and economically viable maize cultivation in resource-constrained agroecosystems.

In conclusion, the integration of granular and liquid bioorganic fertilizers significantly improved the growth, yield, and economic performance of corn cultivated on light chestnut soils. BioEcoGum foliar application enhanced vegetative development, particularly leaf area expansion, while granular organic fertilizer contributed to overall biomass accumulation and yield stability. The combined treatments not only increased grain weight and total dry matter but also promoted earlier and more synchronized flowering, supporting reproductive efficiency. Soil fertility improvements were evident through increased phosphorus availability, although potassium depletion highlights the need for balanced nutrient management. Economically, the most intensive treatment (G2-P3) yielded the highest net income and lowest cost per unit output, confirming its viability for adoption despite higher input costs. These outcomes are consistent with previous studies on humic substances and organic amendments, reaffirming their effectiveness in semi-arid and nutrient-limited environments. The findings underscore the potential of integrated bioorganic fertilization as a sustainable intensification strategy that addresses both productivity and soil health challenges in marginal agroecosystems. While short-term gains are promising, longer-term trials are recommended to assess cumulative effects on soil quality and nutrient dynamics. Overall, this study provides a practical and ecologically sound basis for scaling up the use of bioorganic inputs in dryland maize production systems.

REFERENCES

Alfarisy MY, Yassi A, Mustari K. 2021. Increasing productivity and biomass of corn plants toward grant organic fertilizer and liquid organic fertilizer. ENDLESS Intl J Future Stud 4: 236-248. DOI: 10.54783/endless.v4i2.81.

Andriucă V, Bacean I, Cazmalî N, Macrii L, Melnic R. 2016. Productivity elements in conservative and conventional tillage systems. Sci Paper Ser A Agron 59: 27-32.

Ayoubi S, Khormali F, Sahrawat KL. 2009. Relationships of barley biomass and grain yields to soil properties within a field in the arid region: Use of factor analysis. Acta Agric Scandinavica Sect B-Soil Plant Sci 59 (2): 107-117. DOI: 10.1080/09064710801932417.

Bhattachary A. 2021. Dry matter production, partitioning, and seed yield under soil water deficit: a review. In: Bhattachary A (eds). Soil Water Deficit and Physiological Issues in Plants. Springer, Singapore. DOI: 10.1007/978-981-33-6276-5_7.

Chatzistathis T, Papaioannou E, Giannakoula A, Papadakis IE. 2021. Zeolite and vermiculite as inorganic soil amendments modify shoot-root allocation, mineral nutrition, photosystem ii activity and gas exchange parameters of chestnut (*Castanea sativa* Mill) plants. Agronomy 11 (1): 109. DOI: 10.3390/agronomy11010109.

Edmeades GO, Trevisan W, Prasanna BM, Campos H. 2017. Tropical Maize (*Zea mays* L.). In: Campos H, Caligari PDS. Genetic Improvement Of Tropical Crops. Springer International Publishing, Cham. DOI: 10.1007/978-3-319-59819-2_3.

Gao C, El-Sawah AM, Ali DFI, Alhaj Hamoud Y, Shaghaleh H, Sheteiwy MS. 2020. The integration of bio and organic fertilizers improve plant growth, grain yield, quality and metabolism of hybrid maize (*Zea mays* L.). Agronomy 10 (3): 319. DOI: 10.3390/agronomy10030319.

Habib A. 2021. Response of pearl millet to fertilization by mineral phosphorus, humic acid and mycorrhiza under calcareous soils conditions. Egypt J Soil Sci 61 (4): 399-411. DOI: 10.21608/ejss.2021.104285.1474.

Imran. 2024. Integration of organic, inorganic and bio fertilizer, improve maize-wheat system productivity and soil nutrients. J Plant Nutr 47 (15): 2494-2510. DOI: 10.1080/01904167.2024.2354190.

Khan A. 2024. Soil health and fertility: Modern approaches to enhancing soil quality. Front Agric 1 (2): 283-324.

Lavanya SM. 2022. Effect of Humic Acid Based Liquid Nutrient Formulation on Soil Biological Properties, Growth and Yield of Paddy (Oryza Sativa L.), maize (*Zea mays* L.) and tomato (*Lycopersicon esculentum* Mill.) under field condition. [Dissertation]. University of Agricultural Sciences, GKVK, Bangalore.

Liu J, Shu A, Song W, Shi W, Li M, Zhang W, Li Z, Liu G, Yuan F, Zhang S, Liu Z, Gao Z. 2021. Long-term organic fertilizer substitution increases rice yield by improving soil properties and regulating soil bacteria. Geoderma 404: 115287. DOI: 10.1016/j.geoderma.2021.115287.

Lumactud RA, Gorim LY, Thilakarathna, M. S. 2022. Impacts of humic-based products on the microbial community structure and functions toward sustainable agriculture. Front Sustain Food Syst 6: 977121. DOI: 10.3389/fsufs.2022.977121.

Maiti RK, Singh VP. 2017. Physiological basis of maize growth and productivity-A review. Farm Manag 2 (2): 59-88. DOI: 10.5958/2456-8724.2017.00010.8.

Ochieng J, Afari-Sefa V, Muthoni F, Kansiime M, Hoeschle-Zeledon I, Bekunda M, Thomas D. 2022. Adoption of sustainable agricultural technologies for vegetable production in rural Tanzania: Trade-offs, complementarities and diffusion. Intl J Agric Sustain 20 (4): 478-496. DOI: 10.1080/14735903.2021.1943235.

Pankova EI, Chernousenko GI. 2018. Comparison of chestnut soils of Central Asia with their analogs in other soil-geographical provinces of the dry-steppe zone of the Eurasian subboreal belt. Arid Ecosyst 8 (2): 89-96. DOI: 10.1134/S2079096118020051.

Rigobel EC. 2024. Humic substances in combination with PGPR. In: Rigobelo EC (eds). Microbial services for cereal crops: reducing costs and environmental impact. Springer Nature Switzerland, Cham. DOI: 10.1007/978-3-031-63149-8.

Samenova G. 2024. Preferences and Factors Affecting Decision of Agricultural Enterprises in Kazakhstan to Adopt Improved Maize Seeds [Dissertation]. Istanbul Sabahattin Zaim University, Turkey.

Song X, Guo W, Xu L, Shi L. 2022. Beneficial effect of humic acid urea on improving physiological characteristics and yield of maize (*Zea mays* L.). Acta Physiol Plant 44 (7): 72. DOI: 10.1007/s11738-022-03401-x.

Srivastava AK, Ngullie E. 2009. Integrated nutrient management: Theory and practice. Dynamic Soil Dynamic Plant 3 (1): 1-30.

Suleimenov B, Saparov A, Kan V, Kolesnikova L, Seitmenbetova A, Karabayev K. 2019. The effect of bioorganic liquid fertilizer "BioEcoGum" on the productivity of grain maize in the conditions of Southeast Kazakhstan. Eurasian J Biosci 13 (2): 1639-1644.

Tefera ML, Carletti A, Altea L, Rizzu M, Migheli Q, Seddaiu G. 2024. Land degradation and the upper hand of sustainable agricultural intensification in sub-Saharan Africa-A systematic review. J Agric Rural Dev Trop Subtrop 125 (1): 63-83.

Tellarini V, Caporali F. 2000. An input/output methodology to evaluate farms as sustainable agroecosystems: An application of indicators to farms in central Italy. Agric Ecosyst Environ 77 (1-2): 111-123. DOI: 10.1016/S0167-8809(99)00097-3.

Tembhekar AN. 2013. Effect of Foliar Application of Plant Growth Regulators on Assimilates Partitioning Growth, Seed Yield and Quality of Soybean (*Glycine max* (L.) Merrill). [Dissertation]. Jawaharlal Nehru Krishi Vishwavidyalaya, Madhya Pradesh.

Tian S, Zhu B, Yin R, Wang M, Jiang Y, Zhang C, Li D, Chen X, Kordol P, Liu M. 2022. Organic fertilization promotes crop productivity through changes in soil aggregation. Soil Biol Biochem 165: 108533. DOI: 10.1016/j.soilbio.2021.108533.

Ualiyeva RM, Kukusheva AN, Insebayeva MK, Akhmetov KK, Zhangazin SB, Krykbayeva MS. 2022. Agrotechnological methods of plant feeders applying for spring wheat agrocenoses-North-Eastern Kazakhstan varieties. J Water Land Dev 55 (10-12): 28-40. DOI: 10.24425/jwld.2022.142301.

Uribelarrea M, Cárcova J, Borrás L, Otegui ME. 2008. Enhanced kernel set promoted by synchronous pollination determines a tradeoff between kernel number and kernel weight in temperate maize hybrids. Field Crop Res 105 (3): 172-181. DOI: 10.1016/j.fcr.2007.09.002.

Verlinden G, Pycke B, Mertens J, Debersaques F, Verheyen K, Baert G, Bries J, Haesaert G. 2009. Application of humic substances results in consistent increases in crop yield and nutrient uptake. J Plant Nutr 32 (9): 1407-1426. DOI: 10.1080/01904160903092630.

Vittori Antisari L, Falsone G, Carbone S, Vianello G. 2013. Short-term effects of forest recovery on soil carbon and nutrient availability in an experimental chestnut stand. Biol Fertil Soil 49 (2): 165-173. DOI: 10.1007/s00374-012-0708-z.

Wu J, Xu H, Song B. 2024. Traditional vs. modern maize cultivation practices: A comparative study. Field Crop 7 (2): 93-104.

CELL BIOLOGY & DEVELOPMENT
Volume 9, Number 1, June 2025
Pages: 64-70

E-ISSN: 2580-4499
DOI: 10.13057/cellbioldev/v090106

Antidiabetic and hepatoprotective effects of *Cymbopogon citratus* (lemongrass) oil in streptozotocin-nicotinamide-induced diabetic male rats: Biochemical and histopathological evaluation

QUADRI OLAIDE NURUDEEN[1], SAAD ABDULKADIR[2], SHEU MOHAMMED JAMIU[1], MOSES ADONDUA ABAH[3,4,♥], EKELE JIATA UGWAH[5]

[1]Department of Biochemistry, Faculty of Natural and Life Sciences, University of Ilorin. Ilorin, Kwara State, Nigeria
[2]Department of Biochemistry, Faculty of Pure and Applied Sciences, Kwara State Polytechnic. Ilorin, Kwara State, Nigeria
[3]Department of Biochemistry, Faculty of Pure and Applied Sciences, Federal University Wukari. Wukari, Taraba State, Nigeria. Tel.: +23-480-000-0000, ♥email: M.abah@fuwukari.edu.ng
[4]Department of Medical Biochemistry, Faculty of Basic Medical Sciences, Federal University Wukari. Wukari, Taraba State, Nigeria
[5]Department of Sustainable Agriculture and Food Security, Newcastle University. NE1 7RU, United Kingdom

Manuscript received: 24 October 2023. Revision accepted: 22 June 2025.

Abstract. *Nurudeen QO, Abdulkadir S, Jamiu SM, Abah MA, Ugwah EJ. 2025. Antidiabetic and hepatoprotective effects of* Cymbopogon citratus *(lemongrass) oil in streptozotocin-nicotinamide-induced diabetic male rats: Biochemical and histopathological evaluation. Cell Biol Dev 9: 64-70.* This study investigated the antidiabetic and hepatoprotective effects of *Cymbopogon citratus* (lemongrass) essential oil in male rats with streptozotocin–nicotinamide-induced diabetes. Forty-two rats were randomly assigned to seven groups (n=6): non-diabetic control, diabetic control, diabetic + metformin (150 mg/kg), and diabetic + lemongrass oil at doses of 50, 100, and 200 mg/kg. Diabetes was induced by a single intraperitoneal injection of streptozotocin (60 mg/kg) 15 minutes after nicotinamide (120 mg/kg), followed by 28 days of oral treatment. Parameters assessed included fasting blood glucose, body weight, and key biochemical markers—superoxide dismutase (SOD), catalase (CAT), glutathione (GSH), and alanine aminotransferase (ALT)—along with histological evaluation of liver tissue. Treatment with lemongrass oil significantly lowered fasting blood glucose and enhanced antioxidant enzyme activity in diabetic rats, with the 100 mg/kg dose showing effects comparable to metformin. Histopathological analysis confirmed improvements in hepatic structure and reduced degenerative changes. These findings indicate that *C. citratus* essential oil exhibits notable antidiabetic and hepatoprotective effects, likely mediated through its antioxidant properties, and may serve as a promising adjunct in diabetes therapy.

Keywords: Antioxidant enzymes, *Cymbopogon citratus*, diabetes mellitus, liver histology, streptozotocin-nicotinamide

INTRODUCTION

Diabetes mellitus (DM) is a chronic metabolic disorder characterized by persistent hyperglycemia resulting from both impaired insulin action and defects in insulin secretion (American Diabetes Association 2021). The prevalence of diabetes worldwide has increased substantially, with an estimated 537 million people affected in 2021, and this number is predicted to reach 643 million by 2030 (Sun et al. 2022). The most common form, type 2 diabetes mellitus (T2DM), is often associated with insulin resistance, oxidative stress, and progressive β-cell dysfunction (Szkudelski 2012; Rena et al. 2017). Despite the availability of several pharmacological agents such as metformin, sulfonylureas, and insulin analogues, the long-term management of diabetes remains challenging due to adverse side effects, economic burden, and inconsistent patient responsiveness (Patel et al. 2012). This has prompted the exploration of alternative therapeutic options, particularly plant-derived treatments with antioxidant and antihyperglycemic properties.

At the same time, oxidative stress has been increasingly recognized as a key contributor to the complications and pathogenesis of diabetes mellitus (Evans et al. 2002; Maritim et al. 2003). Hyperglycemia-induced overproduction of reactive oxygen species (ROS) contributes to the impairment of cellular functions, lipid peroxidation, and organ damage, particularly in the pancreas and liver (Matsui et al. 2006). The liver, as a central organ in glucose metabolism, is frequently affected in diabetic conditions, as evidenced by elevated liver enzymes, oxidative injury, and structural abnormalities (Hamdy and Taha 2009). Therefore, agents that can mitigate oxidative stress and preserve hepatic architecture are of great interest in diabetes research, especially those that also address glucose regulation.

In recent years, essential oils from medicinal plants have gained attention for their bioactive properties, including antioxidant, anti-inflammatory, and antidiabetic effects (Bakkali et al. 2008; Eidi and Eidi 2009). Among these, *Cymbopogon citratus* (commonly known as lemongrass) is an aromatic plant widely used across Asia, Africa, and South America in traditional medicine. The essential oil of *C. citratus* contains major constituents such as citral, geraniol, myrcene, and limonene, which have been reported to possess significant pharmacological effects, including free radical scavenging and enzyme-modulating activity (Adeneye et al. 2006; Shah et al. 2011).

Preliminary studies have shown that *C. citratus* extracts may reduce blood glucose levels and improve lipid profiles in diabetic animal models (Oyedeji et al. 2009; Falode et al. 2023). However, the majority of these studies have focused on aqueous or ethanolic extracts, while the therapeutic efficacy of the volatile-rich essential oil remains underexplored. Moreover, studies that integrate both biochemical and histopathological evaluations to assess the hepatoprotective role of *C. citratus* oil in diabetic models are still lacking. Given the central role of the liver in glucose regulation and its sensitivity to oxidative damage, it is crucial to assess the dual-function effects—antidiabetic and hepatoprotective—of such natural agents.

To establish a reliable model for studying diabetes and evaluating therapeutic agents, the combination of streptozotocin (STZ) and nicotinamide (NA) has been widely adopted (Srinivasan et al. 2005). STZ selectively destroys pancreatic β-cells, while NA partially protects these cells, mimicking the pathophysiology of type 2 diabetes. This model is considered effective for evaluating both insulin sensitivity and β-cell preservation under therapeutic intervention. The use of this model, in conjunction with biochemical and histological analyses, provides a robust platform for testing the potential of botanical-based antidiabetic agents.

The present study aimed to evaluate the synergistic antidiabetic and hepatoprotective properties of *C. citratus* essential oil in male Wistar rats with STZ-NA-induced diabetes. Specifically, this research assessed fasting blood glucose levels, antioxidant enzyme activities (SOD, CAT, GSH), liver enzyme levels (ALT), and histological changes in hepatic tissue following oral administration of lemongrass oil. By examining both biochemical and histological parameters, this study provides a comprehensive assessment of the therapeutic potential of *C. citratus* oil, and supports its consideration as a complementary and functional treatment in the management of diabetes mellitus.

MATERIALS AND METHODS

Experimental animals

Forty-two healthy adult male Wistar rats (150-200 g) were collected from the Animal House of the Faculty of Basic Medical Sciences, University of Ilorin, Ilorin, Kwara State, Nigeria. The animals were sheltered in polypropylene cages under standard laboratory conditions (temperature 22-25°C, 12 h light/dark cycle) with unrestricted access to standard rat chow and clean water. All procedures were conducted in conformity with the National Institutes of Health (NIH) Guide for the Care and Use of Laboratory Animals (2011) and in conformity with institutional guidelines for the care and use of laboratory animals.

Induction of diabetes

Type 2 diabetes mellitus was induced by a single intraperitoneal injection of streptozotocin (STZ, 60 mg/kg body weight), freshly dissolved in 0.1 M cold citrate buffer (pH 4.5), 15 minutes after an intraperitoneal injection of nicotinamide (NA, 120 mg/kg) in normal saline. After 72 hours, blood glucose levels were measured using a glucometer (Accu-Chek®, Roche, Germany). Then, rats with fasting blood glucose levels greater than 200 mg/dL (>200 mg/dL) were considered diabetic and included in the experiment.

Experimental design

The diabetic rats were randomly assigned into seven groups (n = 6 per group), as outlined below: (i) Group 1: Non-diabetic control (received distilled water only), (ii) Group 2: Diabetic control (STZ–NA-induced, no treatment), (iii) Group 3: Diabetic + metformin (150 mg/kg/day), (iv) Group 4: Diabetic + *C. citratus* oil (50 mg/kg/day), (v) Group 5: Diabetic + *C. citratus* oil (100 mg/kg/day), (vi) Group 6: Diabetic + *C. citratus* oil (200 mg/kg/day), (vii) Group 7: Non-diabetic + *C. citratus* oil (100 mg/kg/day). All treatments were administered orally by gavage once daily for 28 consecutive days.

Group 7 was included to assess the tolerability and baseline physiological effects of *C. citratus* essential oil in normoglycemic (non-diabetic) animals. A higher dose (200 mg/kg) was not applied to this group to reduce animal usage and to avoid the potential confounding effects of supraphysiological exposure in healthy subjects. The 100 mg/kg dose was selected for this purpose based on prior reports demonstrating both its pharmacological effectiveness and safety in rodent models (Falode et al. 2023). This dose thus served as a suitable reference for evaluating safety outcomes in non-diabetic conditions.

Preparation of *Cymbopogon citratus* oil

The essential oil of *C. citratus* was obtained through steam distillation of fresh leaves collected from a local farm and authenticated at the Faculty of Natural and Life Sciences, University of Ilorin. The oil was then stored in amber glass bottles at 4°C until use. Doses of 50, 100, and 200 mg/kg body weight were prepared in 1% Tween-80 as the vehicle and administered by oral gavage. Although the GC-MS profiling of the oil used in this study was not conducted, previous studies have reported that lemongrass essential oil from West Africa typically contains citral (as a mixture of neral and geranial), geraniol, and limonene as dominant constituents (Oyedeji et al. 2009; Shah et al. 2011). These components are believed to contribute to the observed bioactivities.

Measurement of blood glucose and body weight

Fasting blood glucose levels were analyzed on days 0, 7, 14, 21, and 28 using tail vein blood and a digital glucometer. Body weights were also recorded weekly. Glucose measurements were taken after an of 12 hours overnight fasting.

Biochemical analysis

At the end of the treatment period, rats were fasted again overnight and euthanized under light anesthesia. Then, the blood samples were collected via cardiac puncture into plain tubes. To obtain the serum, the samples were allowed to clot and centrifuged for 10 minutes at 3,000 rpm. The following biochemical parameters were assayed

using commercial diagnostic kits (Randox Laboratories, UK): Alanine aminotransferase (ALT) - liver function marker, Superoxide dismutase (SOD) - antioxidant enzyme, Catalase (CAT) - an antioxidant enzyme, Reduced glutathione (GSH) - an oxidative stress indicator. All assays were performed following the manufacturers' protocols, and an UV-visible spectrophotometer read absorbance.

Histological analysis

Liver tissues were excised, washed with normal saline, and fixed in 10% neutral-buffered formalin. The tissues were processed, embedded in paraffin wax, and sectioned at 5 µm thickness. Next, those sections were stained with hematoxylin and eosin (H&E) and analyzed using a light microscope for structural changes. Photomicrographs were captured to document histopathological findings.

Statistical analysis

Data were expressed analysis as the mean ± standard deviation (SD), and the statistical comparisons among groups were performed by a one-way analysis of variance (ANOVA), followed by Tukey's post hoc test for multiple comparisons. Effect sizes (η^2) and F-values were calculated for each test, and exact p-values were reported where relevant. Confidence intervals (95% CI) were computed for key outcome variables. Then, a p-value of less than 0.05 ($p<0.05$) was regarded statistically significant. Next, all analyses were conducted using SPSS version 25.0 (IBM Corp., USA).

RESULTS AND DISCUSSION

Induction of diabetes and baseline glucose levels

Diabetes mellitus was successfully induced in experimental rats using the streptozotocin–nicotinamide (STZ–NA) protocol, as confirmed by significant elevations in fasting blood glucose (FBG) levels within 72 hours post-injection. Rats with FBG values exceeding 200 mg/dL were regarded as diabetic and included in the study. Baseline FBG levels before treatment (Day 0) are shown in Table 1. Diabetic groups (Groups 2 to 6) exhibited hyper-glycemia compared to the non-diabetic control (Group 1), confirming successful induction of diabetes. The initial blood glucose levels ranged from 210 to 267 mg/dL across diabetic groups, with no statistically significant differences among them, indicating uniform baseline hyperglycemia.

Effect of treatments on fasting blood glucose and body weight

Oral administration of *C. citratus* oil resulted in reduced fasting blood glucose (FBG) levels significantly over the 28-day treatment period in diabetic rats. As shown in Figure 1, all treatment groups (Groups 3-6) demonstrated progressive decreases in FBG compared to the diabetic control (Group 2), which maintained elevated glucose levels throughout the study. The group receiving 100 mg/kg of lemongrass oil (Group 5) exhibited the greatest glycemic reduction by Day 28, with efficacy comparable to that of the metformin-treated group (Group 3). The analyses, using one-way ANOVA followed by Tukey's post hoc test, showed statistically significant differences ($p<0.05$) in fasting blood glucose levels between the treated diabetic groups and the untreated diabetic control group from Day 14 onward.

Table 2 summarizes body weight changes. Diabetic control rats (Group 2) showed a gradual decrease in body weight over 28 days, a common feature of uncontrolled diabetes. In contrast, treatment with metformin or lemongrass oil (Groups 3-6) helped preserve or slightly increase body weight, suggesting improved metabolic stability. Notably, the 100 mg/kg dose of *C. citratus* oil (Group 5) was most effective in maintaining body weight close to baseline levels.

Effect on antioxidant enzyme activities (SOD, CAT, GSH)

Oxidative stress markers were significantly altered in diabetic rats, as shown in Table 3. In the diabetic control group (Group 2), levels of superoxide dismutase (SOD), catalase (CAT), and reduced glutathione (GSH) were significantly decreased compared to the non-diabetic control (Group 1), indicating increased oxidative stress due to hyperglycemia.

Figure 2 illustrates the observed changes in serum antioxidant enzyme activities across all groups. Group 5 (100 mg/kg) showed a near-complete restoration of SOD and GSH levels, while Group 3 (metformin) exhibited the highest CAT activity among treated groups. Treatment with *C. citratus* oil led to dose-dependent improvements in antioxidant enzyme activities. Among the treated groups, Group 5 (100 mg/kg lemongrass oil) showed the most significant restoration of SOD, CAT, and GSH levels, closely approximating the effects of metformin (Group 3). Group 6 (200 mg/kg) also improved antioxidant markers, though less effectively than the 100 mg/kg dose. These findings support the hypothesis that lemongrass oil exerts its antidiabetic effects, at least in part, by enhancing endogenous antioxidant defenses.

Table 1. Fasting blood glucose levels before treatment (Day 0)

Group	Description	FBG (mg/dL)
1	Non-diabetic control	93.6±4.8a
2	Diabetic control	235.4±11.2b
3	Diabetic + Metformin	232.1±12.5b
4	Diabetic + lemongrass (50 mg/kg)	243.6±9.3b
5	Diabetic + lemongrass (100 mg/kg)	267.2±14.0b
6	Diabetic + lemongrass (200 mg/kg)	252.3±13.4b
7	Non-diabetic + Lemongrass	91.5±5.1a

Note: Values are expressed as mean ± SD (n=6 per group). Superscripts indicate no significant difference among diabetic groups (Groups 2–6), but a significant difference exists between diabetic and non-diabetic ($p<0.05$; ANOVA+Tukey post hoc)

Table 2. Body weight changes over the 28-day treatment period

Group	Description	Day 0 (g)	Day 28 (g)	% Change
1	Non-diabetic control	185.2±5.3	204.8±4.7	+10.6%
2	Diabetic control	182.4±6.0	162.7±5.9	−10.8%
3	Diabetic + Metformin	183.3±4.2	192.6±4.1	+5.1%
4	Diabetic + Lemongrass oil (50 mg/kg)	184.0±5.6	187.2±5.3	+1.7%
5	Diabetic + Lemongrass oil (100 mg/kg)	181.5±6.2	191.3±5.7	+5.4%
6	Diabetic + Lemongrass oil (200 mg/kg)	183.7±4.8	189.4±5.0	+3.1%
7	Non-diabetic + Lemongrass oil	184.9±5.5	203.5±5.2	+10.0%

Note: Those values are expressed as mean ± SD (n=6)

Table 3. Effect of treatments on antioxidant enzyme activities in serum (day 28)

Group	Description	SOD (U/mL)	CAT (U/mL)	GSH (µmol/mL)
1	Non-diabetic control	9.45±0.36a	8.23±0.29a	7.31±0.32a
2	Diabetic control	4.27±0.28b	3.89±0.21b	3.12±0.18b
3	Diabetic + Metformin	8.32±0.34a	7.44±0.30a	6.87±0.25a
4	Diabetic + lemongrass (50 mg/kg)	6.78±0.31c	5.65±0.26c	5.03±0.19c
5	Diabetic + lemongrass (100 mg/kg)	8.16±0.29a	7.21±0.22a	6.75±0.24a
6	Diabetic + lemongrass (200 mg/kg)	7.36±0.35ac	6.49±0.24ac	5.98±0.27ac
7	Non-diabetic + Lemongrass	9.28±0.33a	8.11±0.26a	7.20±0.28a

Note: Values are expressed as mean ± SD (n=6 per group). Different superscript letters suggest statistically significant differences (p<0.05) based on one-way ANOVA followed by Tukey's post hoc test

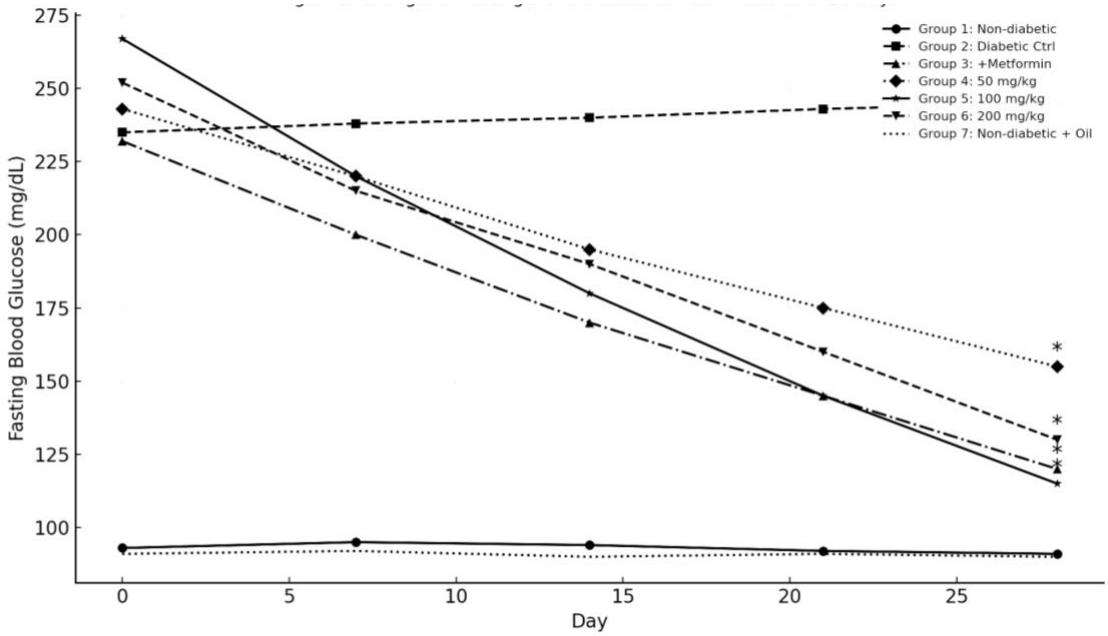

Figure 1. Changes in fasting blood glucose levels in rats over 28 days. Data were analyzed using one-way ANOVA followed by Tukey's post hoc test. Those values are expressed as mean ± SD (n=6 per group). Asterisks (*) indicate significant differences from diabetic control (Group 2), *p<0.05

Effect on liver function marker (ALT)

Serum alanine aminotransferase (ALT) levels, a marker of hepatocellular injury, were markedly elevated in the diabetic control group (Group 2) compared to the non-diabetic control group (Group 1), indicating liver damage associated with hyperglycemia and oxidative stress (Table 4).

Treatment with *C. citratus* oil significantly reduced ALT levels in diabetic rats in a dose-dependent method. The most pronounced reduction was observed in Group 5 (100 mg/kg), which showed ALT values statistically comparable to those of the metformin-treated group (Group 3). Group 4 (50 mg/kg) and Group 6 (200 mg/kg) also showed moderate improvements, suggesting a hepatoprotective effect of lemongrass oil.

Figure 3 presents these group-wise differences in serum ALT levels. Group 5 (100 mg/kg) exhibited ALT values close to those of the non-diabetic control, indicating effective hepatoprotection, whereas the diabetic control group showed the highest elevation. These findings suggest that *C. citratus* oil may confer protection against diabetes-induced hepatic injury, possibly via its antioxidant components.

Histological observations of liver tissue

Histological analysis of liver sections revealed marked differences in tissue architecture among the experimental groups (Figure 4). The non-diabetic control group (Group 1) exhibited normal hepatic histoarchitecture, with well-preserved hepatocytes arranged in radial plates around the central vein, intact sinusoids, and no signs of cellular damage.

In contrast, the diabetic control group (Group 2) showed severe hepatocellular degeneration, including cytoplasmic vacuolation, sinusoidal congestion, pyknotic nuclei, and inflammatory infiltration. These changes indicate substantial liver injury resulting from hyperglycemia-induced oxidative stress. Treatment with metformin (Group 3) and *C. citratus* oil (Groups 4-6) alleviated these pathological features to varying degrees. The 100 mg/kg lemongrass oil group (Group 5) showed the most substantial histological improvement, with reduced vacuolation and nearly normal hepatocyte appearance, comparable to metformin-treated rats. Groups 4 (50 mg/kg) and 6 (200 mg/kg) exhibited partial restoration of hepatic structure, though some mild degeneration remained.

The non-diabetic + lemongrass group (Group 7) maintained normal histological features, suggesting the oil is non-toxic at the administered dose. Overall, these findings support the hepatoprotective role of *C. citratus* oil in diabetes-induced hepatic injury.

Discussion

The present study demonstrated that *Cymbopogon citratus* (lemongrass) oral administration of essential oil exerted significant antidiabetic and hepatoprotective effects in streptozotocin-nicotinamide (STZ-NA) induced diabetic rats. These effects were evident from the reduction in fasting blood glucose levels, the improvement in antioxidant enzyme activities, the normalization of liver enzyme ALT, and the restoration of hepatic histoarchitecture. Among the tested doses, 100 mg/kg showed the most consistent and significant improvements, comparable to the standard antidiabetic drug, metformin.

The ability of lemongrass oil to reduce hyperglycemia may be attributed to its phytoconstituents, such as citral, geraniol, and limonene, which have been reported to enhance insulin secretion, improve peripheral glucose uptake, and inhibit gluconeogenesis (Shah et al. 2011; Falode et al. 2023). Citral, in particular, has been shown to upregulate PPAR-γ expression and modulate GLUT4 translocation in insulin-sensitive tissues (Chen et al. 2019), suggesting a plausible mechanism for insulin sensitization.

Table 4. Effect of treatments on serum ALT levels (U/L)

Group	Description	ALT (U/L)
1	Non-diabetic control	42.3±3.1a
2	Diabetic control	86.7±4.5b
3	Diabetic + Metformin	48.2±2.8a
4	Diabetic + Lemongrass oil (50 mg/kg)	61.7±3.6c
5	Diabetic + Lemongrass oil (100 mg/kg)	49.5±2.9a
6	Diabetic + Lemongrass oil (200 mg/kg)	55.3±3.2ac
7	Non-diabetic + Lemongrass oil	43.5±2.6a

Note: Values are expressed as mean ± SD (n=6). Different superscripts suggest statistically significant differences between groups (p<0.05; one-way ANOVA followed by Tukey's post hoc test)

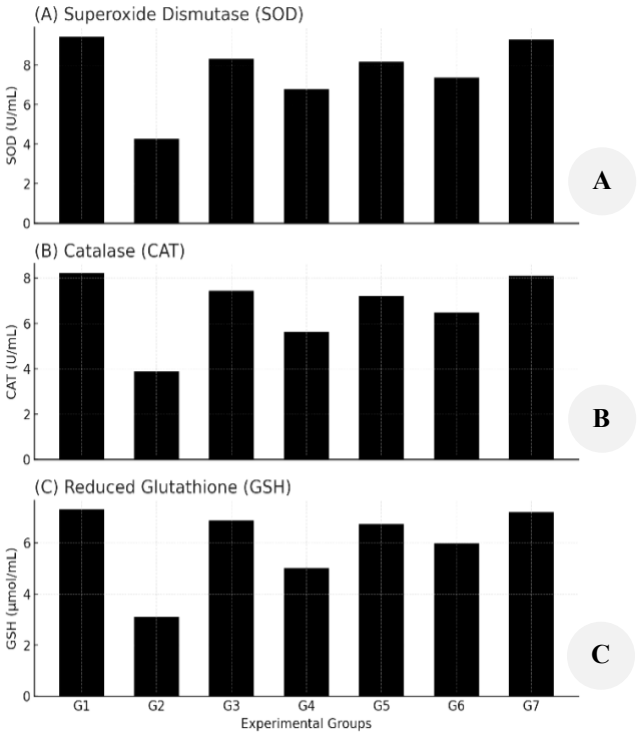

Figure 2. Antioxidant enzyme activities in serum on day 28. A. Superoxide Dismutase (SOD), B. Catalase (CAT), C. Reduced Glutathione (GSH). Note: Bars represent mean ± SD (n=6). A one-way ANOVA followed by Tukey's post hoc test was used to compare the groups. Bars with different letters suggest significant differences (p<0.05)

These findings align with previous reports using the STZ-NA model to evaluate plant-based interventions. For instance, Zamanian et al. (2024) demonstrated that *Curcuma longa* extract significantly lowered fasting glucose and improved liver histology in diabetic rats via suppression of NF-κB-mediated inflammatory pathways. Similarly, Eidi and Eidi (2009) reported that garlic essential oil enhanced antioxidant defense and restored hepatic function through modulation of SOD and GSH levels. The current results confirm and expand on these findings by showing that lemongrass oil can exert comparable hepatoprotective effects, possibly through the synergistic action of its terpenoid components.

The STZ-NA model is considered a mild and reproducible model for type 2 diabetes, characterized by partial β-cell dysfunction and insulin resistance (Srinivasan et al. 2005). In this context, the observed improvement in antioxidant enzyme levels (SOD, CAT, GSH) suggests that *C. citratus* oil may attenuate oxidative stress, a key driver of diabetic complications. Oxidative stress has been implicated in mitochondrial dysfunction, β-cell apoptosis, and hepatic inflammation (Rains and Jain 2011). Therefore, the normalization of these markers may reflect both direct free radical scavenging and indirect effects on redox-sensitive signaling pathways.

At the same time, the exact molecular mechanisms remain to be elucidated; it is plausible that citral and related terpenoids modulate signaling cascades such as the Nrf2/ARE pathway, which regulates the transcription of endogenous antioxidant enzymes (Ma 2013; Rabelo et al. 2015). This regulatory axis has been shown to be activated by several monoterpenes and may underlie the observed restoration of SOD, CAT, and GSH levels in this study.

Furthermore, lemongrass oil may influence AMPK activation, a central energy sensor that promotes glucose uptake and lipid metabolism (Hardie et al. 2012). These proposed mechanisms merit further investigation using transcriptomic or proteomic approaches. One strength of this study lies in its combined evaluation of biochemical and histopathological endpoints, providing a more holistic view of organ-level effects. However, certain limitations should be acknowledged. The study did not measure plasma insulin levels or conduct oral glucose tolerance tests, which could provide deeper insight into β-cell function and systemic glucose handling. Additionally, the absence of GC-MS profiling of the essential oil limits the ability to correlate specific compounds with observed bioactivities. Future studies should aim to isolate individual constituents and validate their actions in vitro and in vivo.

The findings suggest that lemongrass essential oil, particularly at 100 mg/kg, holds promise as a natural therapeutic agent for diabetes management, offering dual benefits on glycemic control and liver protection. These outcomes justify further exploration, including clinical translation and mechanistic studies that target the molecular pathways of insulin action and oxidative stress. Moreover, the observed safety of *C. citratus* oil in non-diabetic rats supports its therapeutic potential. However, further studies are important to assess long-term toxicity, pharmacokinetics, and interactions with standard antidiabetic drugs. Previous findings suggest low acute toxicity, but data on chronic and reproductive effects are lacking. Translational development would also require standardization of active compounds, optimized formulations, and clinical validation.

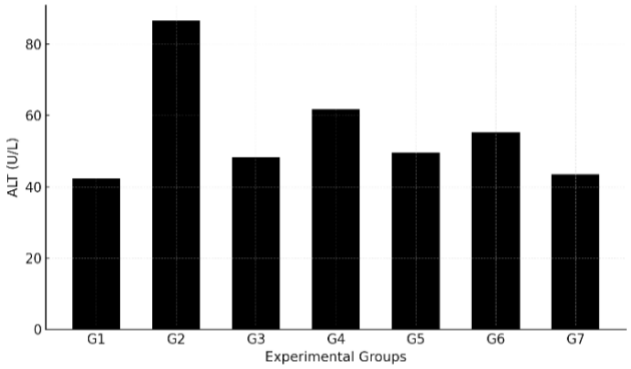

Figure 3. Serum ALT levels in rats on day 28, and the values were expressed as mean ± SD (n=6 per group). Group-wise differences were analyzed using one-way ANOVA followed by Tukey's post hoc test. Bars with different superscript letters suggest statistically significant differences ($p<0.05$)

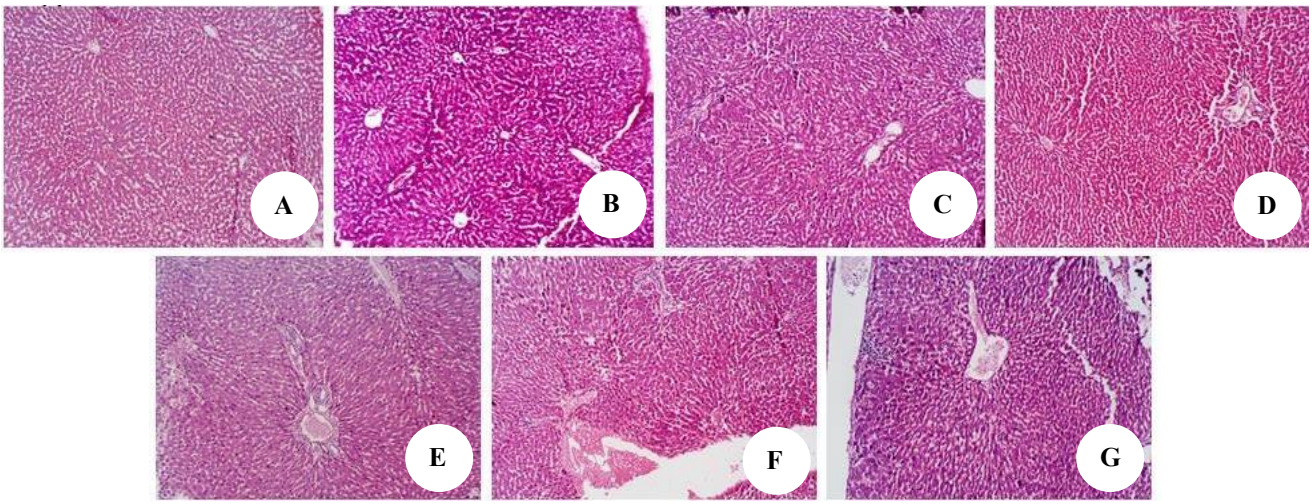

Figure 4. Representative photomicrographs of the liver sections from experimental groups (H&E staining, 400×). A. Group 1: Normal hepatic cords and central vein. B. Group 2: Degeneration, inflammation, congestion. C. Group 3: Near-normal architecture. D. Group 4: Mild cytoplasmic changes. E. Group 5: Well-preserved structure. F. Group 6: Partial recovery. G. Group 7: Normal histology

This study has certain limitations. Only male rats were used, which may overlook sex-specific metabolic responses. The 28-day duration limits insight into long-term efficacy or adverse effects. Important metabolic parameters, such as insulin levels, lipid profiles, and glucose tolerance, were not assessed, which constrains mechanistic interpretation. Additionally, the essential oil was not chemically profiled, which makes it difficult to attribute effects to specific constituents. Lastly, while the STZ-NA model reflects aspects of type 2 diabetes, it does not fully capture the complexity of human disease. Future studies should address these gaps.

In conclusion, this study demonstrated that oral administration of *C. citratus* essential oil, particularly at a dose of 100 mg/kg, significantly improved glycemic control, enhanced antioxidant enzyme activities, and protected liver tissue in streptozotocin-nicotinamide-induced diabetic rats. The comparable efficacy to metformin, along with observed histological improvements and normalization of liver enzyme markers, suggests that *C. citratus* oil possesses both antidiabetic and hepatoprotective properties. These findings support its potential use as a complementary therapeutic agent in the management of type 2 diabetes. However, further studies are needed to validate its clinical relevance and elucidate its molecular mechanisms.

REFERENCES

Adeneye AA, Amole OO, Adeneye AK. 2006. Hypoglycemic and hypolipidemic effects of the aqueous leaf and seed extract of *Phyllanthus amarus* in mice. Fitoterapia 77 (7-8): 511-514. DOI: 10.1016/j.fitote.2006.05.030.

Hamdy NM, Taha RA. 2009. Effects of *Nigella sativa* oil and thymoquinone on oxidative stress and neuropathy in streptozotocin-induced diabetic rats. Pharmacology 84 (3): 127-134. DOI: 10.1159/000234466.

Falode JA, Olofinlade TB, Fayeun GS, Adeoye AO, Bamisaye FA, Ajuwon OR, Obafemi TO. 2023. Free and bound phenols from *Cymbopogon citratus* mitigated hepatocellular injury in streptozotocin-induced type 1 diabetic male rats via decrease in oxidative stress, inflammation, and other risk markers. Pharmacol Res-Mod Chin Med 7: 100234. DOI: 10.1016/j.prmcm.2023.100234.

American Diabetes Association. 2021. Classification and diagnosis of diabetes: Standards of Medical Care in Diabetes—2021. Diabetes Care 44: S15-S33. DOI: 10.2337/dc21-S002.

Bakkali F, Averbeck S, Averbeck D, Idaomar M. 2008. Biological effects of essential oils - a review. Food Chem Toxicol 46 (2): 446-475. DOI: 10.1016/j.fct.2007.09.106.

Eidi A, Eidi M. 2009. Antidiabetic effects of sage (*Salvia officinalis* L.) leaves in normal and streptozotocin-induced diabetic rats. Diabetes Metab Syndr: Clin Res Rev 3: 40-44. DOI: 10.1016/j.dsx.2008.11.004.

Evans JL, Goldfine ID, Maddux BA, Grodsky GM. 2002. Oxidative stress and stress-activated signaling pathways: A unifying hypothesis of type 2 diabetes. Endocr Rev 23: 599-622. DOI: 10.1210/er.2001-0039.

Maritim AC, Sanders RA, Watkins JB. 2003. Diabetes, oxidative stress, and antioxidants: A review. J Biochem Mol Toxicol 17 (1): 24-38. DOI: 10.1002/jbt.10058.

Matsui H, Shimosawa T, Uetake Y, Wang H, Ogura S, Kaneko T, Liu J, Ando K, Fujita T. 2006. Protective effect of potassium against the hypertensive cardiac dysfunction: association with reactive oxygen species reduction. Hypertension 48 (2): 225-231. DOI: 10.1161/01.HYP.0000232617.48372.cb.

Oyedeji OO, Lawal OA, Shode FO, Oyedeji AO. 2009. Chemical composition and antibacterial activity of the essential oils of *Callistemon citrinus* and *Callistemon viminalis* from South Africa. Molecules 14 (6): 1990-1998. DOI: 10.3390/molecules14061990.

Patel DK, Prasad SK, Kumar R, Hemalatha S. 2012. An overview on antidiabetic medicinal plants having insulin mimetic property. Asian Pac J Trop Biomed 2: 320-330. DOI: 10.1016/S2221-1691(12)60032-X.

Rabelo TK, Zeidán-Chuliá F, Caregnato FF, Schnorr CE, Gasparotto J, Serafini MR, de Souza Araújo AA, Quintans-Junior LJ, Moreira JCF, Gelain DP. 2015. In vitro neuroprotective effect of shikimic acid against hydrogen peroxide-induced oxidative stress. J Mol Neurosci 56 (4): 956-965. DOI: 10.1007/s12031-015-0559-9.

Rena G, Hardie DG, Pearson ER. 2017. The mechanisms of action of metformin. Diabetologia 60 (9): 1577-1585. DOI: 10.1007/s00125-017-4342-z.

Shah G, Shri R, Panchal V, Sharma N, Singh B, Mann AS. 2011. Scientific basis for the therapeutic use of *Cymbopogon citratus*, stapf (Lemon grass). J Adv Pharm Technol Res 2 (1): 3-8. DOI: 10.4103/2231-4040.79796.

Srinivasan K, Viswanad B, Asrat L, Kaul CL, Ramarao P. 2005. Combination of high-fat diet-fed and low-dose streptozotocin-treated rat: A model for type 2 diabetes and pharmacological screening. Pharmacol Res 52 (4): 313-320. DOI: 10.1016/j.phrs.2005.05.004.

Sun H, Saeedi P, Karuranga S et al. 2022. IDF Diabetes Atlas: Global and regional diabetes prevalence estimates for 2021 and projections for 2045. Diabetes Res Clin Pract 183: 109119. DOI: 10.1016/j.diabres.2021.109119.

Szkudelski T. 2012. Streptozotocin-nicotinamide-induced diabetes in the rat. Characteristics of the experimental model. Exp Biol Med 237 (5): 481-490. DOI: 10.1258/ebm.2012.011372.

Chen T, Zhang Y, Liu Y, Zhu D, Yu J, Li G, Sun Z, Wang W, Jiang H, Hong Z. 2019. MiR-27a promotes insulin resistance and mediates glucose metabolism by targeting PPAR-γ-mediated PI3K/AKT signaling. Aging 11 (18): 7510. DOI: 10.18632/aging.102263.

Zamanian MY, Alsaab HO, Golmohammadi M, Yumashev A, Jabba AM, Abid MK, Joshi A, Alawadi AH, Jafer NS, Kianifar F, Obakiro SB. 2024. Nf-κb pathway as a molecular target for curcumin in diabetes Mellitus treatment: Focusing on oxidative stress and inflammation. Cell Biochem Funct 42 (4): e4030. DOI: 10.1002/cbf.4030.

Rains JL, Jain SK. 2011. Oxidative stress, insulin signaling, and diabetes. Free Radic Biol Med 50 (5): 567-575. DOI: 10.1016/j.freeradbiomed.2010.12.006.

Ma Q. 2013. Role of nrf2 in oxidative stress and toxicity. Ann Rev Pharmacol Toxicol 53 (1): 401-426. DOI: 10.1146/annurev-pharmtox-011112-140320.

Hardie DG, Ross FA, Hawley SA. 2012. AMPK: A nutrient and energy sensor that maintains energy homeostasis. Nat Revi Mol Cell Biol 13 (4): 251-262. DOI: 10.1038/nrm3311.